Controls of mRNA degradation in Arabidopsis: Investigating cold stress response and mRNA decay machinery

（シロイヌナズナにおける mRNA 分解制御：低温ストレス応答および mRNA 分解酵素複合体に関する研究）

By

Toshihiro Arae

A Dissertation
Submitted to the Graduate School of Life Science
Hokkaido University
In partial fulfillment of the Requirements for
the Degree of Doctor of Life Science

Graduate Course of Biosystems Science
Graduate School of Life Science
Hokkaido University, Sapporo, Japan

March 2019

Contents

Abbreviations

BiFC: Bimolecular fluorescence complementation

CAF1: CCR4-associated factor 1

CCR4: Carbon catabolite repressor 4

CFP: Cyan fluorescence protein

CGFP: C-terminal fragment of GFP

DCP1: Decapping 1

GFP: Green fluorescent protein

NGFP: N-terminal fragment of GFP

PABP: Poly(A) binding protein

PAN2: Poly(A) nuclease 2

PARN: Poly(A) ribonuclease

P-body: Processing body

XRN1: Exoribonuclease 1

Chapter 1

General Introduction

The regulation of gene expression is important for all organisms. Most studies on the control of gene expression have focused on the rate of mRNA synthesis, while only a few attempts have been made to understand the functional relevance of mRNA stability control. However, considering that the actual mRNA level is determined by the balance between mRNA synthesis and degradation, it is important to explore the regulation of mRNA stability in addition to transcription for understanding the control of mRNA amounts.

General mRNA degradation pathway

In 1990, Exoribonuclease 1 (XRN1) was identified as an enzyme responsible for 5'-3' degradation in *Saccharomyces cerevisiae* (yeast) (Larimer and Stevens 1990). To date, a variety of enzymes involved in the mRNA degradation have been identified. mRNA degradation pathways have been extensively studied in yeast. Poly(A) shortening by deadenylases is the first and apparently the rate-limiting step of mRNA degradation for most transcripts (Shyu *et al.* 1991). After deadenylation, the 5' cap structure is removed by Decapping 1/2 (DCP1/2) complex, and then the mRNA body is degraded in the 5'-3' direction by XRN1. Alternatively, deadenylated mRNA is degraded in the 3'-5' direction by EXOSOME complex (Beelman *et al.* 1996, Larimer and Stevens 1990, Mitchell *et al.* 1997) (Figure 1-1). The conservation of enzymes responsible for each of these steps suggests the existence of similar mRNA degradation pathways in eukaryotes, including plants (Morris *et al.* 2005, Morita *et al.* 2007, Chiba and Green 2009, Nagarajan *et al.* 2013).

mRNA degradation in plants

Plants cannot move to escape from any unfavorable environmental conditions due to their sessile life style. Therefore, to adapt to the environmental stresses, an ability of accurate and rapid regulations of gene expression is required in plants. mRNA degradation controls coordinate the level of mRNA with transcriptional regulations. However, transition speed of mRNA level is only dependent on the mRNA stability. Responding to ever-changing environments, controls of the transition speed of mRNA levels are also important. To understand the regulations of mRNA degradation during stress responses, genome-wide measurement of mRNA stability is useful. Narsai *et al.* (2007) measured mRNA degradation rates globally under normal growth condition, identifying several features of transcript, such as intron and sequence motifs, related to the mRNA degradation rate. Our group first challenged global analysis of mRNA degradation changes at 24 h after cold stress treatment (Chiba *et al.* 2013), revealing that a large number of cold responsive genes are relatively destabilized. However, we realized that temporal changes of the mRNA degradation in response to stress have to be determined to understand the importance of mRNA degradation controls coordinated with transcription regulation. So far, such an analysis has not been reported in plants.

Recent studies on several mutants lacking mRNA degradation factor reveal that the control of mRNA degradation is important for developmental processes and stress responses. AtXRN4, a yeast XRN1 homolog in Arabidopsis, is involved in ethylene signaling response

through the regulations of EIN3 binding F-box protein 1 (EBF1) and EBF2 (Olmedo *et al.* 2006). AtXRN4 is also involved in heat stress response. AtXRN4 catalyze the decay of specific mRNAs at an early stage of heat stress response. In this regulation, an RNA-binding protein, La-related protein 1 (LARP1), functions as a heat-specific cofactor of AtXRN4 (Merret *et al.* 2013). Sm-Like (LSM) proteins have been identified as RNA decay related proteins in all eukaryotes, and Arabidopsis AtLSM1-7 complex promotes decapping and 5'-3' decay of mRNA in cytoplasm (Golisz *et al.* 2013). Recent study showed that AtLSM1-7 complex negatively regulates tolerance to cold and drought stresses, whereas positively regulates the salt stress tolerance (Perea-Resa *et al.* 2016). These results indicate the important role of mRNA degradation controls during developmental processes and environmental stress responses.

Poly(A) tail and its regulatory mechanism

Poly(A) tails are added by a nuclear poly(A) polymerase (PAP) following cleavage of the primary transcript during transcriptional termination. The distribution of poly(A) lengths is varied among species; the median of tail-length averages for individual gene are 33.1 nucleotides (nt) in yeast, 82.6 nt in HeLa cells and 58.1 nt in *Arabidopsis thaliana* (Subtelny *et al.* 2014). In cytoplasm, mRNA molecules form circular structures by an interaction between eukaryotic initiation factor 4G (eIF4G) and poly(A) binding proteins (PABPs). PABPs binding to poly(A) tail protect the mRNA from exoribonuclease attack, therefore poly(A) tail is important for mRNA stability. Moreover, the circular structure is also important for mRNA translational efficiency. The interaction between eIF4F and PABPs enhances recycle of the small ribosomal subunit which just dissociated from the mRNA by translation termination. Therefore, eIF4F and PABPs enhances the translation initiation. Global analysis revealed the positive correlation between the poly(A) length and ribosome occupancy in yeast (Lackner *et al.* 2007). However, in another report, this positive correlation was only observed in cells under early developmental stages (Subtelny *et al.* 2014). In contradiction, negative correlation was also reported in *Caenorhabditi selegance* (Lima *et al.* 2017) Therefore, we still cannot conclude the effect of poly(A) length on translational status.

Poly(A) tails are removed by several nucleases called deadenylases. In mammals, poly(A) tails are first trimmed to ~150 nt by deadenylase complex, Poly(A) nuclease 2/3 (PAN2/3). PAN2/3 selectively trims long poly(A) tails (>150 nt) in mammals. Then, the remaining poly(A) tails are degraded by two major cytoplasmic deadenylases, Carbon catabolite repressor 4 (CCR4) and Ccr4-associated factor 1 (CAF1) (Yamashita *et al.* 2005, Yi *et al.* 2018). CCR4, containing a DNase I-like domain, belongs to the endo-exonuclease/phosphatase (EEP) superfamily. CAF1, PAN2 and another widely conserved deadenylase, Poly(A) specific ribonuclease (PARN) belong to the DEDD nuclease family. DEDD type nucleases require three aspartates (D) and one glutaminate (E) to the enzymatic activity. Xenopus PARN deadenylates the *cyclin B1* mRNA and represses its translation during pre-mature oocyte (Kim and Richter 2006). In yeast and mammals, CCR4 and CAF1 form a large complex called CCR4-NOT complex, that includes Negative on TATA 1

(NOT1) as a scaffold protein and various NOT proteins (Oberholzer and Collart 1998, Lau *et al.* 2009).

Deadenylases in plants

A. thaliana has homologs of mammalian deadenylases other than PAN2 and PAN3. Phenotypic analyses of mutants of the Arabidopsis CCR4 homolog (AtCCR4), CAF1 homolog (AtCAF1) and the PARN homolog (AtPARN) have suggested distinct roles for these deadenylases. AtCCR4a and AtCCR4b are involved in sucrose and starch metabolism through the poly(A) length control of *Granule-bound starch synthase 1* (*GBSS1*) mRNA (Suzuki *et al.* 2015). AtCAF1a and AtCAF1b are involved in pathogen defense responses and in stress responses (Liang *et al.* 2009, Walley *et al.* 2010). AtPARN is an essential deadenylase that is required for embryogenesis and controls poly(A) length of mitochondrial mRNA (Chiba *et al.* 2004, Reverdatto *et al.* 2004, Hirayama *et al.* 2013). In *Oryza sativa*, functional CCR4 homolog (OsCCR4) and CAF1 homolog (OsCAF1) are identified. These two deadenylases interact with NOT1 homolog (OsNOT1) as shown in other eukaryotes (Chou *et al.* 2017), suggesting that the CCR4-NOT complex is also conserved in plants. However, the overall picture of the CCR4-NOT complex in plants has not been elucidated yet.

In this dissertation

I took two differential approaches to clarify the importance of mRNA stability control for plant stress responses: On one hand, I focused on the regulated transcripts at the level of mRNA stability under stress condition (Topic 1). On the other hand, I focused on the regulator of mRNA stability (Topic 2).

Topic1: Cold stress adversely affects plant growth and development. To adapt to changes in ambient temperature, plants regulate gene expression at multiple levels. However, most studies on the regulation of gene expression in response to cold stress have focused on the rate of mRNA synthesis, while few studies have explored the functional significance of regulating mRNA stability. In Chapter 2, I describe the functional significance of mRNA stability regulation in the cold stress response in Arabidopsis cells by monitoring temporal changes in mRNA concentrations and half-lives on a global scale. The global analysis revealed that several cold-responsive genes, including *Cold-regulated 15a*, were relatively destabilized, whereas the mRNA amounts were increased during cold treatment. Furthermore, by using mathematical approaches, we propose a possible coordination between mRNA synthesis and degradation, in which the destabilization was overcome by accelerating the transcription rate to achieve the quick induction of mRNA in the cold-responsive genes.

Topic 2: The CCR4-NOT complex includes the deadenylases CCR4/CAF1, which are important for determining the polyA length of mRNAs, and several RNA binding proteins to recognize the specific target mRNAs of the deadenylases. Revealing the components and composition of the

plant CCR4-NOT complex is indispensable for understanding its function as a regulator of mRNA stability, as well as the target recognition mechanism for deadenylases in plants. In Chapter 3, I exhibit the presence of CCR4-NOT complexes in Arabidopsis containing different combinations of deadenylase subunits. I also show that the RNA binding protein APUM5, a member of the Pumilio family, interacts with AtCCR4 in cytoplasmic processing bodies, where most mRNA degradation machinery components accumulate. This discovery is the first step to understanding the function of the CCR4-NOT complex in plants.

Figures and legends

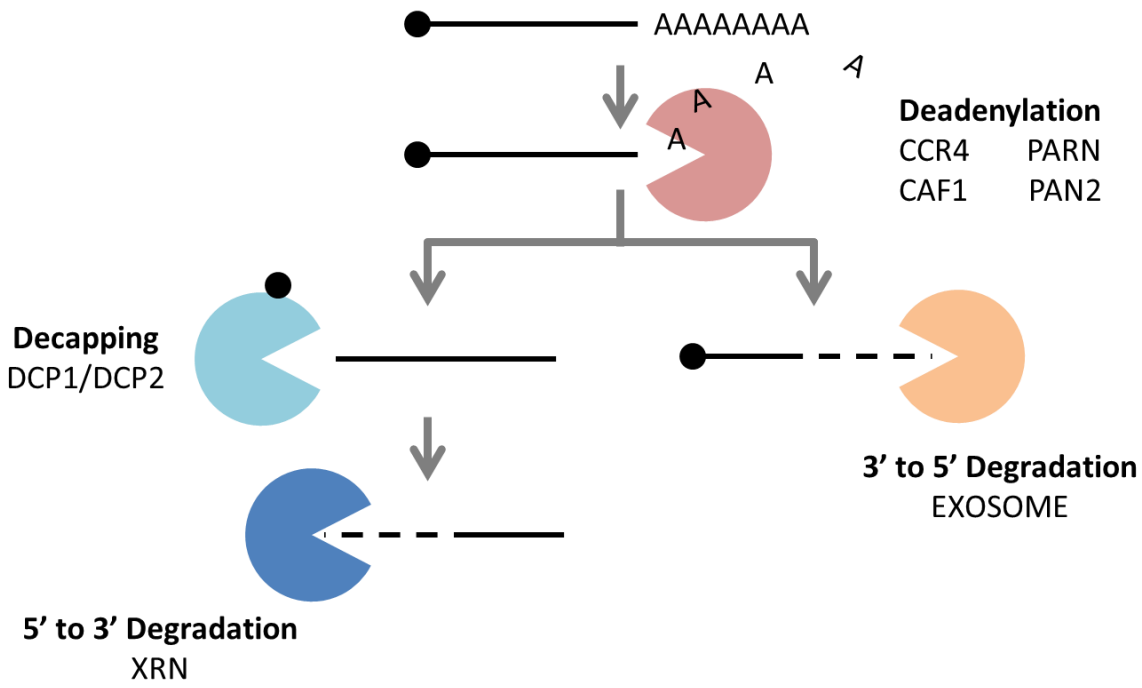

Figure 1-1. General mRNA degradation pathways in eukaryotes.

The mRNA body is protected from degradation by a cap structure at the 5' end and poly(A) tail at the 3' end, respectively. Initially, the poly(A) tail is removed by deadenylases, such as CCR4, CAF1, PARN and PAN2. Deadenlyated mRNA is degraded by 5' to 3' degradation followed by decapping, or alternatively, by 3' to 5' degradation.

References

Beelman, C.A., Stevens, A., Caponigro, G., LaGrandeur T.E., Hatfiedl, L., Fortner, D.M. and Parker, R. (1996) An essential component of the decapping enzyme required for normal rates of mRNA turnover. *Nature*, **15**: 642-646.

Chiba, Y., Johnson, M.A., Lidder, P., Vogel, J.T., Van Erp, H. and Green, P.J. (2004) AtPARN is an essential poly(A) ribonuclease in *Arabidopsis*. *Gene*, **328**: 95-102.

Chiba, Y. and Green, P.J. (2009) mRNA degradation machinery in plants. *J. Plant Biol.*, **52**: 114-124.

Chiba, Y., Mineta, K., Hirai, M.Y., Suzuki, Y., Kanaya, S., Takahashi, H., Onouchi, H., Yamaguchi, J. and Naito, S. (2013) Changes in mRNA stability associated with cold stress in Arabidopsis cells. *Plant Cell Physiol.* **54**: 180-194.

Chou, W.L., Chung, Y.L., Fang, J.C. and Lu, C.A. (2017) Novel interaction between CCR4 and CAF1 in rice CCR4-NOT deadenylase complex. *Plant Mol. Biol.* **93**, 79-96.

Golisz, A., Sikorski, P.J., Kruszka, K. and Kufel, J. (2013) *Arabidopsis thaliana* LSM proteins function in mRNA splicing and degradation. *Nucleic Acid Res.*, **41**: 6232-6249.

Hirayama, T., Matsuura, T., Ushiyama, S., Narusaka, M., Kurihara, Y., Yasuda, M., Ohtani, M., Seki, M., Demura, T., Nakashita, H., Narusaka, Y. and Hayashi, S. (2013) A poly(A)-specific ribonuclease directly regulates the poly(A) status of mitochondrial mRNA in Arabiedopsis. *Nat. Commun.*, **4**: 2247.

Kim, J.H. and Richter, J.D. (2006) Opposing polymerase-deadenylase activities regulate cytoplasmic polyadenylation. *Mol. Cell*, **24**: 173-183.

Lackner, D.H., Beilharz, T.H., Marguerat, S., Mata, J., Watt, S., Schubert, F., Preiss, T. and Bahler, J. (2007) A network of multiple regulatory layers shapes gene expression in fission yeast. *Mol. Cell*, **26**: 145-155.

Larimer, F.W. and Stevens, A. (1990) Disruption of the gene *XRN1*, coding for a 5'→3' exoribonuclease restricts yeast cell growth. *Gene*, **95**: 85-90.

Lau, N.C., Kolkman, A., van Schaik, F.M., Mulder, K.W., Pijnappel, W.W., Heck, A.J. and Timmers, H.T. (2009) Human Ccr4-Not complexes contain variable deadenylase subunits. *Biochem. J.* **422**: 443-453.

Liang, W., Li, C., Liu, F., Jiang, H., Li, S., Sun, j., Wu, X. and Li, C. (2009) The *Arabidopsis* homologs of CCR4-associated factor1 show mRNA deadenylation activity and play a role in plant defence responses. *Cell Rep.*, **19**: 307-316.

Lima, S.A., Chipman, L.B., Nicholson, A.L., Chen, Y.H., Yee, B,A., Yeo, G.W., Coller, J. and Pasquinelli, A.E. (2017) Short poly(A) tails are a conserved feature of highly expressed genes. *Nat. Struct. Mol. Biol.*, **24**: 1057-1063.

Merret, R., Descombin, J., Juan, Y.T., Favory, J.J., Carpentier, M.C., Chaparro, C., Charng Y.Y., Deragon, J.M. and Bousquet-Antonelli, C. (2013) XRN4 and LARP1 are required for a heat-triggered mRNA decay pathway involved in plant acclimation and survival during thermal stress. *Cell Rep.*, **5**: 1279-1293.

Mitchell, P., Petfalski, E., Shevchenko, A., Mann, M. and Tollervey, D. (1997) The exosome: a conserved eukaryotic RNA processing complex containing multiple 3'-->5' exoribouncleases. *Cell*, **91**: 457-466.

Morita, M., Suzuki, T., Nakamura, T., Yokoyama, K., Miyasaka, T. and Yamamoto, T. (2007) Depletion of mammalian CCR4b deadenylase triggers elevation of the *p27Kip1* mRNA level and impairs cell growth. *Mol. Cell. Biol.*, **27**: 4980-4990.

Morris, J.Z., Hong, A., Lilly, M.A. and Lehmann, R. (2005) *twin*, a *CCR4* homolog, regulates cyclin poly(A) tail length to permit *Drosophila* oogenesis. *Development*, **132**: 1165-1174.

Nagarajan, V.K., Jones, C.I., Newbury, S.F. and Green, P.J. (2013) XRN 5'-->3' exoribonucleases: structure, mechanisms and functions. *Biochim. Biophys. Acta*, **1829**: 590-603.

Narsai, R., Howell, K.A., Millar, A.H., O'Toole, N. and Whelan, J. (2007) Genome-wide analysis of mRNA decay rates and their determinants in *Arabidopsis thaliana*. *Plant Cell*, **19**: 3418-3436.

Oberholzer, U. and Collart, M.A. (1998) Characterization of NOT5 that encodes a new component of the Not protein complex. *Gene*, **207**: 61-91.

Olmedo, G., Guo, H., Gregory, B.D., Nourizadeh, S.D., Aguilar-Henonin, L., Li, H., An, F., Guzman, P. and Ecker, J.R. (2006) ETHYLENE-INSENSITIVE5 encodes a 5'→3' exoribonuclease required for regulation of the EIN3-targeting F-box proteins EBF1/2. *Proc. Natl. Acad. Sci. U.S.A.*, **103**: 13286-13293.

Perea-Resa, C., Carrasco-López, C., Catalá, R., Turečkova, V., Navak, O., Zhang, W., Sieburth, L. Jiménez-Gómez, J.M. and Salinas, J. (2016) The LSM1-7 complex

differentially regulates Arabidopsis tolerance to abiotic stress conditions by promoting selecetive mRNA decapping. *Plant Cell*, **28**: 505-520.

Reverdatto, S.V., Dutko, J.A., Chekanova, J.A., Hamilton, D.A. and Belostotsky, D.A. (2004) mRNA deadenylation by PARN is essential for embryogenesis in higher plants. *RNA*, **10**: 1200-1214.

Shyu, A.B., Belasco, J.G. and Greenberg, M.E. (1991) Two distinct destabilizing elements in the c-*fos* message trigger deadenylation as a first step in rapid mRNA decay. *Genes Dev.*, **5**: 221-231.

Subtelny, A.O., Eichhorn, S.W., Chen, G.R., Sive, H. and Bartel, D.P. (2014) Poly(A)-tail profiling reveals an embryonic switch in translational controls. *Nature*, **508**: 66-71.

Suzuki, Y., Arae, T., Green, P.J., Yamaguchi, J. and Chiba, Y. (2015) AtCCR4a and AtCCR4b are Involved in Determining the Poly(A) Length of *Granule-bound starch synthase 1* Transcript and Modulating Sucrose and Starch Metabolism in *Arabidopsis thaliana*. *Plant Cell Physiol.* **56**: 863-874.

Walley, J.W., Kelley, D.R., Nestorova, G., Hirschberg, D.L. and Dehesh, K. (2010) Arabidopsis deadenylases AtCAF1a and AtCAF1b play overlapping and distinct roles in mediating environmental stress responses. *Plant Physiol.*, **152**: 866-875.

Yamashita, A., Chang, T.C., Yamashita, Y., Zhu, W., Zhong, Z., Chen, C.Y. and Shyu, A.B. (2005) Concerted action of poly(A) nucleases and decapping enzyme in mammalian mRNA turnover. *Nat. Struct. Mol. Biol.*, **12**: 1054-1063.

Yi, H., Park, J., Ha, M., Lim, J., Chang, H. and Kim, V.N. (2018) PABP cooperates with the CCR4-NOT complex to promote mRNA deadenylation and precocious decay. *Mol. Cell*, **70**: 1081-1088.

Chapter 2

Co-ordinated Regulations of mRNA Synthesis and Decay during Cold Acclimation in Arabidopsis Cells

Summary

Plants possess a cold acclimation system to acquire freezing tolerance through pre-exposure to non-freezing low temperatures. The transcriptional cascade of C-repeat-binding factors (CBFs)/dehydration response element-binding factors (DREBs) is considered a major transcriptional regulatory pathway during cold acclimation. However, little is known regarding the functional significance of mRNA stability regulation in the response of gene expression to cold stress. The actual level of individual mRNAs is determined by a balance between mRNA synthesis and degradation. Therefore, it is important to assess the regulatory steps to increase our understanding of gene regulation. Here, we analyzed temporal changes in mRNA amounts and half-lives in response to cold stress in Arabidopsis cell cultures based on genome-wide analysis. In this mRNA decay array method, mRNA half-life measurements and microarray analyses were combined. In addition, temporal changes in the integrated value of transcription rates were estimated from the above two parameters using a mathematical approach. Our results showed that several cold-responsive genes, including *Cold-regulated 15a*, were relatively destabilized, whereas the mRNA amounts were increased during cold treatment by accelerating the transcription rate to overcome the destabilization. Considering the kinetics of mRNA synthesis and degradation, this apparently contradictory result supports that mRNA destabilization is advantageous for the swift increase in CBF-responsive genes in response to cold stress.

Introduction

Adaptation of plants to environmental changes is important for their growth and development. Plants have developed various strategies to sense and adapt to biotic and abiotic stresses, including ambient temperature changes. Cold acclimation, which is induced by pre-exposure to low, non-freezing temperatures, leads to several metabolic and biochemical changes to acquire freezing tolerance in plants. Extensive investigations of the molecular mechanisms underlying cold acclimation have revealed transcriptional regulation by C-repeat-binding factors (CBFs)/dehydration response element-binding factors (DREBs) as a major regulatory system (Yamaguchi-Shinozaki and Shinozaki 2006, Zhu *et al.* 2007, Thomashow 2010). CBFs/ DREBs are cold-inducible transcriptional activators that interact with a specific cis-element in the promoter of various cold-responsive genes. The importance of controlling the mRNA levels of cold-responsive genes has been shown by reverse genetic analyses of components in the CBF transcriptional cascade (Fowler and Thomashow 2002, Maruyama *et al*. 2004, Vogel *et al*. 2005, Park *et al*. 2015, Zhao *et al*. 2015). Considering that the actual mRNA level is determined by the balance between mRNA synthesis and degradation, it is important to explore the regulation of mRNA stability as well as transcription to understand the control of the amount of mRNA in response to cold stress. However, studies that have focused on regulation of the mRNA stability in response to cold stress are limited (Chiba *et al*. 2013, Zhang *et al*. 2013). Global profiling of uncapped mRNAs via parallel analysis of RNA ends was performed to detect multiple types of degradation intermediates in response to cold stress in the monocotyledonous model plant *Brachypodium distachyon*. The majority of the intermediates were generated through the decapping pathway responsible for mRNA degradation. In addition, endonucleolytic cleavage products, including microRNA targets, have been identified (Zhang *et al*. 2013). These results were suggestive of a role for mRNA degradation control in the cold stress response.

The half-life of mRNA can be measured by monitoring the amount of mRNA remaining after inhibition of transcription. As a direct approach, we previously developed a method to analyze the half-life of mRNA on a global-scale, known as the mRNA decay array (Chiba *et al*. 2013). This analysis has an advantage in that changes in two parameters, namely the mRNA amount and half-life, are determined simultaneously. The mRNA decay array using Arabidopsis cells before and 24 h after cold treatment revealed that the majority of mRNAs elongate their half-lives at low temperatures, which can be accounted for by a general decrease in enzymatic activity toward mRNA degradation. Taking this ‘general shift’ into account, we identified thousands of relatively stabilized and destabilized transcripts with longer and shorter half-lives, respectively, than those expected from the general shift (EGS). Functional classification analysis showed that stress response- and hormonal response-related transcripts are enriched in the relatively destabilized class. Thus, we identified active changes in mRNA stability in response to cold stress. However, it is difficult to determine the functional significance of these stability changes using the mRNA decay array at a single time point of 24 h after cold treatment (Chiba *et al*. 2013), because the majority of transcripts in Arabidopsis have not reached the steady-state condition by 24 h (Oono *et al*. 2006).

In the present study, we performed the mRNA decay array on a larger scale to detect temporal changes in mRNA amount and stability after cold treatment. The objective of this study is to demonstrate the fundamental response of mRNA stability to cold stress by using Arabidopsis T87 cells (Axelos *et al*. 1992), which is widely accepted as a versatile model system without complex developmental changes and organ communications. The present study showed that CBF-responsive genes could be classified into two groups based on changes in mRNA stability in response to cold stress: those relatively destabilized vs. those showing no obvious changes in mRNA stability during cold treatment. Furthermore, by applying a mathematical approach to estimate changes in transcription rates, we explored the associations between transcriptional and mRNA stability regulations.

Results

Temporal changes in mRNA level and stability in response to cold stress

To understand temporal changes in mRNA levels and stability in response to cold stress, we performed an mRNA decay array using Arabidopsis T87 cells under control conditions (22°C) and 12, 24, and 36 h after the start of cold treatment at 4°C. The mRNA decay rate was measured by monitoring the decrease in mRNA over time after applying cordycepin, a transcriptional inhibitor (Fig. 2-1). Cordycepin effectively inhibited transcription in cells both before and after cold treatment. To achieve similar levels of transcriptional inhibition, a higher concentration of cordycepin was used for cold-treated cells (Fig. 2-2). Since longer mRNA half-lives are expected under cold conditions due to general stabilization, the time period for mRNA half-life measurements was extended in cold-treated cells. Total RNA was extracted at each time point with three biological replicates. RNA samples are often pooled in microarray analysis to reduce the effects of biological variation by averaging. Although statistical analysis cannot be applied to individual mRNA accumulation levels, determination of the expression levels in most genes is not adversely affected by pooling, as discussed by Kendziorski *et al*. (2005). Also, this strategy is beneficial to minimize subject-to-subject variations of microarray, making it easier to find the specific features of gene populations (Kendziorski *et al*. 2005). Thus, in this study, the three biological replicate RNA samples at each time point were pooled before being used for microarray analysis. The mRNA half-lives showed a bell-shaped distribution in both control and cold-treated cells after $\log_2$ conversion. The mean mRNA half-lives in the control cells was 1.3 h, and those in the 12, 24 and 36 h cold-treated cells were 19.6, 24.1 and 26.0 h, respectively (Fig. 2-3, left). The distribution of mRNA half-lives in control cells and 24 h cold-treated cells supported our previous data, in which the mean half-lives were 1.8 h in control cells and 22.7 h in 24 h cold-treated cells (Chiba *et al*. 2013). As expected, general stabilization was observed to a similar extent at all time points during cold treatment. The bell-shaped distribution was also observed among the mRNA amounts of individual transcripts after $\log_2$ conversion. In contrast to the mRNA half-lives, the mean mRNA amounts before and after cold treatment were almost unchanged (Fig. 2-3, right). Considering that no obvious differences were observed in the total RNA levels extracted from cells (Fig. 2-4A) and total poly(A) RNA levels (Fig. 2-4B) before and after cold treatment, the effect of general stabilization is probably offset by the general decrease in transcription rate during cold treatment.

Clustering of transcripts based on time-course profiles of mRNA levels and stability

Time-course profiles of mRNA amount and mRNA half-life were normalized to the values before cold treatment and then $\log_2$ converted to compare these two parameters. We focused on transcripts that showed a >2-fold difference from the general shift in mRNA amount and/or

mRNA half-life. The $\log_2$-converted changes in mRNA amount and half-lives were used for clustering analyses using the simple batch-learning self-organizing map (BL-SOM) method (Kanaya *et al*. 2001). The analyzed transcripts were divided into 15 clusters (Fig. 2-5). Averaged transcripts in Clusters 00, 01, 02, 40 and 42 showed a >2-fold differences (i.e. >1or <–1 in $\log_2$-converted values) from the general shift in mRNA amount and/or mRNA half-life for at least one time point during cold treatment. Among them, averaged transcripts in Cluster 02 showed >2-fold differences in both mRNA amount and half-life at 24h after cold treatment, whereas no obvious difference was observed in transcripts in Cluster 21.

We verified mRNA decay array data using conventional quantitative reverse transcription–PCR (qRT–PCR) with 27 randomly selected transcripts in Clusters 00, 02, 21, 40 and 42 (data of 15 transcripts are shown in Fig. 2-6). The average Pearson's correlation coefficient between the mRNA decay array and qRT–PCR results for the $\log_2$ ratios of mRNA amounts after cold treatment to before was 0.82 and that of mRNA half-lives was 0.94, supporting the reliability of the mRNA decay array.

Classification by Gene Ontology terms of the transcripts in the clusters

To characterize transcripts in each cluster, we performed Gene Ontology (GO)-based enrichment analysis (Berardini *et al*. 2004). Transcripts in Clusters 02, 40, 41 and 42 were associated with several significantly enriched GO terms (Fig. 2-7; Table 2-1). Averaged transcripts in Cluster 02 and Cluster 40 showed >2-fold differences from the general shift in mRNA amount for at least one time point. The levels of averaged transcripts in Cluster 02 showed large increases, whereas these transcripts were relatively destabilized during cold treatment (Fig. 2-5). The GO terms significantly over-represented in this cluster included 'regulation of transcription' and a number of GO terms related to the responses to various biotic and abiotic stresses (Fig. 2-7A). Averaged transcripts in Cluster 40 showed decreased levels during cold treatment, whereas no >2-fold change in mRNA stability at any time point was observed compared with the general shift (Fig. 2-5). Transcripts in this cluster were significantly over-represented in a number of GO terms related to cell cycle, such as 'DNA endoreduplication', 'regulation of cell cycle', 'regulation of cell proliferation' and 'regulation of DNA replication' (Fig. 2-7B).

Conserved sequence motif in relatively stabilized transcripts in Cluster 42

Several cis-acting elements involved in the determination of mRNA stability have been identified mostly in the 5'- or 3'- untranslated regions (UTRs) of various transcripts (Newman *et al*. 1993, Chen and Shyu 1995). To identify putative cis-acting elements, we searched for conserved sequence motifs in the 5'- and 3'-UTRs of transcripts in Clusters 00, 01, 02, 40 and 42 by MEME (Bailey *et al*. 2009). Average transcripts in Clusters 00, 01 and 02 showed relative destabilization and those in Clusters 40 and 42 showed stabilization at least at one time point during cold treatment

(Fig. 2-5). A UAGGGUUU motif was identified in the 5'-UTR of transcripts in Cluster 42 (Fig. 2-8). In addition, several over-represented purine- or pyrimidine-rich motifs (*E*-values<0.05) were identified in the 5'-UTR of transcripts in Clusters 00, 01, 02, 40 and 42, and in the 3'-UTR of transcripts in Cluster 42 (Fig. 2-9). Despite the significant enrichment, these sequences were not limited to the destabilized or stabilized clusters. Therefore, we considered that these motifs are not specific elements for regulation of mRNA stability.

Enrichment of CBF-responsive genes in Cluster 02 and Cluster 12

CBFs/DREBs are cold-inducible transcription factors that interact with a specific cis-element in the promoter of CBF-responsive genes. Transcriptional activation of CBF-responsive genes during cold treatment is critical for acquiring cold stress tolerance in plants (Jaglo-Ottosen *et al*. 1998, Hsieh *et al*. 2002, Ito *et al*. 2006). To explore temporal changes in the mRNA amount and stability of CBF-responsive genes, we performed enrichment analysis of the 15 clusters. CBF-responsive genes were obtained from the public transcriptome database, as described previously in Chiba *et al*. (2013). A total of 32 CBF-responsive genes were identified among the transcripts analyzed using the mRNA decay array in this study. The CBF-responsive genes were significantly enriched in Clusters 02 and 12 (q< 0.05; Table 2-2): 16 in Cluster 02 and six in Cluster 12 (Table 2-2). Among them, nine out of 16 CBF-responsive genes in Cluster 02 (~60%) showed >2-fold destabilization at least at one time point, whereas only one out of six CBF-responsive genes in Cluster 12 (~17%) did so. Also, when we counted the number of CBF-responsive genes which showed destabilization at more than two time points during cold treatment, 12 genes (~75%) were found in Cluster 02 while none was found in Cluster 12 (Fig. 2-10). Thus, CBF-responsive genes in Cluster 02 have a tendency to be relatively destabilized, whereas those in Cluster 12 do not. In addition, greater induction of the mRNA amount in most of the CBF-responsive genes in Cluster 02 was observed compared with those in Cluster 12, suggesting that destabilization contributes to achieving a dynamic increase at least in some of the CBF-responsive genes in Cluster 02.

Kinetics of mRNA synthesis and degradation of CBF-responsive genes

Actual levels of mRNA are determined by the balance between mRNA synthesis and degradation. Transcription can be measured by monitoring the incorporation of a non-toxic ribonucleoside analog, such as 4-thiouridine (Melvin *et al*. 1978). Although this method has been used in various eukaryotic systems (Miller *et al*. 2011, Rabani *et al*. 2011, Schwanhausser *et al*. 2011), this approach is technically difficult in cold-treated cells, because the transcription rate is expected to be much slower under cold conditions at 4°C than under control conditions, as is the case for mRNA degradation. The general shift in mRNA half-life during cold treatment was approximately 20-fold, while the mRNA amount was almost unchanged. Hence, the general transcription rate is expected to be approximately 20-fold less than that of the control condition.

Furthermore, changes in plasma membrane proteins and lipid composition occur in cold-treated cells (Uemura *et al*. 2006). Therefore, we suspected that efficiency of incorporation of ribonucleoside analogs may be too low to be used in monitoring the transcription rate under cold conditions. Consequently, we employed a mathematical approach to estimate temporal changes in the transcription rate to understand the functional relevance of destabilization in CBF-responsive genes, in which the mRNA levels were dynamically up-regulated, despite destabilization, in response to cold.

We selected five transcripts from Cluster 02 for further analyses that showed typical changes in mRNA amount and half-life, in that the mRNA amount was increased during cold treatment, whereas the mRNA half-life was decreased compared with the general shift, indicative of relative destabilization (Fig. 2-11). Three of them, *Cold-regulated 15a* (*Cor15a*: AT2G42540), *Early response to dehydration 10* (*ERD10*: AT1G20450) and *Plant invertase pectin methylesterase inhibitor* (*PMEI*: AT5G62350), are selected as the direct targets of CBF3 (Maruyama *et al*. 2004). Among them, *Cor15a* is the most well-known target of CBF3, which encodes a chloroplast-localized protein. Constitutive expression of *Cor15a* enhances freezing tolerance in chloroplasts in vivo and in protoplasts, possibly through increased cryostability of cellular membranes (Artus *et al*. 1996, Steponkus *et al*. 1998, Thalhammer *et al*. 2014). We also analyzed *rad29A* and *AtGols3* as direct targets of CBF3, as well as the CBF3 gene itself. However, for these three genes, the expression levels before cold treatment were too low to measure their mRNA half-lives.

The remaining two genes are *Calcineurin B-like (CBL) protein-interacting serine/threonine-protein kinase 25* (*CIPK25*: AT5G25110) and *MYB domain protein 32* (*AtMYB32*: AT4G34990). Arabidopsis has 26 CIPK members (Kolukisaoglu *et al*. 2004), some of which function as a calcium sensor together with specific CBLs in signaling pathways in response to various abiotic stresses (Manik *et al*. 2015). AtMYB32 is a member of the R2R3 MYB gene family encoding functionally diverse transcription factors (Ambawat *et al*. 2013). Various transcriptomic analyses, including our data, showed strong induction of *CIPK25* and *AtMYB32* expression by cold stress (Kilian *et al*. 2007, Barah *et al*. 2013, Chiba *et al*. 2013); however, their actual functions in the cold stress response remain unclear.

We calculated the integrated transcription rate (*K*), which represents the sum of transcripts that are newly synthesized by a specific time (*T*) after the start of cold treatment. The *K* value is calculated from two experimentally determined parameters, the mRNA amount (*A*) (Fig. 2-11A) and mRNA decay rate [λ; $\lambda = \ln(2)/\tau$; for detailed calculations, see Equation 3 in the Materials and Methods] (Fig. 2-11B). To visualize the interplay between transcriptional activation and destabilization in response to cold stress, we compared the *K* values over the time course with the hypothetical *K*, which was calculated by assuming that the mRNA decay rate (λ) follows the general shift, and that the mRNA amount (*A*) follows the observed value. Therefore, the hypothetical *K* represents the level of transcription required to support the actual changes in mRNA level when mRNA was only passively stabilized at low temperatures. For any of the five transcripts

in Cluster 02, most of the *K* values were significantly enhanced compared with the hypothetical *K* (Fig. 2-11C), suggesting that greater transcriptional activation, compared with that under the hypothetical condition, was required to overcome mRNA destabilization and increase mRNA amounts under cold conditions.

Discussion

Plants effectively regulate gene expression to adjust for changes in ambient temperature. Most studies on the regulation of gene expression in response to cold stress have focused on transcription, although the mRNA amount is determined by the balance between mRNA synthesis and degradation. To explore the physiological significance of mRNA stability regulation, we used the mRNA decay array to explore temporal changes in mRNA amount and stability during cold treatment. Our results showed that mean whole-mRNA half-lives became longer during cold treatment without appreciable changes in the mean mRNA amount, suggesting that mRNA degradation as well as transcriptional activities are passively decreased under cold conditions.

Determination of temporal changes in mRNA amount and stability of individual transcripts allows us to perform deeper clustering analysis of transcripts based on these two parameters, which capture changes in not only mRNA degradation but also mRNA accumulation levels individually. Transcripts in Cluster 02 showed a large increase in mRNA amount; however, these transcripts were relatively destabilized (Fig. 2-5). Interestingly, GO term-based enrichment analysis revealed that the transcripts in Cluster 02 were significantly over-represented in various stress response-related functions, including the cold stress response (Fig. 2-7A). Based on the simple kinetics of mRNA turnover, assuming that the rates of mRNA synthesis and degradation are constant, regulation of mRNA stability influences both the level of mRNA and speed of transition to a new mRNA level. Accumulation levels of mRNA are determined by two parameters; the rates of mRNA synthesis and degradation, whereas time required for the transition of mRNA level to a new steady state is solely attributed to the rate of mRNA degradation (for details, see 'Kinetics of mRNA synthesis and degradation' in the Materials and Methods) (Perez-Ortin *et al*. 2007). However, rates of mRNA synthesis and degradation alter during the time course of cold treatment as shown in this study. Thus, we simulated the pattern of transient up-regulation of mRNA levels using various mRNA degradation rates (Fig. 2-12). The simulation model showed that faster mRNA turnover under the same transcription rate caused not only a decrease in the level of mRNA, but also a more rapid peak in the amount of mRNA (Fig. 2-12A). Moreover, the simulation model, in which mRNA half-lives were shortened and transcription rates were increased to compensate the decrease in the mRNA level, clearly showed that destabilization shifts the peak of mRNA accumulation to an earlier time point (Fig. 2-12B). Thus, destabilization is advantageous to achieve a rapid response to stress conditions in terms of mRNA levels, even when the rates of mRNA synthesis and degradation are variable. Therefore, transcripts in Cluster 02 are likely to maintain a high rate of mRNA turnover to achieve a rapid up-regulation in response to temperature changes.

Specific mRNA targets for stabilization or destabilization are determined by the cis-acting elements in their sequences. The well-studied example is the AU-rich element identified in the 3'-UTR of mRNAs of various transcripts encoding proto-oncogenes, transcription factors and cytokines in mammals (Chen and Shyu 1995). The AU-rich element is functional as a destabilizer in other systems including plants (Ohme-Takagi *et al*. 1993). Search for the conserved sequence among relatively stabilized transcripts in Cluster 42 detected a UAGGGUUU motif in the 5'-UTR

(Fig. 2-8). This motif was originally identified as a telobox, which is a transcription factor-binding site around transcription start sites (Bilaud *et al*. 1996, Molina and Grotewold 2005). However, this motif was also identified as an enriched motif in the 5'-UTR of translationally repressed ribosomal protein and translation factor mRNAs in response to transient dark treatment, suggesting a possible involvement in the post-transcriptional regulation (Bailey-Serres and Juntawong 2012). In contrast, no specifically conserved motif was identified from the clusters including destabilized transcripts (Fig. 2-9). Recent global analysis of RNA secondary structures provided insights into the roles of the RNA structure in the regulation of gene expression, including transcript stability (Ding *et al*. 2014, Kwok *et al*. 2015). Temperature could be one of the triggers of RNA secondary structure modification. Therefore, other than conventional cis-elements, the specificity of target mRNA might be determined by the secondary structures of mRNAs under cold conditions.

Low temperatures generally inhibit plant growth and development, which is a critical cause of limited crop productivity. An association between a decrease in the cell cycle rate and stress-induced growth retardation has been suggested in some species (Schuppler *et al*. 1998, Burssens *et al*. 2000, Granier *et al*. 2000, Rymen *et al*. 2007). In maize, exposure to low night temperatures causes specific changes in the expression of cell cycle-related genes. This alteration leads to a prolonged cell cycle duration, resulting in decreased cell proliferation (Rymen *et al*. 2007). In the present study, we used Arabidopsis T87 cells 7 d after subculturing, at which time the control cells were about to begin growing, whereas cells under cold conditions showed almost no growth for several additional days (Fig. 2-13), which is suggestive of a possible retardation in the cell cycle under cold conditions. Consistent with this hypothesis, cell cycle-related genes were over-represented among the transcripts in Cluster 40, which showed a decreased mRNA amount without appreciable changes in mRNA stability. These transcripts included core components of the cell cycle, such as several family members of A-type and B-type cyclins (Fig. 2-7B; Table 2-1). Our results indicated that down-regulation of these cell cycle-related transcripts in response to cold stress occurred not at the level of mRNA stability, but at the transcription level.

The CBF-mediated network of transcriptional regulation plays a pivotal role in cold acclimation in diverse plant species (Sanghera *et al*. 2011, Tondelli *et al*. 2011). In Arabidopsis, the upstream transcription factor, inducer of CBF expression 1 (ICE1), activates the expression of *CBF3* by directly binding to the promoter in response to cold stress. Transcriptomic analysis using the dominant *ice1* mutant revealed that approximately 40% of cold-responsive genes are under the control of the CBF regulon (Lee *et al*. 2005). The expression of CBF-responsive genes is up-regulated in response to cold stress. Thus, it is intuitive that up-regulation of mRNA in response to a stimulus is achieved either by increasing the transcription rate or by decreasing the mRNA degradation rate (or some combination); however, our results showed that plants exert a more complex interplay between mRNA synthesis and degradation. In our BL-SOM analysis, CBF-responsive genes were significantly enriched in two clusters; Cluster 02 and Cluster 12. Most of the CBF-responsive genes in Cluster 02 showed relative destabilization, whereas only one gene in Cluster 12 was relatively destabilized. Although CBF-responsive genes in both clusters were

increased in the amount of mRNA during cold treatment, greater induction of mRNA tends to be observed in CBF-responsive genes in Cluster 02 compared with those in Cluster 12 (Fig. 2-10). Moreover, a comparison between the experimental and hypothetical values of the integrated transcription rate showed that transcriptional activation was enhanced to overcome mRNA destabilization in five of the CBF-responsive genes, including direct targets of CBF3, in Cluster 02 (Fig. 2-11). This strategy is consistent with our simulation, in which increases in both mRNA synthesis and degradation act to reconcile the greater increase in mRNA amount with a rapid response (Fig. 2-12).

In conclusion, we demonstrated that a variety of stress response-related transcripts, including some of the CBF-responsive genes, were relatively up-regulated and concurrently destabilized in response to cold stress. Our mathematical approach demonstrated that greater transcriptional induction compensates for the decrease in transcript levels via destabilization. The opposing changes in transcription and mRNA degradation observed in this study are suggestive of an association between regulation of transcription and regulation of mRNA stability.

Experimental Procedures

Growth conditions of Arabidopsis T87 cell culture

Arabidopsis T87 suspension cells derived from the Columbia ecotype were grown in JPL media (Axelos *et al*. 1992) at 22℃ under constant light (80 μmol m^{-2} s^{-1}) with orbital shaking (120 r.p.m.). Cells were transferred to fresh medium every 2 weeks at an approximately 20-fold dilution. Seven days after subculturing, cells were divided into two groups. Control cells were grown under the same condition, while cells for cold treatment were transferred to 4℃ under dim light (40 μmol m^{-2} s^{-1}) and cultured for 12, 24 and 36 h.

Cordycepin treatment and verification of transcription repression

Cordycepin (3'-deoxyadenosine) is a chain-terminating adenosine analog. Cordycepin was added to control and cold-treated cells to inhibit transcription. Control cells were collected prior to (0 h) and 0.5, 2 and 4 h after cordycepin treatment. Cold-treated cells were incubated with cordycepin for 4, 8 and 12 h, because longer mRNA half-lives were expected in cold-treated cells (Chiba *et al*. 2013). In any experiments using a transcriptional inhibitor, we have to consider the possible secondary effect on some specific cellular functions at later time points. However, 24 h treatment is accepted at the longest to measure the decay rate of transcripts based on the RNA quality and cell viability after the treatment (Narsai *et al*. 2007).

The concentration of cordycepin was determined by verifying the efficiency of transcriptional repression based on the [^{3}H]uridine incorporation test, as described previously in Chiba *et al*. (2013). To achieve >95% inhibition, 200 and 400 μg ml^{-1} cordycepin was added to control and cold-treated cells, respectively (Fig. 2-2)

mRNA decay array and mRNA half-life calculation

Total RNA was extracted from cells using the RNeasy Plant Mini kit, and three biological replicate RNA samples for each time point were pooled for microarray analysis. Biotin-labeled cRNA was prepared from equal amounts of total RNA using the GeneChip 3' IVT Express kit and hybridized to Affymetrix GeneChip Arabidopsis ATH1 genomic arrays (Affymetrix). Data processing was conducted as described previously in Chiba *et al*. (2013). After removing absent calls (*P*-value>0.06 for the 0 h data point), ambiguous calls, possible cross-hybridizations and probes derived from organelle genomes, a total of 12,669 transcripts were used for subsequent analyses.

The decay rate (λ) and its SE (SEλ) for each transcript were estimated by non-linear regression using the least-squares method (n = 9-12) as described previously in Chiba *et al*. (2013). The decay rate of individual transcripts in control cells was estimated after omitting the 0.5 h time point if a smaller SEλ was obtained. The mRNA half-life (τ) was then calculated by the equation $\tau = \ln(2)/\lambda$. The level of mRNA (*A*) of each transcript was obtained based on the value prior to cordycepin treatment. To evaluate the quality of data fitting to the exponential model, the residual

SD for fitting (SDr) was calculated. Microarray data with either $SDr/A_0 \geq 0.2$, $SE\lambda/\lambda \geq 1$ or $\lambda \leq 0$ were eliminated from further analyses, resulting in a final microarray data set of 4,838 transcripts.

The value expected from the general shift of mRNA amount (A_{EGS}) and that of mRNA half-life (τ_{EGS}) for each transcript were calculated based on the ratios of mean whole-mRNA amounts and half-lives before cold treatment to after, respectively.

Detection of total mRNA levels

Total mRNA was measured by dot-blot hybridization with an oligo(dT) probe, as described previously (Harley 1987), with minor modifications. Briefly, 1 μg of total RNA denatured at 65℃ for 15 min in 66% deionized formamide, 7.8% formaldehyde, 26 mM MOPS (pH 7.0), 2.6 mM sodium acetate and 1.3 mM EDTA (pH 8.0) was spotted on a nylon membrane filter (Hybond-N+, GE Healthcare) and UV-cross-linked at 1.2 kJ m^{-2}. $Oligo(dT)_{15}$ (Promega) and oligo DNA complementary to 18S rRNA (5'-ACCTCTGACTATGAAATACGA ATGC-3') were 5' end-labeled by T4 polynucleotide kinase (New England Biolabs) with [γ-^{32}P]ATP (Hungarian Academy of Science). Filters were hybridized at 40℃ overnight with the labeled $oligo(dT)_{15}$ and 18S rRNA probes in the PerfectHyb (Toyobo) and then washed twice in 2×SSC and 0.1% SDS at room temperature for 5 min. Hybridization signals were detected using BAS1800 and quantified using MultiGauge software (Fuji Photo Film). To determine the total amount of mRNA, the hybridization signals using the $oligo(dT)_{15}$ probe were normalized to those using the 18S rRNA probe.

Clustering procedures and classification analysis

mRNA levels and half-lives were normalized to the respective values in control cells. The normalized values were $\log_2$-transformed and standardized for BL-SOM analysis. The Simple BL-SOM method developed by Kanaya *et al*. (2001) was used for clustering. The number of lattice points of the SOM in the first axis was set to five, after which all analyzed transcripts were mapped and classified into 15 clusters.

Enrichment analysis based on GO terms for each cluster was performed using Fisher's exact test in the topGO package (v. 2.20.0) (Alexa *et al*. 2006). The 'weight01' algorithm was used to eliminate hierarchical dependency of the GO terms. Annotated GO terms for each transcript were retrieved from TAIR version 10 (Berardini *et al*. 2015) using org.At.tair.db (v. 3.1.2) in Bioconductor (Huber *et al*. 2015).

Discovery of the motifs within the cluster by MEME

To discover the sequence motif(s) within each cluster, we used MEME version 4.10.2 (Bailey *et al*. 2015). The 5'- and 3'-UTR sequences were downloaded from the Arabidopsis Information Resource release 10 (Berardini *et al*. 2015), and were used for the generation of background files. The parameters of MEME were specified as minimum width = 6, maximum

width = 10 and the maximum number of motifs = 10. The DUST option with the default parameter was applied for masking the low-complexity regions. ZOOPS model was assumed for the analysis.

qRT-PCR analysis

Total RNA was converted to cDNA, followed by DNase I treatment using SuperScript II according to the manufacturer's protocol (Invitrogen). qRT–PCR was performed using SYBR premix ExTaq (TAKARA) under the conditions specified in the Mx3005P instrument protocol (Stratagene). The primers used in this study are listed in Table 2-3.

Kinetics of mRNA synthesis and degradation

The simple kinetics of mRNA turnover assumes zero-order mRNA production and first-order mRNA degradation, as shown in Equation 1. When the transcription rate (k) and mRNA decay rate (λ) are constant, the amount of mRNA (A) follows Equation 2, in which A_0 represents the initial level of mRNA:

$$\frac{dA}{dt} = k - \lambda A \quad \ldots\ldots \text{Eq. 1}$$

$$A(t) = \left(\frac{k}{\lambda} - A_0\right)\left(1 - e^{-\lambda t}\right) \quad \ldots\ldots \text{Eq. 2}$$

Thus, the new mRNA steady-state level is determined by both the transcription rate (k) and decay rate (λ), whereas the response time is determined solely based on the decay rate (λ) (Perez-Ortin *et al*. 2007). To understand the kinetics of mRNA synthesis and degradation, when the transcription rate (k) and decay rate (λ) alter over time, we estimated the integrated transcription rate (K) from the experimentally determined mRNA amount (A) and mRNA decay rate (λ) following Equation 3:

$$K(T) = A(T) - A_0 + \int_0^T \lambda(t)A(t)\,dt \quad \ldots\ldots \text{Eq. 3}$$

References

Alexa, A., Rahnenführer, J. and Lengauer, T. (2006) Improved scoring of functional groups from gene expression data by decorrelating GO graph structure. *Bioinformatics* **22**: 1600–1607.

Ambawat, S., Sharma, P., Yadav, N.R. and Yadav, R.C. (2013) MYB transcription factor genes as regulators for plant responses: an overview. *Physiol. Mol. Biol. Plants* **19**: 307–321.

Artus, N.N., Uemura, M., Steponkus, P.L., Gilmour, S.J., Lin, C. and Thomashow, M.F. (1996) Constitutive expression of the cold-regulated *Arabidopsis thaliana COR15a* gene affects both chloroplast and protoplast freezing tolerance. *Proc. Natl. Acad. Sci. USA* **93**: 13404–13409.

Axelos, M., Curic, C., Mazzolini, L., Bardet, C. and Lescure, B. (1992) A protocol for transient gene expression in Arabidopsis thaliana protoplasts isolated from cell suspension cultures. *Plant Physiol. Biochem.* **30**: 123–128.

Bailey-Serres, J. and Juntawong, P. (2012) Dynamic light regulation of translation status in *Arabidopsis thaliana*. *Front. Plant Sci.* **3**: 66.

Bailey, T.L., Boden, M., Buske, F.A., Frith, M., Grant, C.E., Clementi, L., Ren, J., Li, W.W. and Noble, W.S. (2009) MEME SUITE: tools for motif discovery and searching. *Nucleic Acids Res.* **37**: W202–W208.

Bailey, T.L., Johnson, J., Grant, C.E. and Noble, W.S. (2015) The MEME suite. *Nucleic Acids Res.* **43**: W39–W49.

Barah, P., Jayavelu, N.D., Rasmussen, S., Nielsen, H.B., Mundy, J. and Bones, A.M. (2013) Genome-scale cold stress response regulatory networks in ten Arabidopsis thaliana ecotypes. *BMC Genomics* **14**: 1–16.

Benjamini, Y. and Hochberg, Y. (1995) Controlling the false discovery rate: a practical and powerful approach to multiple testing. *J. R. Stat Soc. B: Stat. Methodol.* **57**: 289–300.

Berardini, T.Z., Mundodi, S., Reiser, L., Huala, E., Garcia-Hernandez, M., Zhang, P., Mueller, L.A., Yoon, J., Doyle, A., Lander, G., Moseyko, N., Yoo, D., Xu, I., Zoeckler, B., Montoya, M., Miller, N., Weems, D. and Rhee, S.Y. (2004) Functional annotation of the Arabidopsis genome using controlled vocabularies. *Plant Physiol.* **135**: 745–755.

Berardini, T.Z., Reiser, L., Li, D., Mezheritsky, Y., Muller, R., Strait, E. and Huala, E. (2015) The Arabidopsis information resource: making and mining the ‘gold standard’ annotated reference plant genome. *Genesis* **53**: 474–485.

Bilaud, T., Koering, C.E., Binet-Brasselet, E., Ancelin, K., Pollice, A., Gasser, S.M. and Gilson, E. (1996) The telobox, a Myb-related telomeric DNA binding motif found in proteins from yeast, plants and human. *Nucleic Acids Res.* **24**: 1294–1303.

Burssens, S., Himanen, K., van de Cotte, B., Beeckman, T., Van Montagu, M., Inzé, D. and Verbruggen, N. (2000) Expression of cell cycle regulatory genes and morphological alterations in response to salt stress in Arabidopsis thaliana. *Planta* **211**: 632–640.

Chen, C.-Y.A. and Shyu, A.B. (1995) AU-rich elements: characterization and importance in mRNA degradation. *Trends Biochem. Sci.* **20**: 465–470.

Chiba, Y., Mineta, K., Hirai, M.Y., Suzuki, Y., Kanaya, S., Takahashi, H., Onouchi, H., Yamaguchi, J. and Naito, S. (2013) Changes in mRNA stability associated with cold stress in Arabidopsis cells. *Plant Cell Physiol.* **54**: 180–194.

Ding, Y., Tang, Y., Kwok, C.K., Zhang, Y., Bevilacqua, P.C. and Assmann, S.M. (2014) In vivo genome-wide profiling of RNA secondary structure reveals novel regulatory features. *Nature* **505**: 696–700.

Edgar, R., Domrachev, M. and Lash, A.E. (2002) Gene Expression Omnibus: NCBI gene expression and hybridization array data repository. *Nucleic Acids Res.* **30**: 207–210.

Fowler, S. and Thomashow, M.F. (2002) Arabidopsis transcriptome profiling indicates that multiple regulatory pathways are activated during cold acclimation in addition to the CBF cold response pathway. *Plant Cell* **14**: 1675–1690.

Granier, C., Inzé, D. and Tardieu, F. (2000) Spatial distribution of cell division rate can be deduced from that of $p34^{cdc2}$ kinase activity in maize leaves grown at contrasting temperatures and soil water conditions. *Plant Physiol.* **124**: 1393–1402.

Harley, C.B. (1987) Hybridization of oligo(dT) to RNA on nitrocellulose. *Gene Anal. Tech.* **4**: 17–22.

Hsieh, T.H., Lee, J.T., Yang, P.T., Chiu, L.H., Charng, Y.Y., Wang, Y.C. and Chan, M.T. (2002) Heterology expression of the Arabidopsis *C-repeat/dehydration response element binding factor 1* gene confers elevated tolerance to chilling and oxidative stresses in transgenic tomato. *Plant Physiol.* **129**: 1086–1094.

Huber, W., Carey, V.J., Gentleman, R., Anders, S., Carlson, M., Carvalho, B.S., Bravo, H.C., Davis, S., Gatto, L., Gottardo, R., Hahne, F., Hansen, K.D., Irizarry, R.A., Lawrence, M., Love, M.I., MacDonald, J., Obenchain, V., Oleś, A.K., Pagès, H., Reyes, A., Shannon, P., Smyth, G.K., Tenenbaum, D., Waldron, L. and Morgan, M. (2015) Orchestrating high-throughput genomic analysis with Bioconductor. *Nat. Methods* **12**: 115–121.

Ito, Y., Katsura, K., Maruyama, K., Taji, T., Kobayashi, M., Seki, M., Shinozaki, K. and Yamaguchi-Shinozaki, K. (2006) Functional analysis of rice DREB1/CBF-type

transcription factors involved in cold-responsive gene expression in transgenic rice. *Plant Cell Physiol.* **47**: 141–153.

Jaglo-Ottosen, K.R., Gilmour, S.J., Zarka, D.G., Schabenberger, O. and Thomashow, M.F. (1998) Arabidopsis *CBF1* overexpression induces *COR* genes and enhances freezing tolerance. *Science* **280**: 104–106.

Kanaya, S., Kinouchi, M., Abe, T., Kudo, Y., Yamada, Y., Nishi, T., Mori, H. and Ikemura, T. (2001) Analysis of codon usage diversity of bacterial genes with a self-organizing map (SOM): characterization of horizontally transferred genes with emphasis on the *E. coli* O157 genome. *Gene* **276**: 89–99.

Kendziorski, C., Irizarry, R.A., Chen, K.-S., Haag, J.D. and Gould, M.N. (2005) On the utility of pooling biological samples in microarray experiments. *Proc. Natl. Acad. Sci. USA* **102**: 4252–4257.

Kilian, J., Whitehead, D., Horak, J., Wanke, D., Weinl, S., Batistic, O., D'Angelo, C., Bornberg-Bauer, E., Kudla, J. and Harter, K. (2007) The AtGenExpress global stress expression data set: protocols, evaluation and model data analysis of UV-B light, drought and cold stress responses. *Plant J.* **50**: 347–363.

Kolukisaoglu, Ü ., Weinl, S., Blazevic, D., Batistic, O. and Kudla, J. (2004) Calcium sensors and their interacting protein kinases: genomics of the Arabidopsis and rice CBL–CIPK signaling networks. *Plant Physiol.* **134**: 43–58.

Kwok, C.K., Tang, Y., Assmann, S.M. and Bevilacqua, P.C. (2015) The RNA structurome: transcriptome-wide structure probing with next-generation sequencing. *Trends Biochem. Sci.* **40**: 221–232.

Lee, B.H., Henderson, D.A. and Zhu, J.K. (2005) The Arabidopsis cold-responsive transcriptome and its regulation by ICE1. *Plant Cell* **17**: 3155– 3175.

Manik, S.M.N., Shi, S., Mao, J., Dong, L., Su, Y., Wang, Q. and Haobao, L. (2015) The calcium sensor CBL–CIPK is involved in plant's response to abiotic stresses. *Int. J. Genomics* **2015**: 493191.

Maruyama, K., Sakuma, Y., Kasuga, M., Ito, Y., Seki, M., Goda, H., Shimada, Y., Yoshida, S., Shinozaki, K. and Yamaguchi-Shinozaki, K. (2004) Identification of cold-inducible downstream genes of the Arabidopsis DREB1A/CBF3 transcriptional factor using two microarray systems. *Plant J.* **38**: 982–993.

Melvin, W.T., Milne, H.B., Slater, A.A., Allen, H.J. and Keir, H.M. (1978) Incorporation of 6-thioguanosine and 4-thiouridine into RNA. *Eur. J. Biochem.* **92**: 373–379.

Miller, C., Schwalb, B., Maier, K., Schulz, D., Dümcke, S., Zacher, B., Mayer, A., Sydow, J., Marcinowski, L., Dölkn, L., Martin, D.E., Tresch, A. and Cramer, P. (2011) Dynamic transcriptome analysis measures rates of mRNA synthesis and decay in yeast. *Mol. Syst. Biol.* **7**: 458.

Molina, C. and Grotewold, E. (2005) Genome wide analysis of Arabidopsis core promoters. *BMC Genomics* **6**: 25–25.

Narsai, R., Howell, K.A., Millar, A.H., O'Toole, N., Small, I. and Whelan, J. (2007) Genome-wide analysis of mRNA decay rates and their determinants in *Arabidopsis thaliana*. *Plant Cell* **19**: 3418–3436.

Newman, T.C., Ohme-Takagi, M., Taylor, C.B. and Green, P.J. (1993) DST sequences, highly conserved among plant SAUR genes, target reporter transcripts for rapid decay in tobacco. *Plant Cell* **5**: 701–714.

Ohme-Takagi, M., Taylor, C.B., Newman, T.C. and Green, P.J. (1993) The effect of sequences with high AU content on mRNA stability in tobacco. *Proc. Natl. Acad. Sci. USA* **90**: 11811–11815.

Oono, Y., Seki, M., Satou, M., Iida, K., Akiyama, K., Sakurai, T., Fujita, M., Yamaguchi-Shinozaki, K. and Shinozaki, K. (2006) Monitoring expression profiles of Arabidopsis genes during cold acclimation and deacclimation using DNA microarrays. *Funct. Integr. Genomics* **6**: 212–234.

Park, S., Lee, C.-M., Doherty, C.J., Gilmour, S.J., Kim, Y. and Thomashow, M.F. (2015) Regulation of the Arabidopsis CBF regulon by a complex low-temperature regulatory network. *Plant J.* **82**: 193–207.

Perez-Ortin, J.E., Alepuz, P.M. and Moreno, J. (2007) Genomics and gene transcription kinetics in yeast. *Trends Genet.* **23**: 250–257.

Rabani, M., Levin, J.Z., Fan, L., Adiconis, X., Raychowdhury, R., Garber, M., Gnirke, A., Nusbaum, C., Hacohen, N., Friedman, N., Amit, I. and Regev, A. (2011) Metabolic labeling of RNA uncovers principles of RNA production and degradation dynamics in mammalian cells. *Nat. Biotechnol.* **29**: 436–442.

Rymen, B., Fiorani, F., Kartal, F., Vandepoele, K., Inzé, D. and Beemster, G.T. (2007) Cold nights impair leaf growth and cell cycle progression in maize through transcriptional changes of cell cycle genes. *Plant Physiol.* **143**: 1429–1438.

Sanghera, G.S., Wani, S.H., Hussain, W. and Singh, N.B. (2011) Engineering cold stress tolerance in crop plants. *Curr. Genomics* **12**: 30–43.

Schuppler, U., He, P.H., John, P.C. and Munns, R. (1998) Effect of water stress on cell division and cell-division-cycle 2-like cell-cycle kinase activity in wheat leaves. *Plant Physiol.* **117**: 667–678.

Schwanhausser, B., Busse, D., Li, N., Dittmar, G., Schuchhardt, J., Wolf, J., Chen, W. and Selbach, M. (2011) Global quantification of mammalian gene expression control. *Nature* **473**: 337–342.

Steponkus, P.L., Uemura, M., Joseph, R.A., Gilmour, S.J. and Thomashow, M.F. (1998) Mode of action of the *COR15a* gene on the freezing tolerance of *Arabidopsis thaliana*. *Proc. Natl. Acad. Sci. USA* **95**: 14570– 14575.

Thalhammer, A., Bryant, G., Sulpice, R. and Hincha, D.K. (2014) Disordered cold regulated15 proteins protect chloroplast membranes during freezing through binding and folding, but do not stabilize chloroplast enzymes in vivo. *Plant Physiol.* **166**: 190–201.

Thomashow, M.F. (2010) Molecular basis of plant cold acclimation: insights gained from studying the CBF cold response pathway. *Plant Physiol.* **154**: 571–577.

Tondelli, A., Francia, E., Barabaschi, D., Pasquariello, M. and Pecchioni, N. (2011) Inside the *CBF* locus in *Poaceae*. *Plant Sci.* **180**: 39–45.

Uemura, M., Tominaga, Y., Nakagawara, C., Shigematsu, S., Minami, A. and Kawamura, Y. (2006) Responses of the plasma membrane to low temperatures. *Physiol. Plant.* **126**: 81–89.

Vogel, J.T., Zarka, D.G., Van Buskirk, H.A., Fowler, S.G. and Thomashow, M.F. (2005) Roles of the CBF2 and ZAT12 transcription factors in configuring the low temperature transcriptome of Arabidopsis. *Plant J.* **41**: 195–211.

Yamaguchi-Shinozaki, K. and Shinozaki, K. (2006) Transcriptional regulatory networks in cellular responses and tolerance to dehydration and cold stresses. *Annu. Rev. Plant. Biol.* **57**: 781–803.

Zhang, J., Mao, Z. and Chong, K. (2013) A global profiling of uncapped mRNAs under cold stress reveals specific decay patterns and endonucleolytic cleavages in *Brachypodium distachyon*. *Genome Biol.* **14**: R92.

Zhao, C., Lang, Z. and Zhu, J.-K. (2015) Cold responsive gene transcription becomes more complex. *Trends Plant Sci.* **20**: 466–468.

Zhu, J., Dong, C.H. and Zhu, J.K. (2007) Interplay between cold-responsive gene regulation, metabolism and RNA processing during plant cold acclimation. *Curr. Opin. Plant Biol.* **10**: 290–295.

Figures and legends

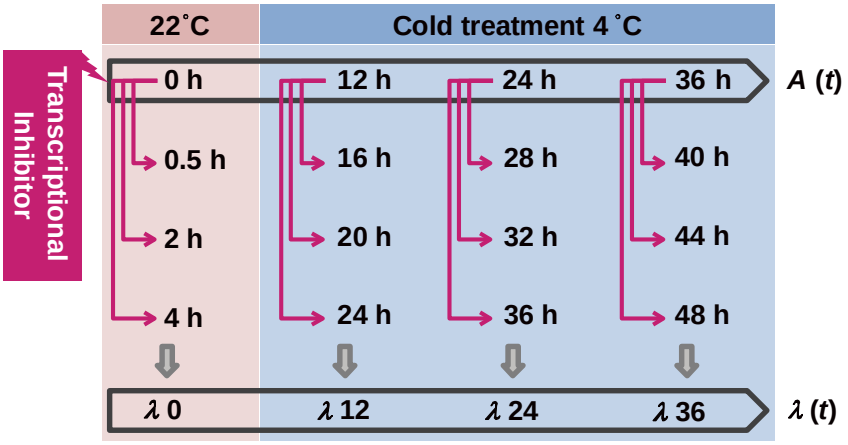

Figure 2-1. Schematic representation of mRNA decay array.

Control cells were cultured for 7 d at 22°C. For cold treatment, the cells were exposed to 4°C for 12, 24 and 36 h. For mRNA half-life measurements, the transcriptional inhibitor, cordycepin, was applied to the cell cultures and total RNA was isolated at several time points as indicated for microarray analysis. mRNA half-lives were calculated from the changes in mRNA levels following transcription arrest. mRNA amounts were determined by the value just before the addition of cordycepin.

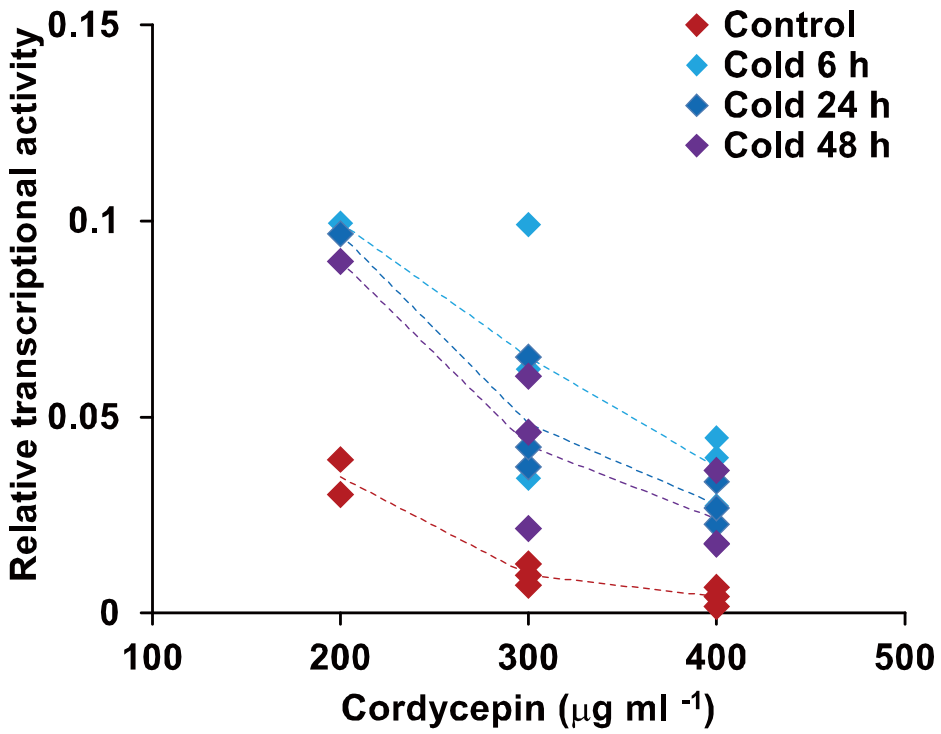

Figure 2-2. Inhibition of transcription by cordycepin in T87 cells.

Cells were treated with cordycepin at the indicated concentrations before (red diamond) or after cold treatment (diamonds in light blue: 6 h, dark blue: 24 h, purple: 48 h). Transcriptional activity was measured by [^{3}H]uridine incorporation, and the values relative to that without cordycepin addition are indicated. Each single mark indicates individual experiment. Averages are shown by dashed lines.

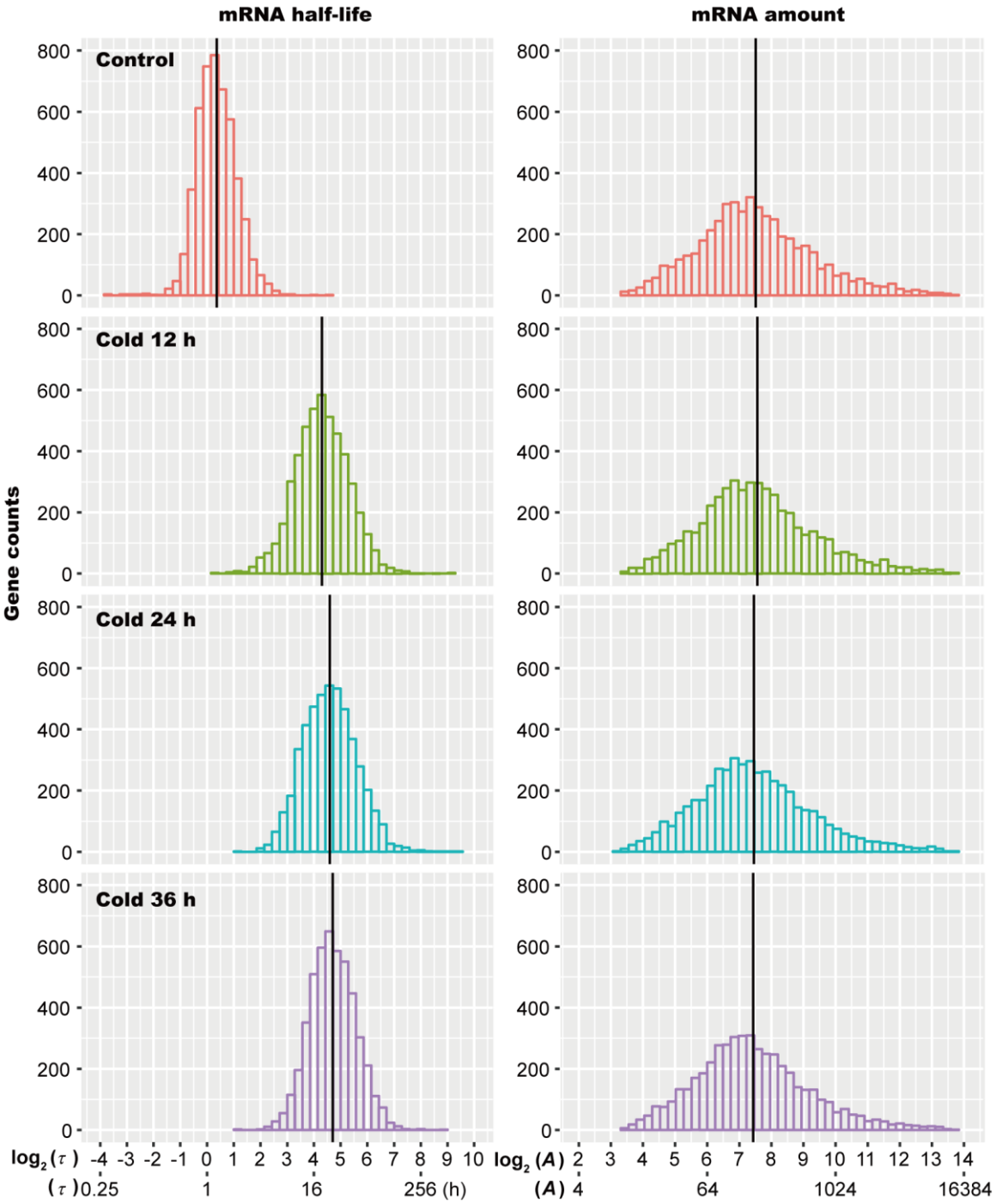

Figure 2-3. Changes in mRNA half-lives and mRNA amounts during cold treatment. Histogram of $\log_2$-converted mRNA half-lives (τ) and mRNA amounts (*A*) are shown. The gene counts of each value before (red) and after (green, 12 h; blue: 24 h; and purple, 36 h) cold treatment are presented. Vertical lines indicate the mean values.

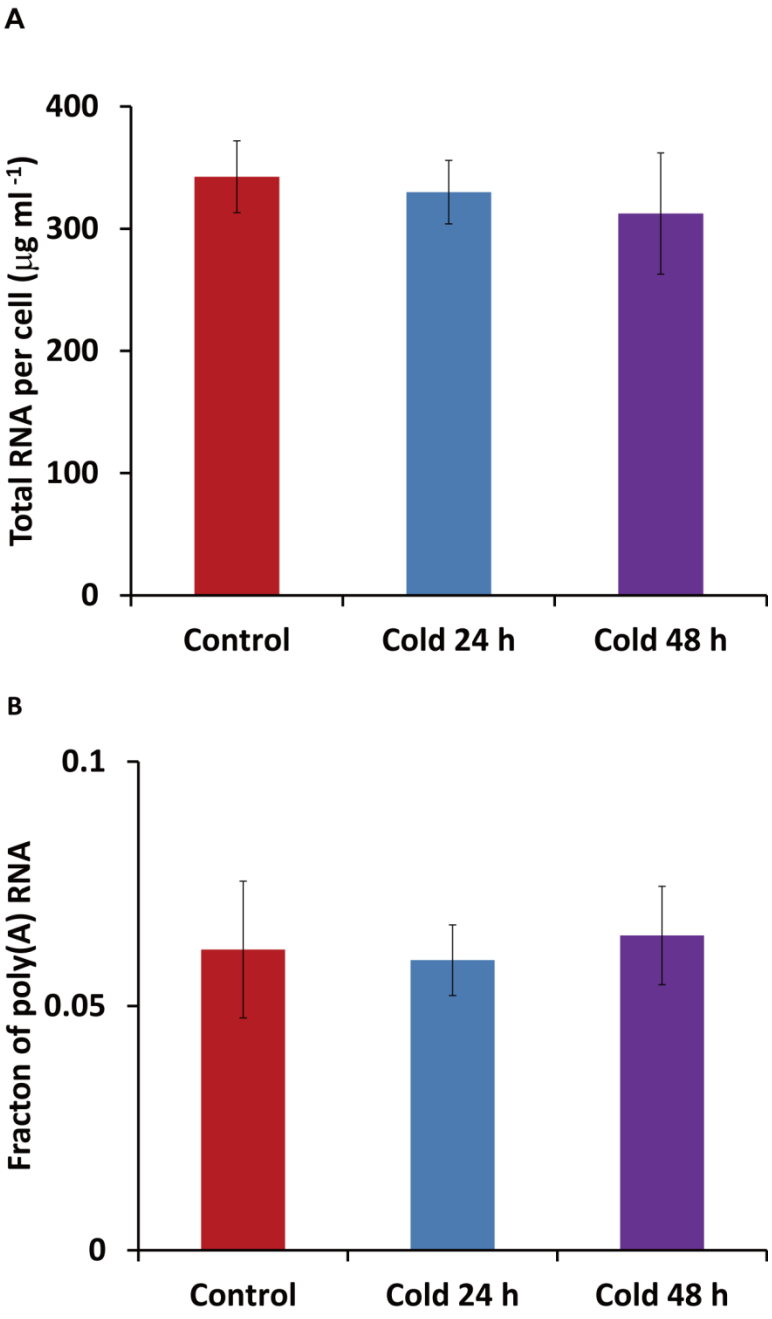

Figure 2-4. Total RNA and poly(A) RNA amounts in Arabidopsis T87 cells under the cold condition.

(A) Amount of total RNA extracted from cells before and after cold treatment and (B) fraction of the poly(A) RNA were measured. Averages ± SD of at least three biological replicates are shown.

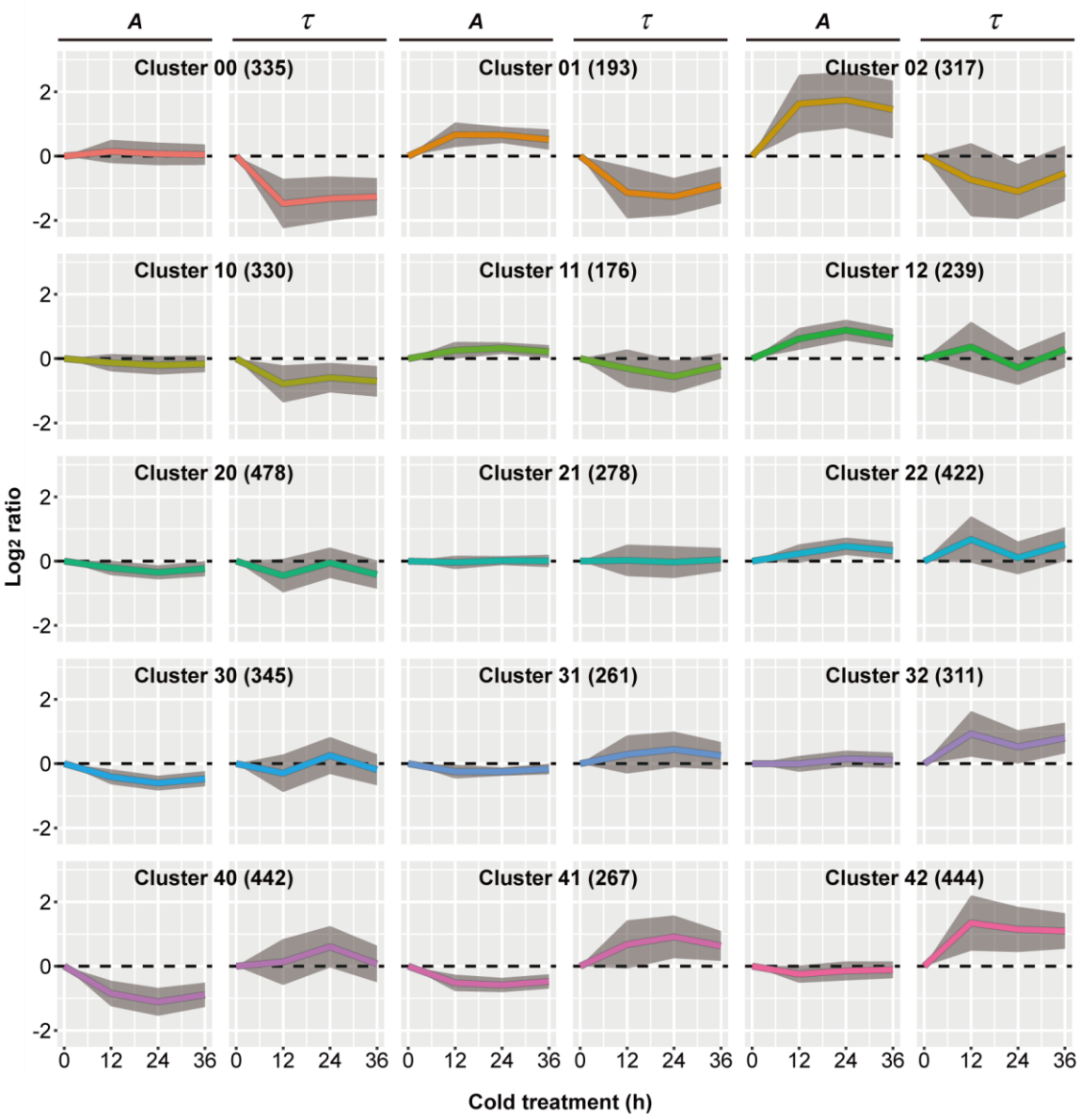

Figure 2-5. Clustering of mRNA decay array data by Simple BL-SOM.

Time course profiles for mRNA amount (*A*) and mRNA half-life (τ) of a total of 4,838 genes were considered for clustering. The number of genes in each cluster is indicated in parentheses. Log_2 ratios of mRNA amount to the value expected from the general shift {*A*: $\log_2[A(t)/A_{EGS}]$} and those of mRNA half-life {τ: $\log_2[\tau(t)/\tau_{EGS}]$} of average transcripts in each cluster with SD are shown by colored lines and gray shadow, respectively.

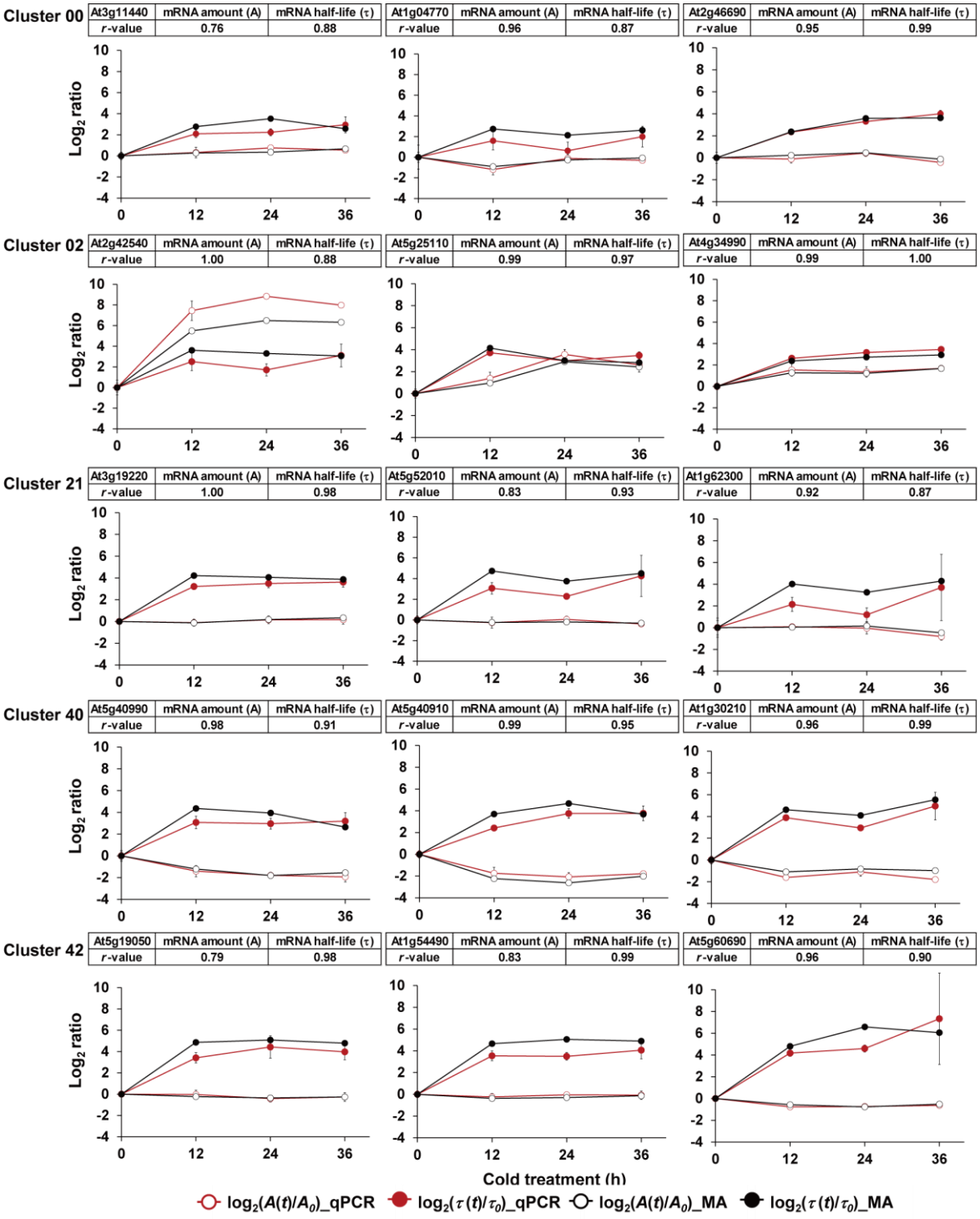
Cluster 00
At3g11440 | mRNA amount (A) | mRNA half-life (τ)
r-value | 0.76 | 0.88
At1g04770 | mRNA amount (A) | mRNA half-life (τ)
r-value | 0.96 | 0.87
At2g46690 | mRNA amount (A) | mRNA half-life (τ)
r-value | 0.95 | 0.99
Cluster 02
At2g42540 | mRNA amount (A) | mRNA half-life (τ)
r-value | 1.00 | 0.88
At5g25110 | mRNA amount (A) | mRNA half-life (τ)
r-value | 0.99 | 0.97
At4g34990 | mRNA amount (A) | mRNA half-life (τ)
r-value | 0.99 | 1.00
Cluster 21
At3g19220 | mRNA amount (A) | mRNA half-life (τ)
r-value | 1.00 | 0.98
At5g52010 | mRNA amount (A) | mRNA half-life (τ)
r-value | 0.83 | 0.93
At1g62300 | mRNA amount (A) | mRNA half-life (τ)
r-value | 0.92 | 0.87
Cluster 40
At5g40990 | mRNA amount (A) | mRNA half-life (τ)
r-value | 0.98 | 0.91
At5g40910 | mRNA amount (A) | mRNA half-life (τ)
r-value | 0.99 | 0.95
At1g30210 | mRNA amount (A) | mRNA half-life (τ)
r-value | 0.96 | 0.99
Cluster 42
At5g19050 | mRNA amount (A) | mRNA half-life (τ)
r-value | 0.79 | 0.98
At1g54490 | mRNA amount (A) | mRNA half-life (τ)
r-value | 0.83 | 0.99
At5g60690 | mRNA amount (A) | mRNA half-life (τ)
r-value | 0.96 | 0.90
Log2 ratio
Cold treatment (h)
log2(A(t)/A0)_qPCR
log2(τ(t)/τ0)_qPCR
log2(A(t)/A0)_MA
log2(τ(t)/τ0)_MA

Figure 2-6. Verification of mRNA decay array by qRT-PCR.

Three each of transcripts were randomly selected from the clusters indicated in the left, and $\log_2$ ratios of mRNA amount after cold treatment to before ($\log_2(A(t)/A_0)$) and those of mRNA half-life ($\log_2(\tau(t)/\tau_0)$) were determined by mRNA decay array (MA) and qRT-PCR (qPCR). Changes in the mRNA amount from the array data are shown by black open circle and those from qRT-PCR data by red open circle. Changes in the mRNA half-life from the array data are shown by black filled circle and those from qRT-PCR data by red filled circle. Results from three biological replications are shown in the qRT-PCR data. Averages ± SD are shown for mRNA amount. Error bars for mRNA half-lives represent SE of τ obtained from SEλ. Error bars are not visible in some time points due to the smaller size of bar than the graph symbols

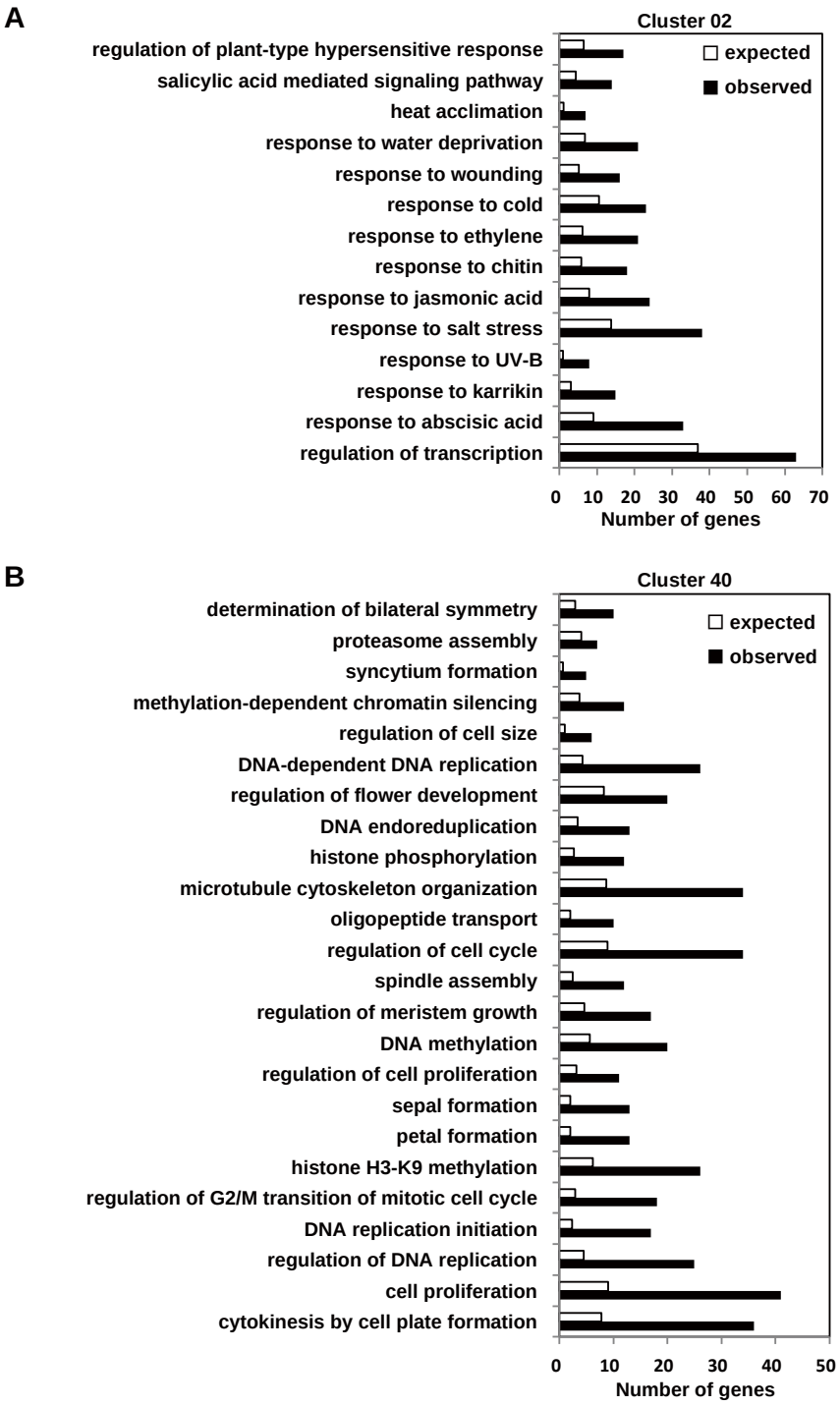

Figure 2-7. Gene ontology analysis of transcripts in Cluster 02 and Cluster 40.

(A) Transcripts in Cluster 02 and (B) those in Cluster 40 were classified according to GO terms. Significantly over-represented GO terms by two-sided Fisher's exact test with Benjamini and Hochberg correction (Benjamini and Hochberg 1995)(q-value< 0.05) are shown. The expected number of genes in each category from the distribution of all analyzed transcripts is represented by open bars, and the observed number of genes is represented by filled bars.

A

B

Gene ID	Strand	Representative gene symbol and annotation
AT4G35020.2	+	*RAC3*, RAC-like 3
AT3G54350.2	+	*emb1967*, Forkhead-associated (FHA) domain-containing protein
AT4G24560.1	+	*UBP16*, ubiquitin-specific protease 16
AT3G05090.1	+	*LRS1*, Transducin/WD40 repeat-like superfamily protein
AT3G08850.1	+	*RAPTOR1B*, HEAT repeat ;WD domain, G-beta repeat protein protein
AT4G35950.1	+	*ARAC6*, RAC-like 6
AT5G12310.1	+	RING/U-box superfamily protein
AT3G12140.2	+	Emsy N Terminus (ENT)/ plant Tudor-like domains-containing protein
AT3G56580.1	+	RING/U-box superfamily protein
AT5G23150.1	+	*HUA2*, Tudor/PWWP/MBT domain-containing protein
AT2G30470.1	+	*HSI2*, high-level expression of sugar-inducible gene 2
AT1G50200.2	+	*ALATS*, Alanyl-tRNA synthetase
AT1G58220.1	+	Homeodomain-like superfamily protein
AT4G31590.1	+	*ATCSLC05*, Cellulose-synthase-like C5
AT1G30690.2	+	Sec14p-like phosphatidylinositol transfer family protein
AT2G40930.1	+	*UBP5*, ubiquitin-specific protease 5
AT3G19860.1	+	*bHLH121*, basic helix-loop-helix (bHLH) DNA-binding superfamily protein
AT5G24760.3	+	GroES-like zinc-binding dehydrogenase family protein
AT5G44560.2	+	*VPS2.2*, SNF7 family protein
AT1G04550.1	+	*IAA12*, AUX/IAA transcriptional regulator family protein
AT2G02090.1	+	*CHR19*, SNF2 domain-containing protein / helicase domain-containing protein
AT3G16310.1	+	mitotic phosphoprotein N' end (MPPN) family protein
AT5G18580.1	+	*FASS*, tonneau 2 (TON2)
AT2G41710.1	+	Integrase-type DNA-binding superfamily protein
AT3G59640.2	+	glycine-rich protein
AT3G02890.1	+	RING/FYVE/PHD zinc finger superfamily protein
AT1G12910.1	+	*ATAN11*, Transducin/WD40 repeat-like superfamily protein
AT2G26470.1	+	unknown protein
AT3G10310.1	+	P-loop nucleoside triphosphate hydrolases superfamily protein with CH (Calponin Homology) domair
AT5G23340.1	+	RNI-like superfamily protein
AT4G15880.1	+	*ESD4*, Cysteine proteinases superfamily protein
AT5G15920.1	+	*SMC5*, structural maintenance of chromosomes 5
AT2G06510.1	+	*ATRPA1A*, replication protein A 1A
AT5G51870.3	+	*AGL71*, AGAMOUS-like 71
AT5G37890.1	+	Protein with RING/U-box and TRAF-like domains

Figure 2-8. Nucleotide sequence motif in transcripts of Cluster 42.

(A) Sequence logo of the eight-nucleotide motif identified in the 5'-UTRs of Cluster 42 transcripts using MEME (*E*-value = 3.9E-06). (B) Gene ID, the strand in which the motif was identified, and representative gene symbol and annotation of the 34 genes that contains the motif.

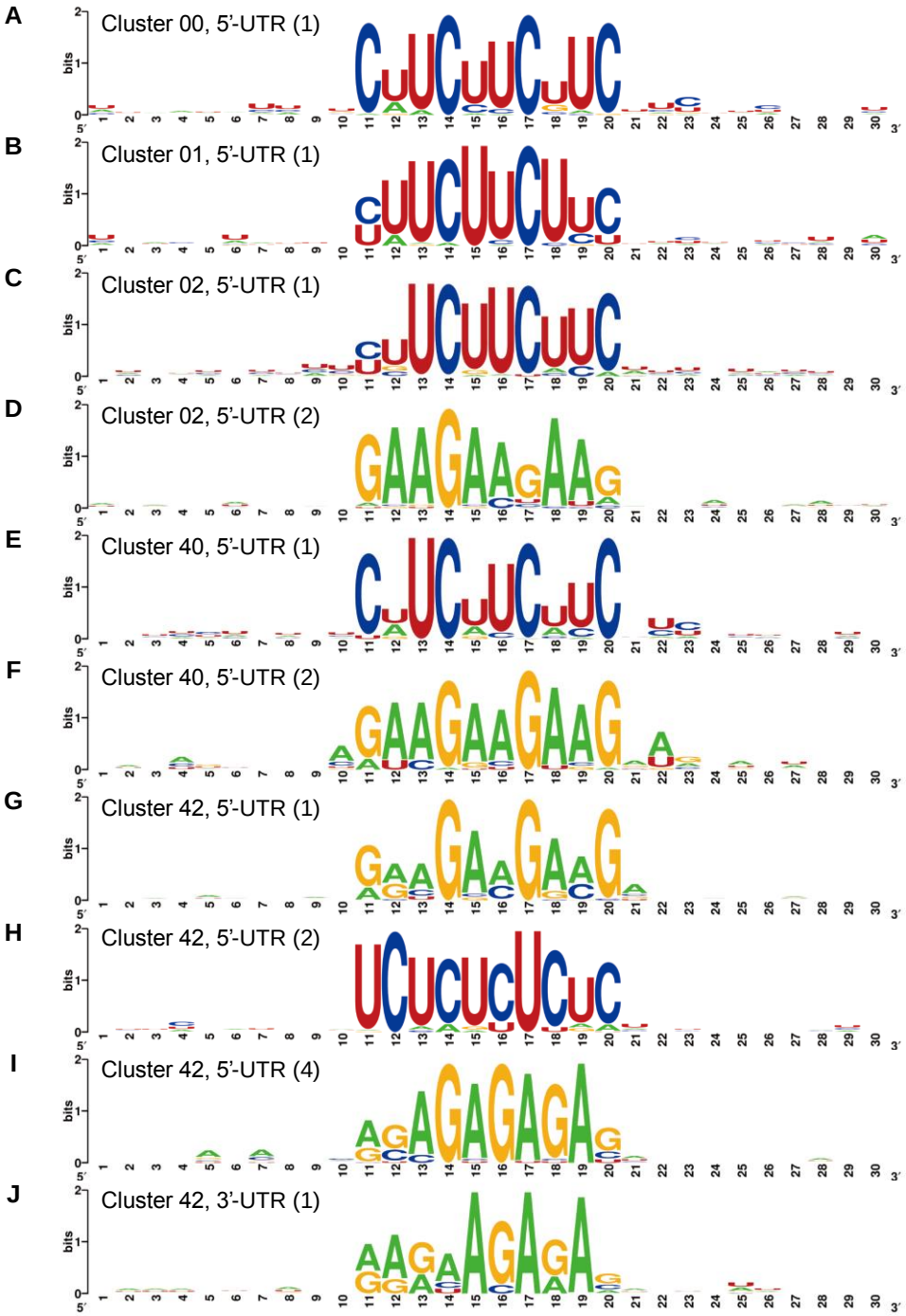

Figure 2-9. Nucleotide sequence motifs identified by MEME in the 5'- and 3'-UTRs. Sequence logo of the motifs identified by MEME in the 5'-UTRs of Clusters 00 (A), 01 (B), 02 (C, D), 40 (E, F), 42 (G–I), and that in the 3'-UTRs of Cluster 42 (J) are shown along with 10 nucleotide flanking regions. Sequence logo of one of the motifs found in the 5'-UTR of Cluster 42 (3) is presented in Fig. 2-8.

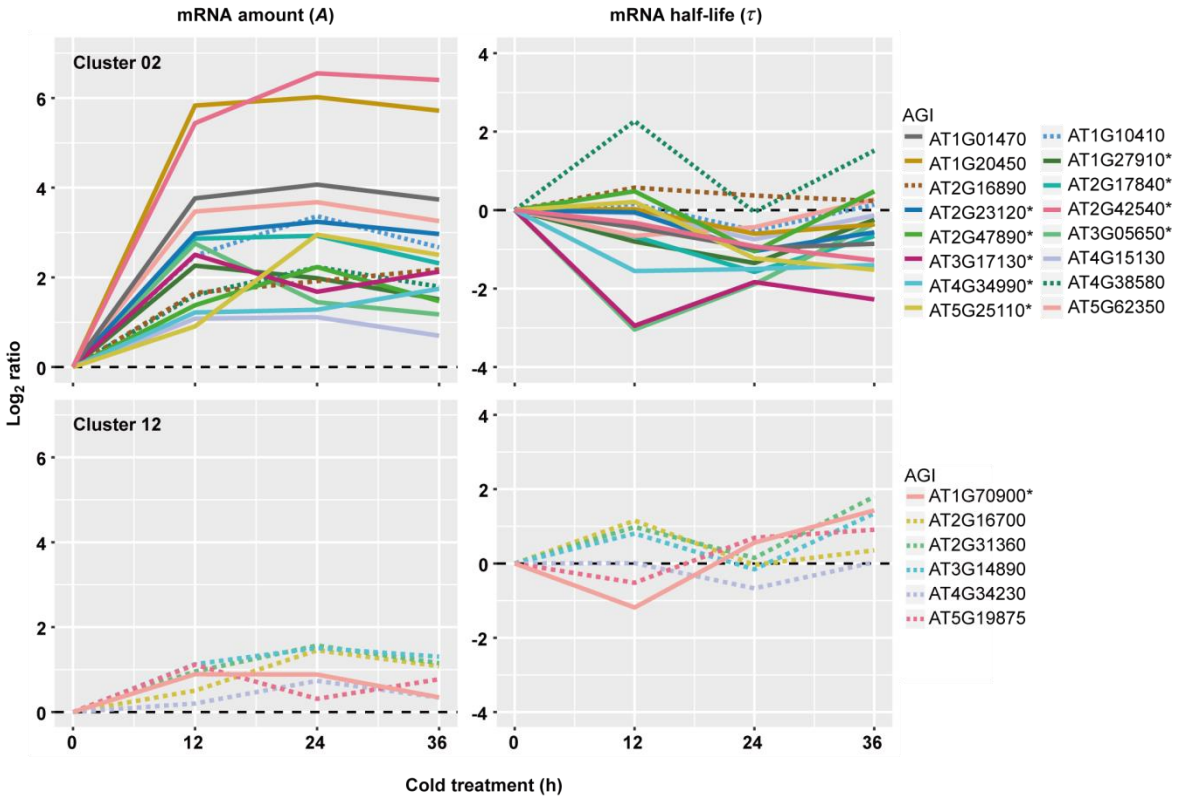

Figure 2-10. Changes in mRNA half-lives and mRNA amounts on CBF-responsive genes.

Log_2 ratios of mRNA amount to the value expected from the general shift {*A*: $\log_2[A(t)/A_{EGS}]$} and those of mRNA half-life {τ: $\log_2[\tau(t)/\tau_{EGS}]$} of CBF-responsive genes in each cluster are shown by colored lines individually with Arabidopsis gene ID (AGI). The CBF-responsive genes which showed >2-fold destabilization at least at one time point (marked by asterisks on the AGI) or destabilization at more than two time points during cold treatment are shown by solid lines, while others are shown by dotted lines.

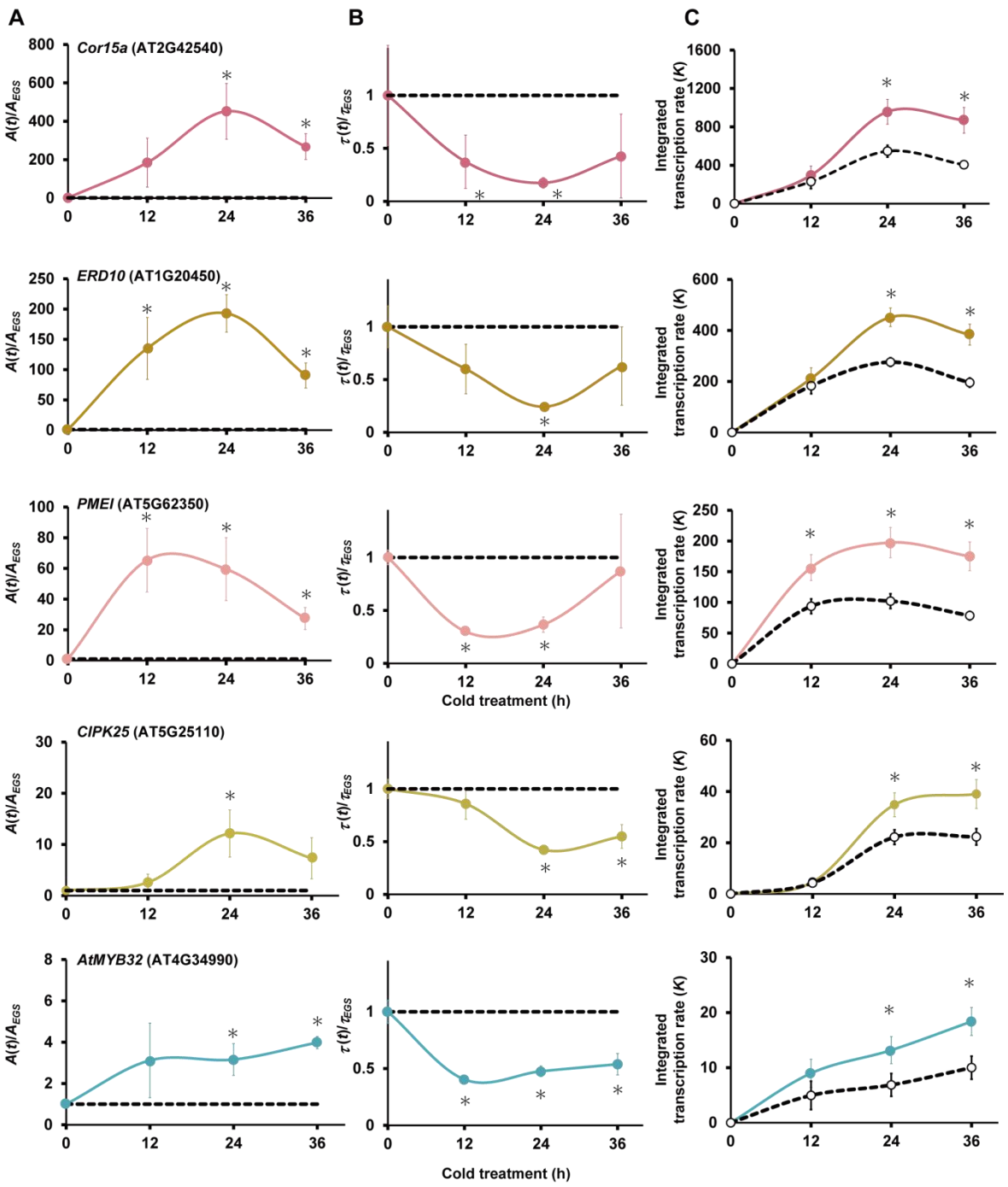
A
B
C
Cor15a (AT2G42540)
ERD10 (AT1G20450)
PMEI (AT5G62350)
CIPK25 (AT5G25110)
AtMYB32 (AT4G34990)
A(t)/A_EGS
τ(t)/τ_EGS
Integrated transcription rate (K)
Cold treatment (h)

Figure 2-11. Kinetics of the CBF-responsive genes in Cluster 02.

(A) Ratios of mRNA amounts to the value expected from the general shift [A(t)/A_{EGS}] and (B) those of mRNA half-lives [τ(t)/τ_{EGS}] in the CBF-responsive genes in Cluster 02 were determined by qRT–PCR. Error bars for mRNA amount represent average ±SD from three biological replications. Error bars for mRNA half-lives represent the SE of t obtained from SEλ. The values expected from the general shift are shown by dashed lines. Asterisks indicate a significant difference from the EGS (one-sample *t*-test, P<0.05). (C) The integrated transcription rate (K) was calculated from the two parameters, mRNA amount (A) and mRNA decay rate [λ = ln(2)/ τ]. The K value indicates the total amount of newly synthesized mRNA by the indicated time. The K value from our experimental data (solid line with filled circles) was compared with the theoretical K values (dashed line with open circles) by assuming that mRNA decay rates follow their general shift during cold treatment. Error bars for integrated transcription rate represent the SE of K obtained from SEs of A and λ. Asterisks indicate a significant difference between experimental and theoretical K by Welch's *t*-test (P< 0.05). Error bars are not visible in some time points due to the smaller size of the bar than the graph symbols. Each transcript is represented by the same colored lines as in Fig. 2-10.

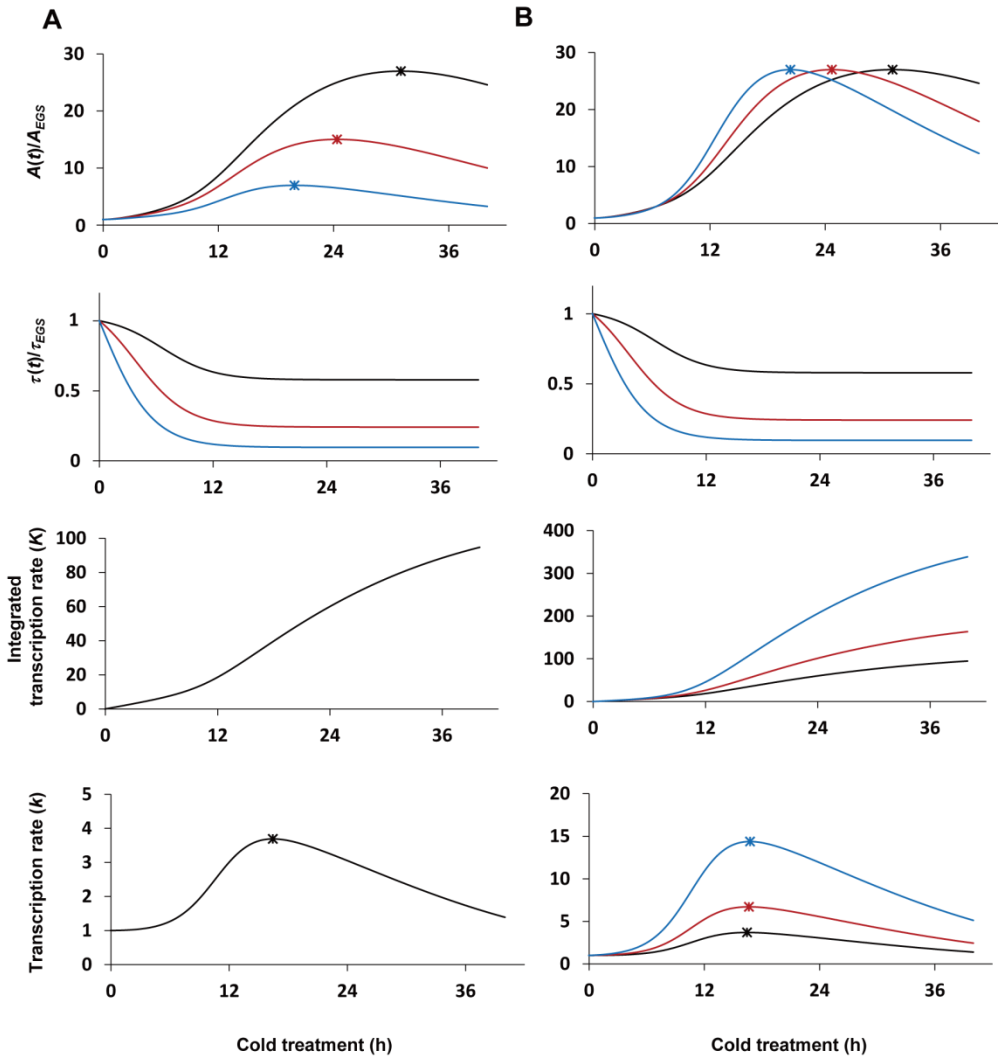

Figure 2-12. Simulation of the effect of mRNA half-lives on the time course pattern of transient upregulation of mRNA levels under the cold condition.

We simulated the parameter changes in the CBF responsive genes in the Cluster 02, in which mRNA amount is upregulated by the transient increase of transcription rate while the mRNA is relatively destabilized in response to cold treatment (black lines). The peak positions of mRNA amounts and transcription rates are indicated by asterisks. Changes in the ratios of mRNA amounts to the value expected from the general shift (A(t)/A_{EGS}) and those of mRNA half-lives (λ(t)/λ_{EGS}), integrated transcription rate (K) and transcription rate (k) are shown. (A) The patterns of transient upregulation of mRNA amounts, when mRNA half-lives were shortened (red to blue lines) while the transcription rate was unchanged. (B) The patterns of transient upregulation of mRNA amounts, when mRNA half-lives were shortened (red to blue lines) while the transcription rates were increased to achieve the same maximum levels of the mRNA accumulation (red to blue lines).

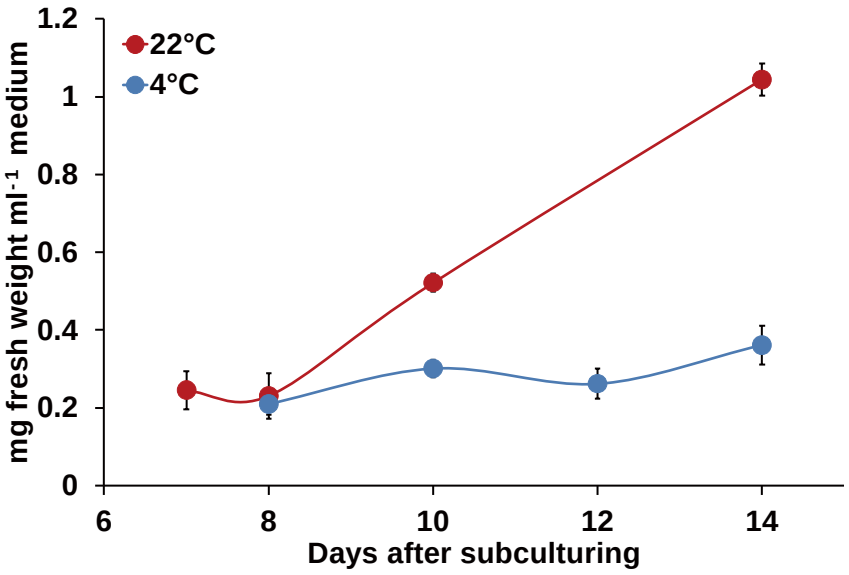

Figure 2-13. Growth of Arabidopsis T87 cells under the control and cold conditions. Fresh weight of the cells grown under 22˚C (red) and 4˚C (blue) was measured at the indicated days after subculturing. Average ± SD of three biological replicates are shown.

Cluster 02						
GO_ID	**GO Term**	**Annotated**	**Expected**	**Observed**	***p*-value**	***q*-value**
GO:0006355	regulation of transcription, DNA-templated	555	37	63	1.5E-09	4.5E-06
GO:0009737	response to abscisic acid	138	9	33	1.2E-08	1.8E-05
GO:0080167	response to karrikin	47	3	15	1.6E-07	1.6E-04
GO:0010224	response to UV-B	15	1	8	1.5E-06	1.1E-03
GO:0009651	response to salt stress	208	14	38	2.3E-06	1.3E-03
GO:0009753	response to jasmonic acid	119	8	24	2.6E-06	1.3E-03
GO:0010200	response to chitin	89	6	18	1.5E-05	6.5E-03
GO:0009723	response to ethylene	94	6	21	2.8E-05	1.0E-02
GO:0009409	response to cold	160	11	23	2.9E-05	1.0E-02
GO:0009611	response to wounding	78	5	16	3.7E-05	1.1E-02
GO:0009414	response to water deprivation	103	7	21	5.2E-05	1.5E-02
GO:0010286	heat acclimation	17	1	7	5.7E-05	1.5E-02
GO:0009862	systemic acquired resistance, salicylic acid mediated signaling pathway	65	4	14	6.5E-05	1.5E-02
GO:0010363	regulation of plant-type hypersensitive response	99	7	17	2.2E-04	4.9E-02
GO:0006355	regulation of transcription, DNA-templated	555	37	63	1.5E-09	4.5E-06
GO:0009737	response to abscisic acid	138	9	33	1.2E-08	1.8E-05
GO:0080167	response to karrikin	47	3	15	1.6E-07	1.6E-04
GO:0010224	response to UV-B	15	1	8	1.5E-06	1.1E-03
GO:0009651	response to salt stress	208	14	38	2.3E-06	1.3E-03
GO:0009753	response to jasmonic acid	119	8	24	2.6E-06	1.3E-03
GO:0010200	response to chitin	89	6	18	1.5E-05	6.5E-03

GO:0009723	response to ethylene	94	6	21	2.8E-05	1.0E-02
GO:0009409	response to cold	160	11	23	2.9E-05	1.0E-02
GO:0009611	response to wounding	78	5	16	3.7E-05	1.1E-02
GO:0009414	response to water deprivation	103	7	21	5.2E-05	1.5E-02

Cluster 40

GO_ID	GO Term	Annotated	Expected	Observed	*p*-value	*q*-value
GO:0000911	cytokinesis by cell plate formation	85	8	36	3.1E-16	9.5E-13
GO:0008283	cell proliferation	99	9	41	2.0E-15	3.1E-12
GO:0006275	regulation of DNA replication	49	4	25	1.1E-13	1.1E-10
GO:0006270	DNA replication initiation	26	2	17	2.2E-12	1.7E-09
GO:0010389	regulation of G2/M transition of mitotic cell cycle	32	3	18	1.9E-11	1.2E-08
GO:0051567	histone H3-K9 methylation	68	6	26	5.1E-11	2.6E-08
GO:0048451	petal formation	22	2	13	5.8E-09	2.2E-06
GO:0048453	sepal formation	22	2	13	5.8E-09	2.2E-06
GO:0042127	regulation of cell proliferation	34	3	11	5.3E-07	1.8E-04
GO:0006306	DNA methylation	62	6	20	6.7E-07	2.1E-04
GO:0010075	regulation of meristem growth	50	5	17	1.3E-06	3.5E-04
GO:0051225	spindle assembly	27	2	12	1.4E-06	3.5E-04
GO:0051726	regulation of cell cycle	98	9	34	2.7E-06	6.4E-04
GO:0006857	oligopeptide transport	23	2	10	1.4E-05	3.0E-03
GO:0000226	microtubule cytoskeleton organization	95	9	34	2.2E-05	4.5E-03
GO:0016572	histone phosphorylation	30	3	12	2.4E-05	4.5E-03
GO:0042023	DNA endoreduplication	37	3	13	4.8E-05	8.7E-03
GO:0009909	regulation of flower development	90	8	20	8.2E-05	1.4E-02
GO:0006261	DNA-dependent DNA	47	4	26	1.3E-04	2.1E-02

	replication					
GO:0008361	regulation of cell size	11	1	6	1.7E-04	2.6E-02
GO:0006346	methylation-dependent chromatin silencing	41	4	12	1.9E-04	2.8E-02
GO:0006949	syncytium formation	8	1	5	2.7E-04	3.8E-02
GO:0043248	proteasome assembly	45	4	7	3.3E-04	4.4E-02
GO:0009855	determination of bilateral symmetry	32	3	10	3.7E-04	4.7E-02

Cluster 41

GO_ID	GO Term	Annotated	Expected	Observed	*p*-value	*q*-value
GO:0009909	regulation of flower development	90	5	20	7.8E-08	2.0E-04
GO:0006306	DNA methylation	62	3	16	1.3E-07	2.0E-04
GO:0051567	histone H3-K9 methylation	68	4	15	2.9E-06	2.9E-03
GO:0006275	regulation of DNA replication	49	3	14	1.3E-05	9.7E-03
GO:0000911	cytokinesis by cell plate formation	85	5	16	3.1E-05	1.7E-02
GO:0031048	chromatin silencing by small RNA	39	2	10	3.4E-05	1.7E-02
GO:0000278	mitotic cell cycle	153	8	31	5.0E-05	2.2E-02
GO:0051225	spindle assembly	27	1	8	6.9E-05	2.7E-02
GO:0009165	nucleotide biosynthetic process	52	3	10	8.4E-05	2.9E-02
GO:0009909	regulation of flower development	90	5	20	7.8E-08	2.0E-04
GO:0006306	DNA methylation	62	3	16	1.3E-07	2.0E-04
GO:0051567	histone H3-K9 methylation	68	4	15	2.9E-06	2.9E-03
GO:0006275	regulation of DNA replication	49	3	14	1.3E-05	9.7E-03
GO:0000911	cytokinesis by cell plate formation	85	5	16	3.1E-05	1.7E-02
GO:0031048	chromatin silencing by small RNA	39	2	10	3.4E-05	1.7E-02
GO:0000278	mitotic cell cycle	153	8	31	5.0E-05	2.2E-02
GO:0051225	spindle assembly	27	1	8	6.9E-05	2.7E-02
GO:0009165	nucleotide biosynthetic	52	3	10	8.4E-05	2.9E-02

	process					
Cluster 42						
GO_ID	**GO Term**	**Annotated**	**Expected**	**Observed**	***p*-value**	***q*-value**
GO:0000956	nuclear-transcribed mRNA catabolic process	49	5	23	3.0E-10	9.3E-07
GO:0009616	virus induced gene silencing	34	3	14	7.3E-07	1.1E-03
GO:0010050	vegetative phase change	20	2	9	3.2E-05	3.2E-02
GO:0010267	production of ta-siRNAs involved in RNA interference	35	3	12	4.2E-05	3.2E-02

Table 2-1. Enriched GO terms in Cluster 02, 40, 41 and 42

Following information for each enriched GO terms in each Cluster is presented. "GO_ID", "GO Term", ID and Term of Gene ontology from TAIR database ver.10; "Annotated", number of annotated genes in each GO term; "Expected", expected number of genes in each GO term; "Observed", observed number of genes in each GO term; "*p*-value", probability with Fisher's exact test; "*q*-value", probability after Benjamini and Hochberg correction.

Cluster	Number of genes	%	Expected	Observed	%	*q*-value
C00	335	6.9	2	0	0.0	0.83
C01	193	4.0	1	2	6.3	0.74
C02	317	6.6	2	16	50.0	3E-10*
C10	330	6.8	2	1	3.1	0.65
C11	176	3.6	1	1	3.1	1.00
C12	239	4.9	2	6	18.8	0.03*
C20	478	9.9	3	1	3.1	0.75
C21	278	5.7	2	0	0.0	0.65
C22	422	8.7	3	1	3.1	0.54
C30	345	7.1	2	1	3.1	0.70
C31	261	5.4	2	1	3.1	0.78
C32	311	6.4	2	0	0.0	0.64
C40	442	9.1	3	1	3.1	0.67
C41	267	5.5	2	0	0.0	0.55
C42	444	9.2	3	1	3.1	0.60
total	4,838	100	32	32	100	

Table 2-2. Enrichment analysis of CBF-responsive genes.

The expected and observed numbers of CBF-responsive genes in each cluster are shown. Significantly overrepresented clusters are marked by asterisks (two-sided Fisher's exact test with Benjamini and Hochberg correction (Benjamini and Hochberg 1995), q-value < 0.05).

AGI/Tair	Forward primers	Reverse primers
At1g04770	TGGGTAGAAGAATGTAGTGAGTGAA	AGACAACGACACCCGAAAA
At1g20450	GTGAATAATAATGATGTGGGAGTGG	AACTTGGAGAACAGCTAGAAAGACA
At1g30210	CAGACCGCGAGGAATTGT	GCAGCCAACAGAATGAGGA
At1g34180	GGAAGACCTCTCTTGTCGTGACCTA	AAAGCCATCAGAGAATCCAGGAAAA
At1g54490	TTGAGGCGCATAAGGAGGTT	GAGAACTGATGGCAGATGATGC
At1g62300	CTCATAAGAATCACCGACG	CGGAGAAGAAATCCACTTC
At2g42540	GATCCATATCCTCTCTCTTCATGTT	TGACGGTGACTGTGGATACC
At2g46690	GATGGGTGGTGATTGTATGTGT	TTTTGTGGGTTAGGCCAGTT
At3g11440	TGGTCGCTGTAACAAAATGAAC	TTACCAAGTCCACAAATCTTCTCTC
At4g34990	AAACAGAGGACAGTAGTAGCAGCA	GTTTAGACCCAAGAAGTCATAACCA
At5g19050	GATGATCCTTGGAGCTAAATCTGC	GTTACGAATCAGCCAAGAAGTGAA
At5g25110	TCTGGTAGTGACTGCTAAGAGAATG	CCTTGAATCTAACAACTGATTAACAAA
At5g40910	AGGAGCCTGAAGCTGTTGAG	GACCACAAGGGAACCAATACA
At5g40990	AGCGGACCATTGAGAGGAA	CAGCGATCTGTCGATTAGCC
At5g52010	TCTGATTCATGGTGAATTGAGTTGC	CTTTGACCACATGAATGCACAAAA
At5g60690	GCTGCATCTGAAGAAAACAACA	ACAGAGACACCTAAACAACAACCA
At5g62350	GTAATGTCTTGCTAAGAGTTTGATGTG	GGGGCAATTTATCCAATCTTAAA

Table 2-3. List of primers

Primer sequences used for qRT-PCR of each transcript are shown. “AGI/Tair”, Arabidopsis gene ID from TAIR database ver. 10.

Chapter 3

Identification of Arabidopsis CCR4-NOT complexes with variable combination of deadenylase subunits

Summary

CCR4/CAF1 are widely conserved deadenylases in eukaryotes. They form a large complex that includes NOT1 as a scaffold protein and various NOT proteins that are core components of multiple levels of gene expression control. The CCR4-NOT complex also contains several RNA-binding proteins as accessory proteins, which are required for target recognition by CCR4/CAF1 deadenylases. AtCCR4a/b, orthologs of human CCR4 in Arabidopsis, have various physiological effects. AtCCR4 isoforms are likely to have specific target mRNAs related to each physiological effect; however, AtCCR4 does not have RNA-binding capability. Therefore, identifying factors that interact with AtCCR4a/b is indispensable to understand its function as a regulator of gene expression, as well as the target mRNA recognition mechanism. Here, we determined components of the AtCCR4-NOT complex by co-immunoprecipitation in combination with mass spectrometry analysis using FLAG-tagged AtCCR4b and yeast two-hybrid assay. Interestingly, 4 of 11 AtCAF1 isoforms interacted with both AtCCR4a/b and AtNOT1, whereas 2 isoforms interacted only with AtNOT1. These results suggest that Arabidopsis has multiple CCR4-NOT complexes with various combinations of deadenylases. We also revealed that the RNA binding protein Arabidopsis Pumilio 5 interacted with AtCCR4a/b, mostly in processing bodies.

Introduction

Almost all eukaryotic mRNA molecules possess poly(A) tails at the 3′ end. The length of a poly(A) tail is important for posttranscriptional regulation because it influences mRNA stability and/or translational efficiency. Poly(A) tails have a critical role in enhancing the translational efficiency of some transcripts (Kojima *et al.* 2012, Udagawa *et al.* 2012), especially in certain developmental stages (Subtelny *et al.* 2014). In addition, poly(A) tails are vital for determining mRNA stability since shortening of the poly(A) tail is the first and apparently rate-limiting step of mRNA degradation in eukaryotes (Chen and Shyu 2011). Various factors in the nucleus and cytoplasm are involved in determining the length of a poly(A) tail. One such cytoplasmic factor is deadenylase, a poly(A)-specific ribonuclease. Carbon catabolite repressor 4 (CCR4) and CCR4-associated factor 1 (CAF1) are widely conserved deadenylases in eukaryotes. In yeast, CCR4 is a major cytoplasmic deadenylase and CAF1 is a regulatory component (Chen *et al.* 2002, Tucker *et al.* 2002). CCR4 and CAF1 are components of a large CCR4-NOT complex, which also contains NOT1 as a scaffold protein. CAF1 binds directly to the MIF4G domain of NOT1, as well as the leucine-rich repeat (LRR) region of CCR4 (Basquin *et al.* 2012, Petit *et al.* 2012). Orthologs of yeast CCR4 and CAF1 have been identified in mammalian cells, including human and mouse. Deadenylation is a biphasic reaction in mammalian cells; CCR4 and CAF1 are involved in the second phase (Yamashita *et al.* 2005). These proteins also form a large CCR4-NOT complex (Lau *et al.* 2009).

Phylogenic analysis of deadenylases identified orthologs of CCR4 and CAF1 in Arabidopsis (Dupressoir *et al.* 2001, Pavlopoulou *et al.* 2013). Two orthologs of CCR4 in Arabidopsis, AtCCR4a/b, have been characterised using reverse genetic strategies showing that they play roles in sucrose and starch metabolism by modulating the poly(A) length of the *Granule-bound starch synthase 1* (*GBSS1*) transcript (Suzuki *et al.* 2015). Two orthologs of CAF1, AtCAF1a/b, are deadenylases involved in defence responses to pathogens, and in stress responses (Liang *et al.* 2009, Walley *et al.* 2010). Four orthologs of CAF1 (OsCAF1A/B/G/H) and two orthologs of CCR4 (OsCCR4A/B) have also been identified and characterised in rice. OsCAF1 isoforms exhibit deadenylation activity in vitro and have diverse expression patterns among tissues under abiotic stress conditions (Chou *et al.* 2014). In addition, interactions among OsCAF1, OsCCR4, and OsNOT1 were evaluated using yeast two-hybrid assays and bimolecular fluorescence complementation (BiFC) analysis, revealing that OsCAF1 functions as an adapter that connects OsCCR4 and OsNOT1 (Chou *et al.* 2017). This suggests that the CCR4-NOT complex is present in rice. However, the components of the CCR4-NOT complex have not been fully elucidated in plants.

Yeast and human CCR4-NOT complexes include factors that regulate different phases of gene expression, from transcription to translation, as well as deadenylase proteins (Collart *et al.* 2013). Therefore, the CCR4-NOT complex has recently attracted attention as a candidate master regulator of gene expression. Moreover, several proteins related to target mRNA recognition by deadenylases are present in the complex as auxiliary components (Fabian *et al.* 2011, Maryati *et al.*

2015). Therefore, it is important to clarify the components of plant CCR4-NOT complex not only to understand its function as a possible master regulator of eukaryotic gene expression, but also to understand the target recognition mechanism of deadenylases in plants.

In this study, we surveyed orthologs of the core components of the human CCR4-NOT complex in several plant species using BLAST searches. Candidate components of the CCR4-NOT complex in Arabidopsis were detected by co-immunoprecipitation assays with mass spectrometry (IP-MS) using FLAG-tagged AtCCR4b. Interactions among the candidate components were evaluated using yeast two-hybrid assays or BiFC analysis. We revealed that Arabidopsis contains two distinct AtCCR4-NOT complexes and also identified several RNA-binding proteins that interact with AtCCR4 and may have a critical role in target mRNA recognition by AtCCR4.

Results

Orthologs of the human CCR4-NOT complex in plants

We performed a phylogenic analysis to identify orthologs of human CCR4-NOT complex components in six plant genomes and evaluate the evolutionary conservation of the complex. *Arabidopsis thaliana* and *Oryza sativa* were chosen as representative dicot and monocot angiosperms, respectively, *Physcomitrella patens* and *Marchantia polymorpha* from bryophytes, *Selaginella moellendorffii* from ferns, and *Chlamydomonas reinhardtii* from green algae. We searched for orthologs of core components of the human CCR4-NOT complex, including NOT1, NOT2, NOT3, NOT9, NOT10, NOT11, and CCR4 and CAF1 deadenylases. All of the analysed plant species possessed orthologs of the CCR4-NOT components (Fig. 3-1A, B; Fig. 3-2). The plant deadenylases CCR4 and CAF1 appeared to be composed of a larger family than other components. Orthologs of CAF1 in *Arabidopsis thaliana* and *Oryza sativa* were divided into three monophyletic groups (group A, B, and C) and those of CCR4 could be separated into four monophyletic groups (group I, II, III, and IV) (Fig. 3-1A, B). To compare the expression levels of AtCAF1 and AtCCR4 family members, we retrieved combined RNA-sequencing data showing the global expression levels in aerial tissue, leaves, and roots from a publicly available database (https://www.araport.org/). In group B, the expression of AtCAF1c/d/f was lower than that of the other AtCAF1 isoforms. In group III, AtCCR4g showed almost no expression in any tissue (Fig. 3-3A, B). Therefore, we excluded these four genes from further analyses.

Identification of candidate components of AtCCR4-NOT complex

To identify candidate components of the AtCCR4-NOT complex in Arabidopsis cells, we performed co-immunoprecipitation experiments in combination with mass spectrometry (IP-MS) using FLAG-tagged AtCCR4b (FLAG-AtCCR4b). FLAG-AtCCR4b was transiently expressed in protoplasts prepared from 4-week-old Arabidopsis seedlings. Protoplasts treated with water was used as a mock (negative control). To increase the number of detectable interactors, IP products extracted using the anti-FLAG antibody were incubated with extracts from Arabidopsis cell suspension culture (MM2d) to reconstitute the AtCCR4-NOT complex. Then, IP was performed again with anti-FLAG antibody followed by MS analysis (Fig. 3-4A, B). A total of 231 proteins were identified as FLAG-AtCCR4b interactors (Fig. 3-4C). Among these, we identified AtCAF1h/i/k, AtNOT2a, AtNOT3, AtNOT9a, and AtNOT10 as candidate components of the AtCCR4-NOT complex (Table 3-1).

Verification of the interactions among AtCCR4-NOT proteins

To verify the interactions among candidate AtCCR4-NOT proteins, we used yeast two-hybrid assays. NOT1 is a scaffold protein in the CCR4-NOT complex in yeast and humans (Lau *et al.* 2009, Maillet *et al.* 2000). We first tested the interaction between AtNOT1 and AtCAF1 isoforms after generating the following truncated AtNOT1 fragments to facilitate expression in

yeast: AtNOT1N including the N-terminal region (residues 1–836), AtNOT1M containing the middle region (830–1,438), and AtNOT1C containing the C-terminal region (1,527–2,377) (Fig. 3-5). Since CAF1 interacts with the MIF4G domain of NOT1 in the central region of the protein in yeast and humans (Basquin *et al.* 2012, Petit *et al.* 2012), we used the AtNOT1M fragment for the interaction analysis with AtCAF1 isoforms. AtCAF1a in group A and AtCAF1h/i/j/k in group C exhibited a significant interaction with AtNOT1M. AtCAF1b also had higher β-galactosidase activity than the negative controls, even though no significant difference was detected due to high variability among biological replicates (Fig. 3-6A). These results suggest that some, but not all, AtCAF1 isoforms interact with AtNOT1. The middle region of AtNOT1 including the AtNOT1M fragment was sufficient for these interactions.

Next, we tested the interaction between AtCAF1 isoforms and AtCCR4 isoforms. We demonstrated previously that AtCCR4a/b are most similar to yeast CCR4 and that they localise to cytoplasmic mRNA processing bodies (P-bodies) (Suzuki *et al.* 2015). P-bodies are specific granules containing many enzymes involved in mRNA turnover. AtCAF1i/k in group C had a significant interaction with both AtCCR4a/b (Fig. 3-6B). Although AtCAF1h/j in group C exhibited a significant interaction with AtCCR4b, no significant interaction with AtCCR4a was observed due to a high background signal with AtCAF1h and high variability among biological replicates in AtCAF1j (Fig. 3-6B). These results suggest that AtCAF1 in group C is likely to interact with AtCCR4a/b.

Even though AtCAF1a/b in group A also interacted with AtNOT1, neither had any significant interaction with AtCCR4a/b (Fig. 3-6A, B). Thus, we evaluated a possible interaction between AtCAF1a/b and other members of the AtCCR4 family. To assess the biological function of other AtCCR4 isoforms, we observed their protein localisation. A C-terminal green fluorescent protein (GFP) fusion with each AtCCR4 isoform was transiently expressed in protoplasts prepared from T87 Arabidopsis cultured cells. The fluorescence of AtCCR4c-GFP was exclusively observed in chloroplasts (Fig. 3-7). Consistent with this, the expression of AtCCR4c was mostly observed in green tissues (Fig 3-3B). In contrast, AtCCR4d-GFP was observed in the cytoplasm and chloroplasts and AtCCR4f-GFP was observed only in the cytoplasm (Fig. 3-7). Even though AtCCR4d/f were likely to be localised in the cytoplasm, P-body-like foci were not observed. No fluorescence image was obtained from AtCCR4e-GFP. Because we were interested in deadenylases that function in the cytoplasm, AtCCR4c was excluded from the interaction analyses with AtCAF1 isoforms. None of AtCCR4d/e/f had any significant interaction with AtCAF1 isoforms that interacted with AtNOT1, including AtCAF1a/b (Fig. 3-8).

Next, we tested the interactions of AtNOT1, AtNOT9, AtNOT10, and AtNOT11. Since NOT1 contains a CAF40/NOT9-binding domain (CN9BD) in the middle region of analogous protein in yeast and humans (Chen *et al.* 2001, Chen *et al.* 2014), we used the AtNOT1M fragment for the interaction analyses with AtNOT9 isoforms (Fig. 3-5). Among the three members of the AtNOT9 family, AtNOT9c was expressed at lower levels in aerial tissues compared with ANOT9a/b (Fig. 3-3C). Therefore, we used AtNOT9a/b for the interaction analysis. AtNOT9a/b

both exhibited a significant interaction with AtNOT1M (Fig.3-9A). NOT10 and NOT11 are components of the human CCR4-NOT complex, but no orthologs are present in yeast (Mauxion *et al.* 2013). Since NOT10 interacts with the N-terminal region of NOT1 through a direct interaction with NOT11 in humans, we used the AtNOT1N fragment for assessing the interactions with AtNOT10/11 (Fig. 3-5). As expected, AtNOT11 had a significant interaction with AtNOT1N, but no significant interaction was observed between AtNOT10 and AtNOT1N. AtNOT10 exhibited a significant interaction with AtNOT11, suggesting that AtNOT10 is included in the AtCCR4-NOT complex via binding to AtNOT11 (Fig. 3-9B).

We also tested the interactions of AtNOT1, AtNOT2a/b and AtNOT3 using yeast two-hybrid assays. NOT2 and NOT3 form heterodimers via their Not-box domains. In addition, NOT2 and NOT3 interact with the C-terminal region of NOT1 in yeast and humans (Bhaskar *et al.* 2013, Boland *et al.* 2013). Therefore, we used the AtNOT1C fragment for assessing the interactions between AtNOT2a/b and AtNOT3 (Fig. 3-5). AtNOT2a/b and AtNOT3 all interacted significantly with the AtNOT1C fragment (Fig. 3-9C). Moreover, AtNOT2a/b had significant interactions with AtNOT3 (Fig. 3-9C).

Taken together, these data suggest that the AtCCR4-NOT complex exists in Arabidopsis cells, with conserved components and a similar composition to those in other eukaryotes. Another type of AtCCR4-NOT complex was also identified, in which AtCAF1a/b did not interact with AtCCR4 isoforms.

APUM5 interacted with AtCCR4a/b in P-bodies

Since *atccr4a/b* double mutants have pleiotropic phenotypes throughout plant growth and development, these deadenylases are thought to have specific target mRNAs (Suzuki *et al.* 2015). However, AtCCR4a/b do not contain an RNA-binding domain in their amino acid sequences, making it highly likely that the AtCCR4-NOT complex includes RNA-binding proteins that recognise the specific targets of AtCCR4a/b. IP-MS analysis using FLAG-AtCCR4b identified several interacting RNA-binding proteins (Table3- 2). Pumilio proteins are evolutionally conserved RNA-binding proteins in eukaryotes. The Pumilio family in Arabidopsis (APUM) consists of 25 isoforms that are divided into five groups (Tam *et al.* 2010). Among them, APUM1 and APUM5 interacted with FLAG-AtCCR4b. These APUM are classified in the same group as pumilio proteins in humans and fruit fly. Several studies indicated that APUM5 is involved in the response to abiotic stresses, as well as defence against viral infections in Arabidopsis (Huh *et al.* 2013, Huh and Paek 2014). Thus, we focused on APUM5 and investigated its subcellular localisation using a C-terminal GFP fusion to APUM5. APUM5-GFP was co-transfected into tobacco leaves with AtDCP1-mCherry and AtDCP2-CFP, that are universal P-body markers (Iwasaki *et al.* 2007, Xu *et al.* 2006), by agroinfiltration. APUM5-GFP fluorescence was observed in the cytoplasm with a few foci. These cytoplasmic foci clearly overlapped with those derived from AtDCP1-mCherry and AtDCP2-CFP, suggesting that APUM5 was localised in P-bodies (Fig. 3-10A).

Our previous study demonstrated that AtCCR4a/b are localised in the cytoplasm with a few foci. Transient co-expression analyses of AtCCR4-GFP with AtDCP1-mCherry and AtDCP2-CFP, as well as BiFC analysis (Weber *et al*. 2008) using an AtCCR4-N-fragment of GFP (NGFP) with AtDCP1- or the AtDCP2-C-fragment of GFP (CGFP), revealed that these cytoplasmic foci were P-bodies (Suzuki *et al.*, 2015).

Since APUM5 was localised to P-bodies, like AtCCR4a/b, we performed BiFC analysis to verify the interaction between APUM5 and AtCCR4a/b. APUM5-CGFP and AtCCR4a-NGFP were transiently co-expressed together with mCherry (as a positive control for transfection) in tobacco leaves by agroinfiltration. The reconstituted GFP fluorescence of these two constructs was detected in the cytoplasmic foci (Fig. 3-10B). Interestingly, the reconstituted GFP fluorescence of APUM5-CGFP with AtCCR4a-NGFP was mostly observed in cytoplasmic foci, even though both proteins were broadly localised in the cytoplasm. No fluorescent signal was detected when any of the fusion proteins were expressed in combination with NGFP or CGFP (Fig. 3-10B). Similar interactions were observed with AtCCR4b (Fig. 3-10B). These results suggest that APUM5 interacts with AtCCR4a/b in P-bodies.

Discussion

In this study, we searched for proteins that interact with FLAG-AtCCR4b to reveal the presence of the CCR4-NOT complex in Arabidopsis. We also identified factors that might be required for target recognition by AtCCR4. We defined the core components of two types of AtCCR4-NOT complex and found that the RNA-binding protein APUM5 interacts with AtCCR4a/b (Fig. 6).

Two types of CCR4-NOT complex are present in Arabidopsis

In the Arabidopsis AtCCR4-NOT complex, AtNOT1 acts as scaffold protein by interacting with various AtNOT proteins and AtCAF1, just like in other eukaryotic CCR4-NOT complexes. Our phylogenic analyses suggested duplication or multiplication of genes encoding several subunits of the CCR4-NOT complex in plants. For example, CAF1 is encoded in two loci in humans, whereas the AtCAF1 family contains 11 members that are divided into three groups (Fig. 3-1A). Among them, AtCAF1a/b in group A and AtCAF1h/i/j/k in group C interacted with AtNOT1, whereas AtCAF1e/g in group B were not part of the AtCCR4-NOT complex (Fig. 3-6A). Consistent with this, amino acid residues in human CAF1 that are important for the interaction with NOT1 are mostly conserved in AtCAF1 isoforms in groups A and C (Fig. 3-12). AtCAF1 isoforms in group B might function as deadenylases independent from the AtCCR4-NOT complex, although we cannot exclude the possibility that these are pseudogenes because they are expressed at much lower levels than the AtCAF1 isoforms in other groups (Fig. 3-3A).

We also revealed two types of AtCCR4-NOT complex. The AtCAF1 in group C interacted with AtCCR4a/b, just like other CCR4-NOT complexes; however, the AtCAF1 in group A did not interact with any AtCCR4 isoforms (Fig. 3-6B, Fig. 3-8). A close ortholog of AtCAF1a/b in rice, OsCAF1b, also does not interact with the full-length OsCCR4a/b, whose catalytic domain inhibits the interaction (Chou *et al.* 2017). Interestingly, AtCAF1a/b and OsCAF1b are strongly expressed in response to abiotic stresses (Chou *et al.* 2014, Walley *et al.* 2010). Therefore, it is possible that these CAF1 in group A are functional without interacting with CCR4, and that they play a specific role in abiotic stress responses. Recently, differences in the substrate specificities of CAF1 and CCR4 were revealed in yeast and human. Specifically, CCR4 showed degradation activity specific to PABP-protected poly(A) segments, whereas CAF1 degraded naked poly(A) segments alone in vitro (Webster *et al.* 2018, Yi *et al.* 2018). Further studies will provide a better understanding of the deadenylation specificities of the two types of AtCAF1 in the AtCCR4-NOT complex.

Arabidopsis Pumilio proteins as interactor of AtCCR4

Pumilio is a widely conserved RNA-binding protein in eukaryotes. Pumilio homology domains (PUM-HD) in the C-terminal region, especially triplets of eight amino acids sequence called Puf repeats, are important for binding to specific RNAs. Here, APUM5 and APUM1 were identified as candidate proteins that interact with FLAG-AtCCR4b using IP-MS analysis (Table

3-2). In the Arabidopsis genome, APUM1 is located in tandem with APUM2 and 3 in one region of chromosome 2. Also, the identity of the amino acid sequences of APUM1/2/3 is very high (> 85%). Thus, APUM1/2/3 likely appear as the result of single gene duplications and are functionally redundant. Peptide signals determined by the IP-MS analysis using FLAG-AtCCR4b protein were identified in APUM 2 and 3 as well; therefore, APUM2 and 3 may also interact with AtCCR4b. APUM1/2/3 and APUM5 belong to the same phylogenic group, which also includes most characterized human and fruit fly Pumilio proteins. All of these APUMs possess eight Puf repeats in their PUM-HD and can bind specifically to Nanos Response Element 1 (NRE1), which is a well-known target RNA sequence of fruit fly Pumilio (Francischini and Quaggio 2009, Tam *et al.* 2010).

APUM5 is involved in both biotic and abiotic stress responses. APUM5-overexpressing plants showed reduced susceptibility to cucumber mosaic virus (CMV) infection via the direct binding of APUM5 to the 3′-UTR or internal motifs in the CMV RNA itself (Huh *et al.* 2013). APUM5-overexpressing plants were also hypersensitive phenotypes to salt, osmotic, and drought stresses. Further results indicated that APUM5 expression was induced in response to these abiotic stresses and that APUM5 bound to a specific motif in the 3′-UTR of several stress-responsive genes (Huh and Paek 2014). Since APUM5 interacted with both AtCCR4a/b in P-bodies (Fig. 3-10B), where most of the mRNA degradation machinery accumulates, it is highly possible that APUM5 is associated with mRNA degradation of stress responsive genes together with AtCCR4a/b. Moreover, it is interesting that the interaction between APUM5 and AtCCR4a/b occurred mostly in P-bodies, even though both APUM5 and AtCCR4a/b were localised broadly in the cytoplasm with foci. These results suggest that an unknown factor in P-bodies might be required to strengthen the interaction between APUM5 and AtCCR4.

The physiological functions of APUM1/2/3 are not yet clear. However, several transcripts related to shoot meristem maintenance contain the specific motif recognised by APUM2 (Francischini and Quaggio 2009), suggesting that, together with AtCCR4, APUM in Arabidopsis is also involved in regulating transcripts related to stem cell maintenance, which is considered to be an ancestral function of Pumilio proteins and the CCR4-NOT complex in animals (Spassov and Jurecic 2003).

In conclusion, we revealed that the CCR4-NOT complex is present in Arabidopsis. The composition of the AtCCR4-NOT complex was mostly conserved, although two types of deadenylase were identified, which may reflect functional differences in these complexes. Moreover, we identified that Pumilio RNA-binding proteins interact with AtCCR4, providing important perspectives into the physiological function of the AtCCR4-NOT complex.

Experimental Procedures

Plant materials and growth conditions

A. thaliana (L.) Heynh. ecotype Columbia (Col-0) was used as a wild-type strain. All seedlings were grown at 22°C on Murashige and Skoog (MS) medium (Murashige and Skoog, 1962) supplemented with 100 mM sucrose under constant light or a 16 h-light/8 h-dark cycle with white light (35 μmol m^{-2} sec^{-1}). MM2d Arabidopsis cell suspension cultures were maintained as described previously (Menges and Murray 2002, 2006).

Phylogenic analyses of human CCR4-NOT orthologs in plants

To identify human CCR4-NOT orthologs in plants, human CCR4s (HsCNOT6, HsCNOT6L), CAF1s (HsCNOT7, HsCNOT8), and NOT proteins (HsCNOT1, HsCNOT2, HsCNOT3, HsCNOT4, HsCNOT9, HsCNOT10, HsCNOT11) were used as queries in the NCBI BLAST+ program (Camacho *et al.* 2009). The amino acid sequences of subunits of the human CCR4-NOT complex were retrieved from UniProt (https://www.uniprot.org/). A BLAST database was created using peptide sequences retrieved from JGI Phytozome v12.1 (https://phytozome.jgi.doe.gov) and BLAST searches (BLASTP) were performed with default parameters. Amino acid sequences were aligned using the Clustal Ω program (Sievers *et al.* 2011) and phylogenetic trees were generated with MEGA7 (Kumar *et al.* 2016) using the neighbour-joining method with pairwise deletion. Bootstrap calculations were performed using 1,000 replicates to ensure statistical reliability.

Plasmid construction

The coding regions lacking the stop codons of AtCCR4a/b/d/e/f, AtCAF1a/b/e/g/h/i/j/k, AtNOT2, AtNOT3, AtNOT9a/b, AtNOT10, AtNOT11, and APUM5 were amplified from Col-0 cDNA by PCR. Truncated versions of AtNOT1 were also PCR-amplified. AtNOT1N, AtNOT1M, and AtNOT1C include amino acids 1–836, 830–1438, and 1527–2377 of the coding region, respectively. The primers used for PCR are listed in Table 3-3. The amplified fragments were introduced into the pENTR/D-TOPO vector (Invitrogen, Carlsbad, CA, USA). After confirming the sequences, the fragments were transferred into destination vectors using the Gateway system according to the manufacture's protocol (Invitrogen).

Yeast two-hybrid assay

The coding regions of AtCCR4a/b/d/e/f, AtCAF1a/b/e/g/h/i/j/k, AtNOT2, AtNOT3, AtNOT9a/b, AtNOT10, and AtNOT11 were transferred into pEG202gw as bait, and those of AtCCR4a/b/d/e/f, AtCAF1a/b/e/g/h/i/j/k, AtNOT2, AtNOT3, AtNOT9a/b, AtNOT10, and AtNOT11 were transferred into pJG4-5gw destination vector as prey. These Gateway-compatible versions of pEG202 and pJG4-5 vectors were kindly provided by Dr. Hironori Kaminaka (Tottori University, Tottori, Japan). The yeast strain EGY48 (pJK103) was used for the two-hybrid assays.

pEG202 and pJG4-5 vectors were used as negative vector controls. Yeast transformation was performed using a Frozen-EZ Yeast Transformation II Kit (Zymo Research, Irvine, CA, USA) according to the manufacturer's protocol. Handling of yeast cultures and β-galactosidase assays were performed as described in the Yeast Protocols Handbook (Clontech, Mountain View, CA, USA). A β-galactosidase unit is defined as the amount of enzyme that hydrolyses 1 μmol of 2-nitrophenyl-β-D-galactopyranoside to 2-nitrophenol and D-galactose per min per cell (Miller 1972).

Co-immunoprecipitation and mass spectrometry analysis

FLAG-tagged AtCCR4b under the control of the CaMV 35S promoter was transiently overexpressed in protoplast cells, as described previously (Yoo *et al.* 2007). Protoplast cells were harvested by centrifugation (200 × *g* for 1 min at room temperature). Protoplast cells were ruptured by vortexing in extraction buffer (50 mM Tris-HCl pH 7.5, 10% (v/v) glycerol, 150 mM NaCl, 1 mM EDTA, 0.1% (v/v) Triton X-100) with 10 μM MG-132 and complete protease inhibitor cocktail (Roche Applied Science, Penzberg, Germany), and cellular debris was removed by centrifugation (20,000 × g for 5 min at 4°C). MM2d cells were harvested 4 days after sub-culture. A mortar and pestle was used to grind cells with liquid nitrogen. Extraction buffer with protease inhibitors was added to ground cells, and cellular debris was removed by centrifugation (20,000 × g for 10 min at 4°C) twice. Anti-FLAG M2 magnetic beads (Sigma-Aldrich, St. Louis, MO, USA) that had been equilibrated with extraction buffer were added to the protoplast mixture and gently rotated for 3 h at 4°C. The beads were washed three times with extraction buffer containing 2% v/v Triton X-100 and then added to MM2d cell extracts and rotated gently for 3 h at 4°C. Finally, the beads were washed three times with extraction buffer and the bound proteins were eluted with 100 μl of 300 μg ml^{-1} 3× FLAG peptides (Sigma-Aldrich) by rotating for 1 h at 4°C. The eluted proteins were concentrated by acetone precipitation and resuspended in 20 μl SDS sample buffer (125 mM Tris-HCl pH 6.8, 20% (v/v) glycerol, 4% (w/v) SDS, 0.02% (w/v) bromophenol blue, 200 mM DTT). The precipitated proteins were separated using 10% SDS-PAGE (Perfect NT Gel; DRC, Tokyo, Japan) and stained with SYPRO Ruby (Lonza, Walkersville, MD, USA) as described in the manufacturer's protocol. Peptides for liquid chromatography–tandem mass spectrometry (LC-MS/MS) analysis were prepared by in-gel digestion using sequencing-grade modified trypsin (Promega, Madison, WI, USA), and LC-MS/MS analysis was performed using an EASY-nLC 1000 liquid chromatograph coupled to an Orbitrap Elite Mass Spectrometer system (Thermo Scientific, Waltham, MA, USA) as described previously (Lu et al. 2016). The MS/MS spectra were compared against Arabidopsis protein sequences retrieved from TAIR10 (https://www.arabidopsis.org/) using the SEQUEST program embedded in Proteome Discoverer 1.4 (Thermo Scientific).

BiFC analysis and transient expression assay using tobacco leaves

The coding regions of APUM5, AtDCP1, and AtDCP2 were transferred into pGWB5, pB4GWmC, and pGWB444, respectively (Nakagawa *et al.* 2007) for tobacco transformation. The coding regions of APUM5 and AtCCR4a/b were transferred into pB4GWnG and pB4GWcG, respectively, for BiFC analysis. A series of pB4 vectors were kindly provided by Dr. Mano (National Institute for Basic Biology, Okazaki, Japan). All constructs for agroinfiltration were introduced into *Agrobacterium tumefaciens* strain GV3101 (pMP90) by electroporation. Transformed *A. tumefaciens* cells were cultured in 2× YT medium overnight at 28°C with shaking and then collected and resuspended in infiltration buffer (10 mM MES, 10 mM $MgCl_2$, 450 μM acetosyringone, pH 5.6). To enhance the transgene expression, *A. tumefaciens* expressing the p19 silencing suppressor was resuspended with all samples. *A. tumefaciens* suspensions transformed with distinct constructs were mixed at equal ratios and then infiltrated into the leaves of 3–5-week-old *Nicotiana benthamiana* plants using a needleless syringe. Confocal microscopy images were obtained with an LSM510 inverted confocal laser microscope (Zeiss, Oberkochen, Germany) with a 40× objective.

References

Basquin, J., Roudko, V.V., Rode, M., Basquin, C., Seraphin, B. and Conti, E. (2012) Architecture of the nuclease module of the yeast Ccr4-Not complex: the Not1-Caf1-Ccr4 interaction. *Mol. Cell* **48**: 207-218.

Bhaskar, V., Roudko, V., Basquin, J., Sharma, K., Urlaub, H., Seraphin, B. and Conti, E. (2013) Structure and RNA-binding properties of the Not1-Not2-Not5 module of the yeast Ccr4-Not complex. *Nat. Struct. Mol. Biol.* **20**: 1281-1288.

Boland, A., Chen, Y., Raisch, T., Jonas, S., Kuzuoglu-Ozturk, D., Wohlbold, L., Weichenrieder, O. and Izaurralde, E. (2013) Structure and assembly of the NOT module of the human CCR4-NOT complex. *Nat. Struct. Mol. Biol.* **20**: 1289-1297.

Camacho, C., Coulouris, G., Avagyan, V., Ma, N., Papadopoulos, J., Bealer, K. and Madden, T.L. (2009) BLAST+: architecture and applications. *BMC Bioinformatics* **10**: 421.

Chen, C.Y. and Shyu, A.B. (2011) Mechanisms of deadenylation-dependent decay. *Wiley Interdiscip. Rev. RNA* **2**: 167-183.

Chen, J., Chiang, Y.C. and Denis, C.L. (2002) CCR4, a 3'-5' poly(A) RNA and ssDNA exonuclease, is the catalytic component of the cytoplasmic deadenylase. *EMBO J.* **21**: 1414-1426.

Chen, J., Rappsilber, J., Chiang, Y.C., Russell, P., Mann, M. and Denis, C.L. (2001) Purification and characterization of the 1.0 MDa CCR4-NOT complex identifies two novel components of the complex. *J. Mol. Biol.* **314**: 683-694.

Chen, Y., Boland, A., Kuzuoglu-Ozturk, D., Bawankar, P., Loh, B., Chang, C.T., Weichenrieder, O. and Izaurralde, E. (2014) A DDX6-CNOT1 complex and W-binding pockets in CNOT9 reveal direct links between miRNA target recognition and silencing. *Mol. Cell* **54**: 737-750.

Chou, W.L., Chung, Y.L., Fang, J.C. and Lu, C.A. (2017) Novel interaction between CCR4 and CAF1 in rice CCR4-NOT deadenylase complex. *Plant Mol. Biol.* **93**: 79-96.

Chou, W.L., Huang, L.F., Fang, J.C., Yeh, C.H., Hong, C.Y., Wu, S.J. and Lu, C.A. (2014) Divergence of the expression and subcellular localization of CCR4-associated factor 1 (CAF1) deadenylase proteins in *Oryza sativa*. *Plant Mol. Biol.* **85**: 443-458.

Collart, M.A., Panasenko, O.O. and Nikolaev, S.I. (2013) The Not3/5 subunit of the Ccr4-Not complex: a central regulator of gene expression that integrates signals between the cytoplasm and the nucleus in eukaryotic cells. *Cell. Signal.* **25**: 743-751.

Dupressoir, A., Morel, A.P., Barbot, W., Loireau, M.P., Corbo, L. and Heidmann, T. (2001) Identification of four families of yCCR4- and Mg^{2+}-dependent endonuclease-related proteins in higher eukaryotes, and characterization of orthologs of yCCR4 with a conserved leucine-rich repeat essential for hCAF1/hPOP2 binding. *BMC Genomics* **2**: 9.

Fabian, M.R., Cieplak, M.K., Frank, F., Morita, M., Green, J., Srikumar, T., Nagar, B., Yamamoto, T., Raught, B. and Duchaine, T.F. (2011) miRNA-mediated deadenylation is orchestrated by GW182 through two conserved motifs that interact with CCR4-NOT. *Nat. Struct. Mol. Biol.* **18**: 1211-1217.

Francischini, C.W. and Quaggio, R.B. (2009) Molecular characterization of *Arabidopsis thaliana* PUF proteins--binding specificity and target candidates. *FEBS J.* **276**: 5456-5470.

Huh, S.U., Kim, M.J. and Paek, K.H. (2013) Arabidopsis Pumilio protein APUM5 suppresses Cucumber mosaic virus infection via direct binding of viral RNAs. *Proc. Natl. Acad. Sci. USA* **110**: 779-784.

Huh, S.U. and Paek, K.H. (2014) APUM5, encoding a Pumilio RNA binding protein, negatively regulates abiotic stress responsive gene expression. *BMC Plant Biol.* **14**: 75.

Iwasaki, S., Takeda, A., Motose, H. and Watanabe, Y. (2007) Characterization of Arabidopsis decapping proteins AtDCP1 and AtDCP2, which are essential for post-embryonic development. *FEBS Lett.* **581**: 2455-2459.

Kojima, S., Sher-Chen, E.L. and Green, C.B. (2012) Circadian control of mRNA polyadenylation dynamics regulates rhythmic protein expression. *Genes Dev.* **26**: 2724-2736.

Kumar, S., Stecher, G. and Tamura, K. (2016) MEGA7: Molecular Evolutionary Genetics Analysis version 7.0 for bigger datasets. *Mol. Biol. Evol.* **33**: 1870-1874.

Lau, N.C., Kolkman, A., van Schaik, F.M., Mulder, K.W., Pijnappel, W.W., Heck, A.J. and Timmers, H.T. (2009) Human Ccr4-Not complexes contain variable deadenylase subunits. *Biochem. J.* **422**: 443-453.

Liang, W., Li, C., Liu, F., Jiang, H., Li, S., Sun, J., Wu, X. and Li, C. (2009) The Arabidopsis homologs of CCR4-associated factor 1 show mRNA deadenylation activity and play a role in plant defence responses. *Cell Res.* **19**: 307-316.

Lu, Y., Yasuda, S., Li, X., Fukao, Y., Tohge, T., Fernie, A.R., Matsukura, C., Eruza, H., Sato, T. and Yamaguchi, J. (2016) Characterization of ubiquitin ligase SlATL31 and

proteomic analysis of 14-3-3 targets in tomato fruit tissue (*Solanum lycopersicum* L.). *J. Proteomics* **143**: 254-264.

Maillet, L., Tu, C., Hong, Y.K., Shuster, E.O. and Collart, M.A. (2000) The essential function of Not1 lies within the Ccr4-Not complex. *J. Mol. Biol.* **303**: 131-143.

Maryati, M., Airhihen, B. and Winkler, G.S. (2015) The enzyme activities of Caf1 and Ccr4 are both required for deadenylation by the human Ccr4-Not nuclease module. *Biochem. J.* **469**: 169-176.

Mauxion, F., Preve, B. and Seraphin, B. (2013) C2ORF29/CNOT11 and CNOT10 form a new module of the CCR4-NOT complex. *RNA Biol.* **10**: 267-276.

Menges, M. and Murray, J.A. (2002) Synchronous Arabidopsis suspension cultures for analysis of cell-cycle gene activity. *Plant J.* **30**: 203-212.

Menges, M. and Murray, J.A. (2006) Synchronization, transformation, and cryopreservation of suspension-cultured cells. *Methods Mol. Biol.* **323**: 45-61.

Miller, J.H. (1972) Experiments in Molecular Genetics. Cold Spring Harbor Laboratory, Cold Spring Harbor, New York.

Nakagawa, T., Kurose, T., Hino, T., Tanaka, K., Kawamukai, M., Niwa, Y., Toooka, K., Matsuoka, K., Jinbo, T. and Kimura, T. (2007) Development of series of gateway binary vectors, pGWBs, for realizing efficient construction of fusion genes for plant transformation. *J. Biosci. Bioeng.* **104**: 34-41.

Pavlopoulou, A., Vlachakis, D., Balatsos, N.A. and Kossida, S. (2013) A comprehensive phylogenetic analysis of deadenylases. *Evol. Bioinform. Online* **9**: 491-497.

Petit, A.P., Wohlbold, L., Bawankar, P., Huntzinger, E., Schmidt, S., Izaurralde, E. and Weichenrieder, O. (2012) The structural basis for the interaction between the CAF1 nuclease and the NOT1 scaffold of the human CCR4-NOT deadenylase complex. *Nucleic Acids Res.* **40**: 11058-11072.

Sievers, F., Wilm, A., Dineen, D., Gibson, T.J., Karplus, K., Li, W., Lopez, R., McWilliam, H., Remmert, M., Söding, J., Thompson, J.D. and Higgins, D.G. (2011) Fast, scalable generation of high-quality protein multiple sequence alignments using Clustal Omega. *Mol. Syst. Biol.* **7**: 539.

Spassov, D.S. and Jurecic, R. (2003) The PUF family of RNA-binding proteins: does evolutionarily conserved structure equal conserved function? *IUBMB Life* **55**: 359-366.

Subtelny, A.O., Eichhorn, S.W., Chen, G.R., Sive, H. and Bartel, D.P. (2014) Poly(A)-tail profiling reveals an embryonic switch in translational control. *Nature* **508**: 66-71.

Suzuki, Y., Arae, T., Green, P.J., Yamaguchi, J. and Chiba, Y. (2015) AtCCR4a and AtCCR4b are involved in determining the poly(A) length of *Granule-bound starch synthase 1* transcript and modulating sucrose and starch metabolism in *Arabidopsis thaliana*. *Plant Cell Physiol.* **56**: 863-874.

Tam, P.P., Barrette-Ng, I.H., Simon, D.M., Tam, M.W., Ang, A.L. and Muench, D.G. (2010) The Puf family of RNA-binding proteins in plants: phylogeny, structural modeling, activity and subcellular localization. *BMC Plant Biol.* **10**: 44.

Tucker, M., Staples, R.R., Valencia-Sanchez, M.A., Muhlrad, D. and Parker, R. (2002) Ccr4p is the catalytic subunit of a Ccr4p/Pop2p/Notp mRNA deadenylase complex in *Saccharomyces cerevisiae*. *EMBO J.* **21**: 1427-1436.

Udagawa, T., Swanger, S.A., Takeuchi, K., Kim, J.H., Nalavadi, V., Shin, J., Lorenz, L.J., Zukin, R.S., Bassell, G.J. and Richter, J.D. (2012) Bidirectional control of mRNA translation and synaptic plasticity by the cytoplasmic polyadenylation complex. *Mol. Cell* **47**: 253-266.

Walley, J.W., Kelley, D.R., Nestorova, G., Hirschberg, D.L. and Dehesh, K. (2010) Arabidopsis deadenylases AtCAF1a and AtCAF1b play overlapping and distinct roles in mediating environmental stress responses. *Plant Physiol.* **152**: 866-875.

Weber, C., Nover, L. and Fauth, M. (2008) Plant stress granules and mRNA processing bodies are distinct from heat stress granules. *Plant J.* **56**: 517-530.

Webster, M.W., Chen, Y.H., Stowell, J.A.W., Alhusaini, N., Sweet, T., Graveley, B.R., Coller, J. and Passmore, L.A. (2018) mRNA deadenylation is coupled to translation rates by the differential activities of Ccr4-Not nucleases. *Mol. Cell* **70**: 1089-1100 e1088.

Xu, J., Yang, J.Y., Niu, Q.W. and Chua, N.H. (2006) Arabidopsis DCP2, DCP1, and VARICOSE form a decapping complex required for postembryonic development. *Plant Cell* **18**: 3386-3398.

Yamashita, A., Chang, T.C., Yamashita, Y., Zhu, W., Zhong, Z., Chen, C.Y. and Shyu, A.B. (2005) Concerted action of poly(A) nucleases and decapping enzyme in mammalian mRNA turnover. *Nat. Struct. Mol. Biol.* **12**: 1054-1063.

Yi, H., Park, J., Ha, M., Lim, J., Chang, H. and Kim, V.N. (2018) PABP cooperates with the CCR4-NOT complex to promote mRNA deadenylation and block precocious decay. *Mol. Cell* **70**: 1081-1088.e5.

Yoo, S.D., Cho, Y.H. and Sheen, J. (2007) Arabidopsis mesophyll protoplasts: a versatile cell system for transient gene expression analysis. *Nat. Protoc.* **2**: 1565-1572.

Figures and legends

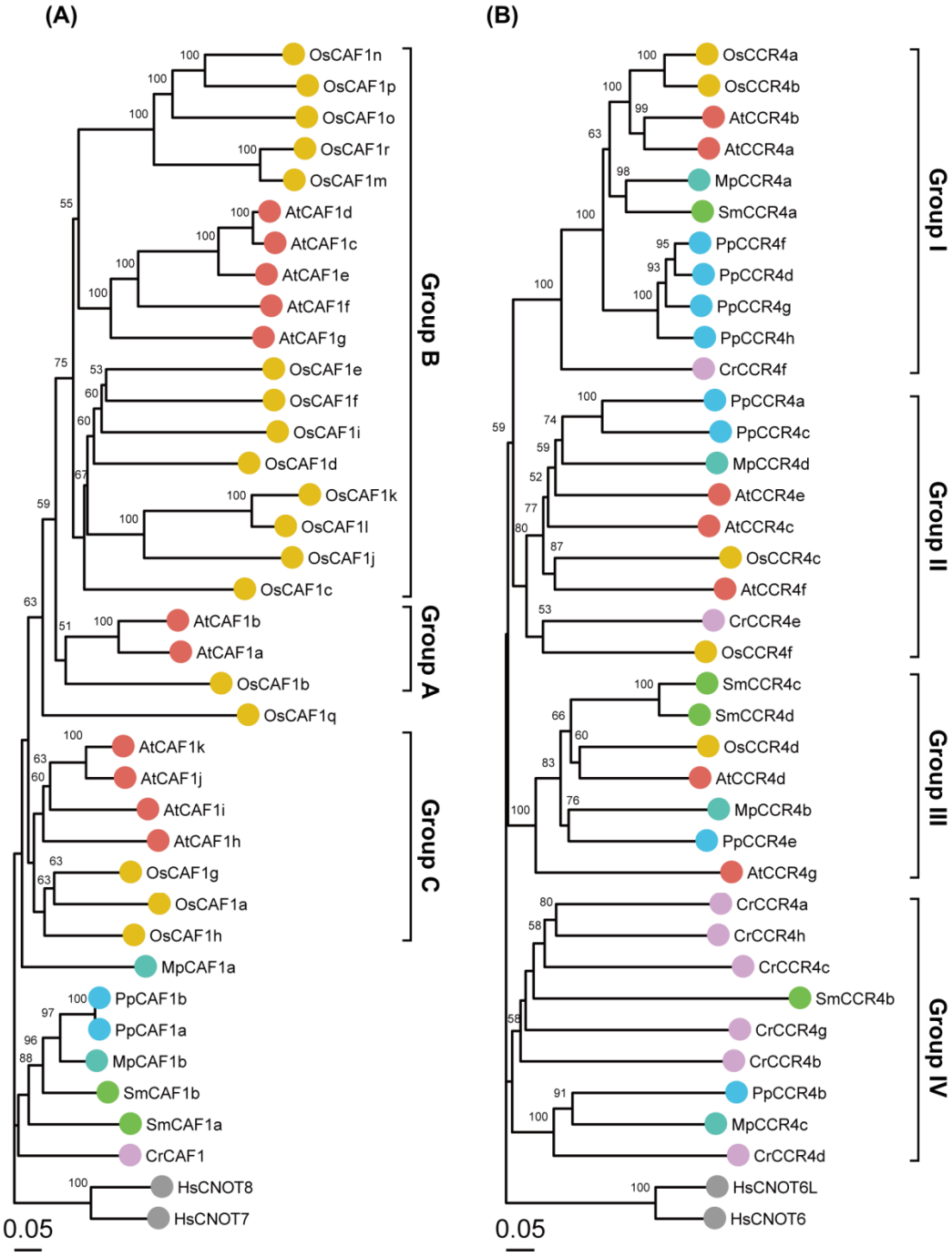

Figure 3-1. Phylogenetic analysis of orthologs of human CAF1 and CCR4 in plants.

Phylogenetic trees of CAF1 orthologs (A) and CCR4 orthologs (B) were constructed using the neighbour-joining method. Numbers with bootstrap value (> 50%) are shown at each branch. The amino acid sequence of each component of the human CCR4-NOT complex was used to identify orthologs in other plant species using BLAST searches in Phytozome v12.1. Orthologs in *Arabidopsis thaliana* are shown in red, *Oryza sativa* in gold, *Physcomitrella patens* in blue, *Marchantia polymorpha* in cobalt-green, *Selaginella moellendorffii* in green, and *Chlamydomonas reinhardtii* in violet. Orthologs in humans are shown in grey.

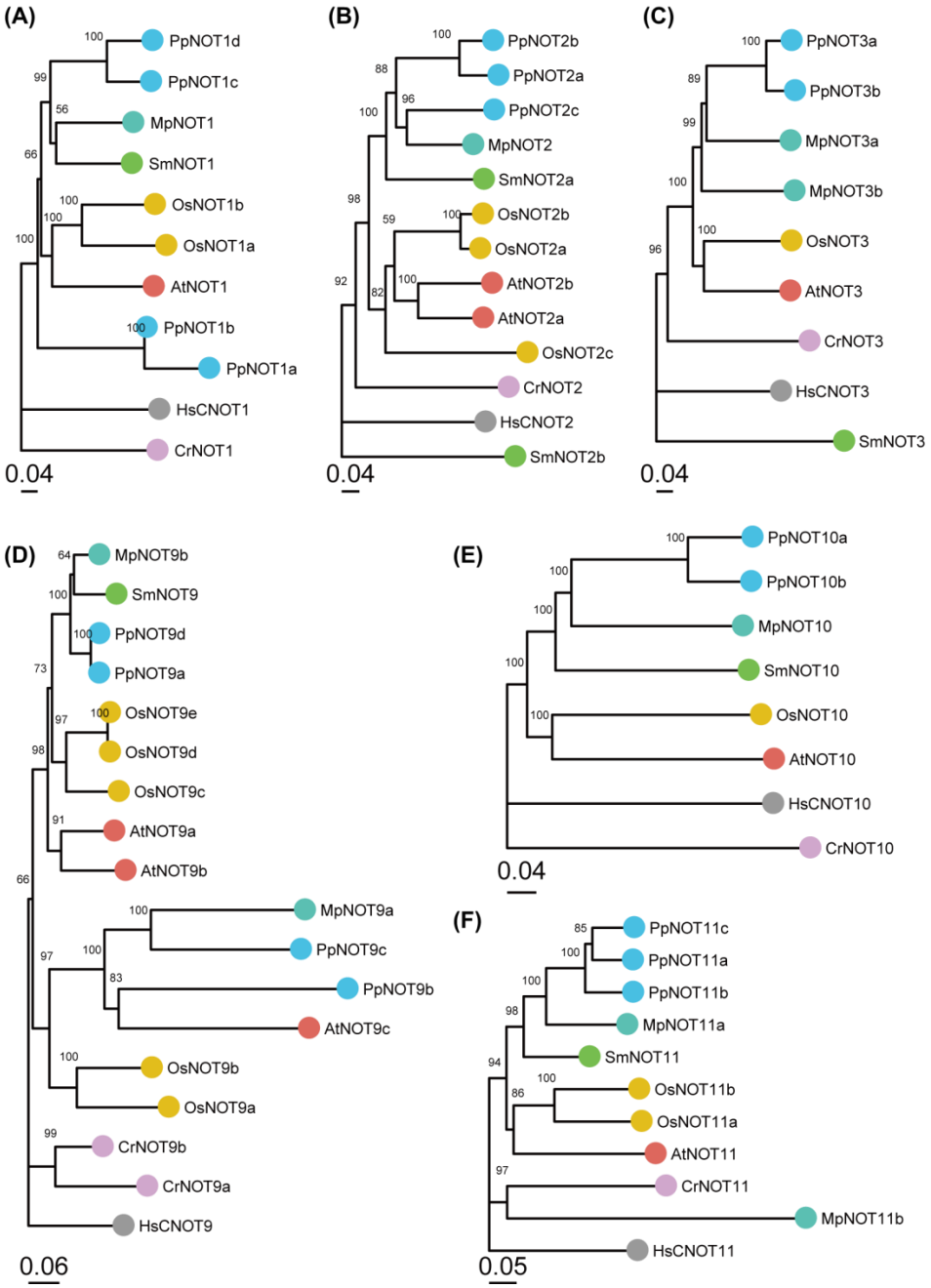

Figure 3-2. Phylogenetic analysis of orthologs of the core components of human CCR4-NOT complex in plants.

Phylogenetic trees of NOT1 orthologs (A), NOT2 orthologs (B), NOT3 orthologs (C), NOT9 orthologs (D), NOT10 orthologs (E), and NOT11 orthologs (F) were constructed using the neighbour-joining method. Bootstrap values (> 50%) are shown at each branch. The amino acid sequence of each component of the human CCR4-NOT complex was used to identify orthologs in other plant species using BLAST searches in Phytozome v12.1. Orthologs in *Arabidopsis thaliana* are shown in red, *Oryza sativa* in gold, *Physcomitrella patens* in blue, *Marchantia polymorpha* in cobalt-green, *Selaginella moellendorffii* in green, and *Chlamydomonas reinhardtii* in violet. Orthologs in human are shown in grey.

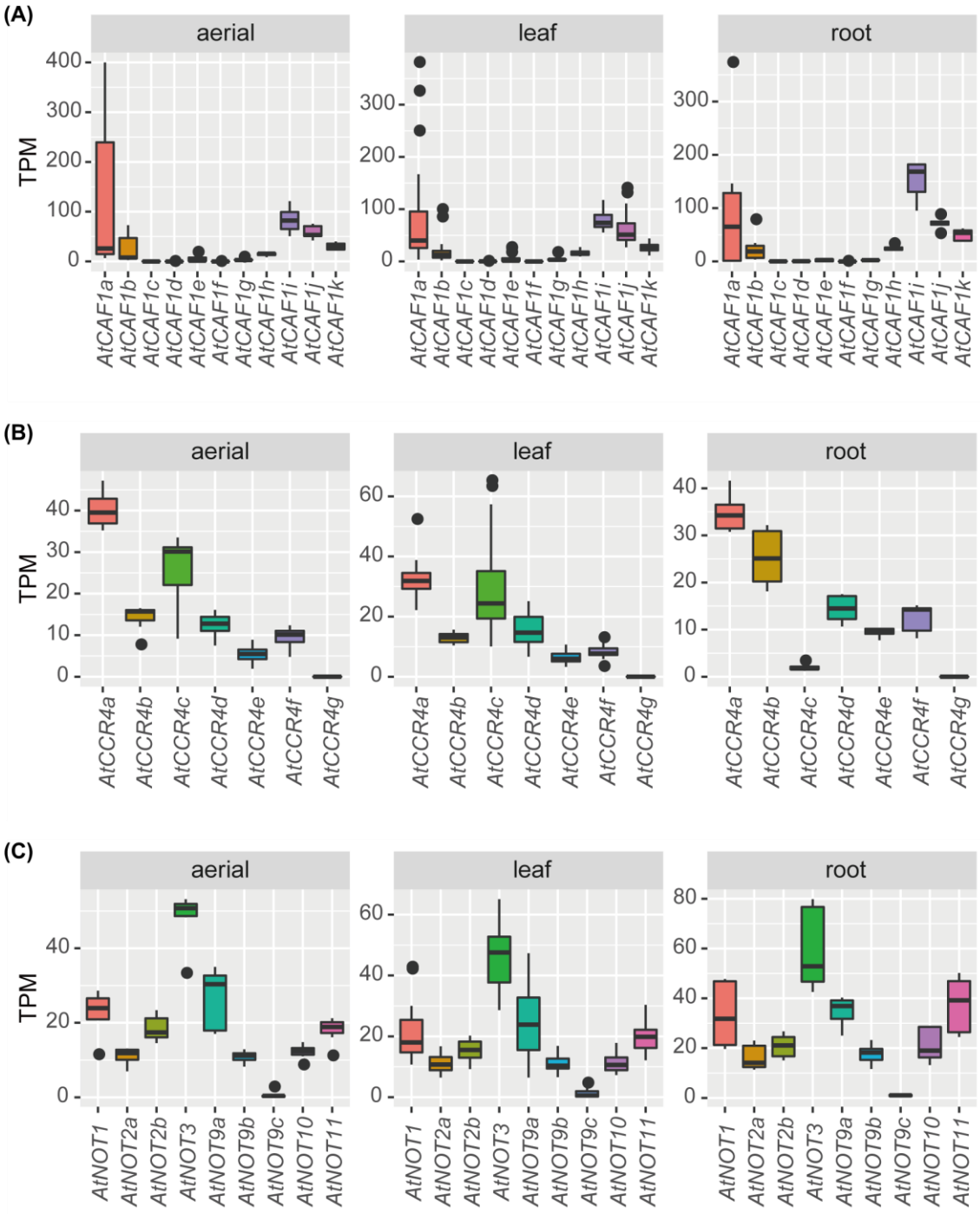

Figure 3-3. Expression patterns of AtCAF1, AtCCR4, and AtNOT families.

Normalised mRNA expression levels (transcripts per kilobase million; TPM) of members of the AtCAF1 (A), AtCCR4 (B), and AtNOT (C) protein families. Expression data from aerial, leaf, and root plant regions are shown as box-and-whisker plots. Data were retrieved from a publicly available database (https://www.araport.org/).

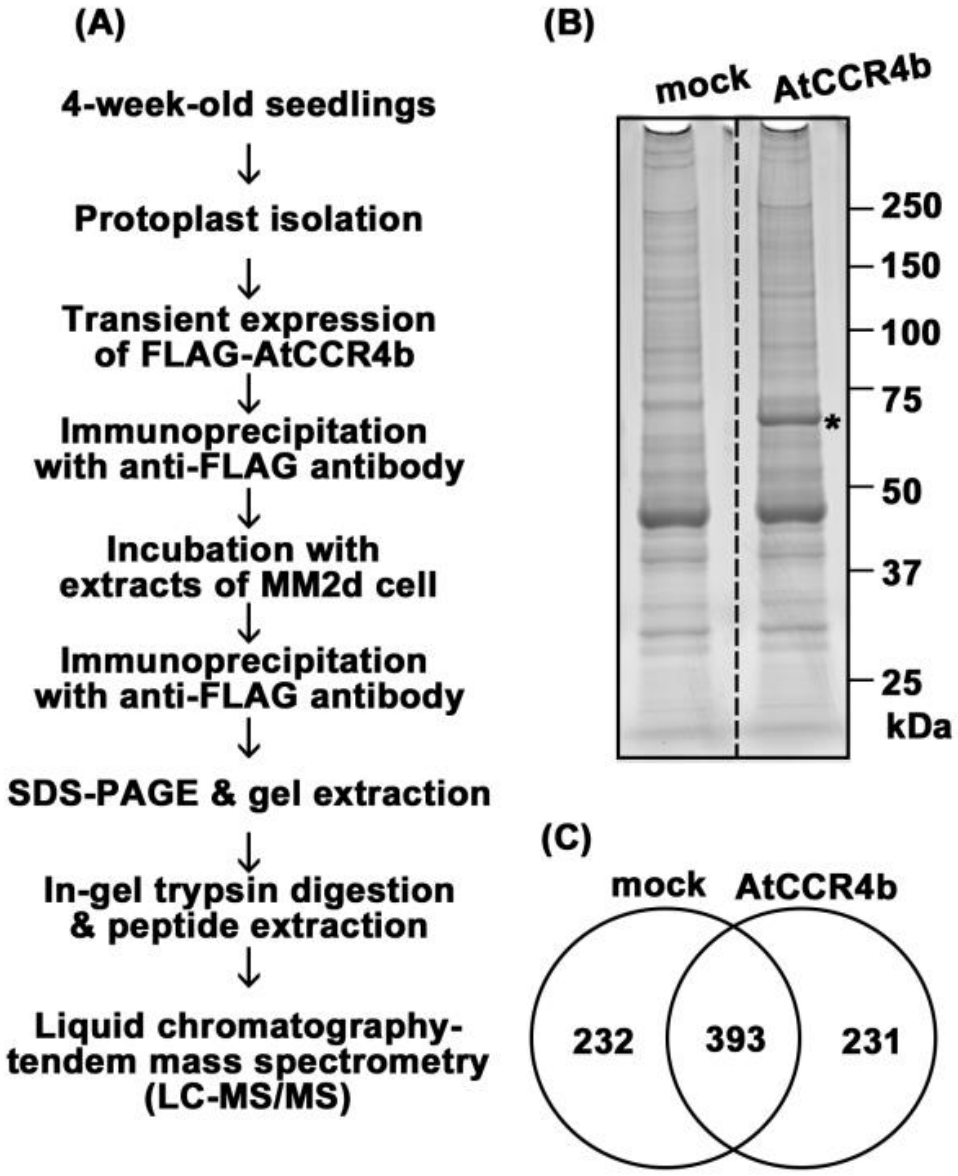

Figure 3-4. Isolation of putative interactors of FLAG-AtCCR4b in vivo.

(A) Scheme of the experimental procedure. (B) Anti-FLAG-immunoprecipitated (IP) products from cells transfected with FLAG-AtCCR4b or mock were incubated with MM2d extracts. Then, second IP products were visualised on the gel using SYPRO Ruby staining. An asterisk indicates the position of FLAG-AtCCR4b proteins. (C) Numbers of proteins identified from cells transfected with FLAG-AtCCR4b and/or mock by IP-MS analysis.

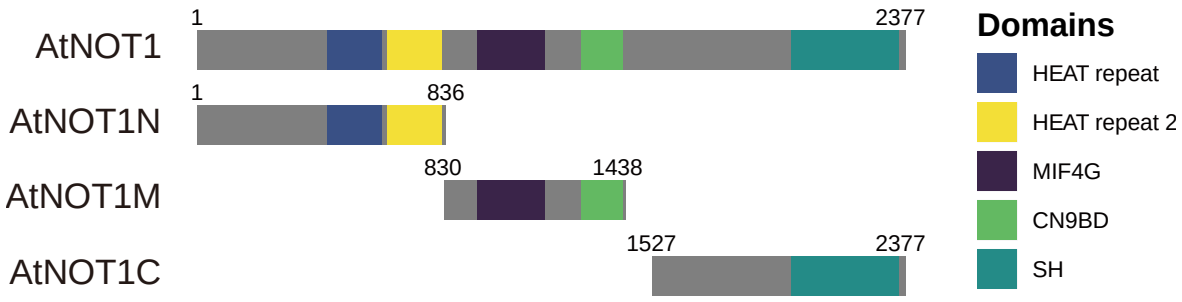

Figure 3-5. Schematic structures of full-length and truncated NOT1 protein.

AtNOT1 represents the full-length protein (1–2377 residues) with HEAT repeat, MIF4G domain, CAF40/NOT9 binding domain (CN9BD), and super homology (SH) domain. AtNOT1N is the N-terminal region (amino acids 1–836 residues) containing two HEAT repeats. AtNOT1M is the middle region (amino acids 830–1438), containing the MIF4G and CN9BD domains. AtNOT1C is the C-terminal region (amino acids 1527–2377), containing the SH domain.

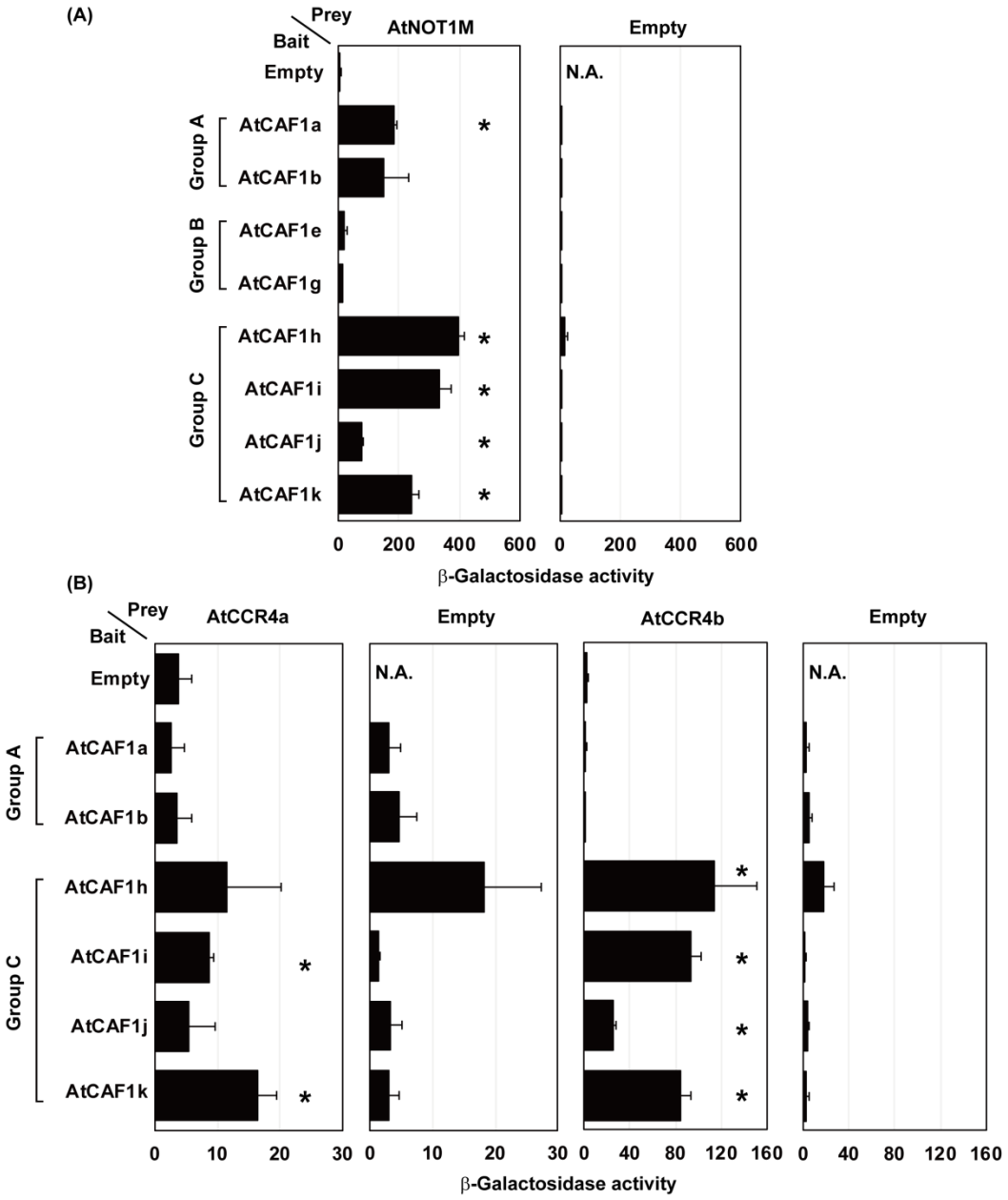

Figure 3-6. AtCCR4a/b and several AtCAF1 isoforms are present in the AtCCR4-NOT complex.

Interactions between AtNOT1M and AtCAF1 isoforms, and AtCCR4a/b and AtCAF1 isoforms were tested by yeast two-hybrid assay. (A) β-Galactosidase units of yeast expressing AtNOT1M and AtCAF1 isoforms or (B) expressing AtCCR4a/b and AtCAF1 isoforms are shown. Means ± SD of three biological replicates are shown. Asterisks indicated significant differences between test sample and both of negative controls (empty vectors) according to one-sided Welch's *t*-tests. N.A., not analysed.

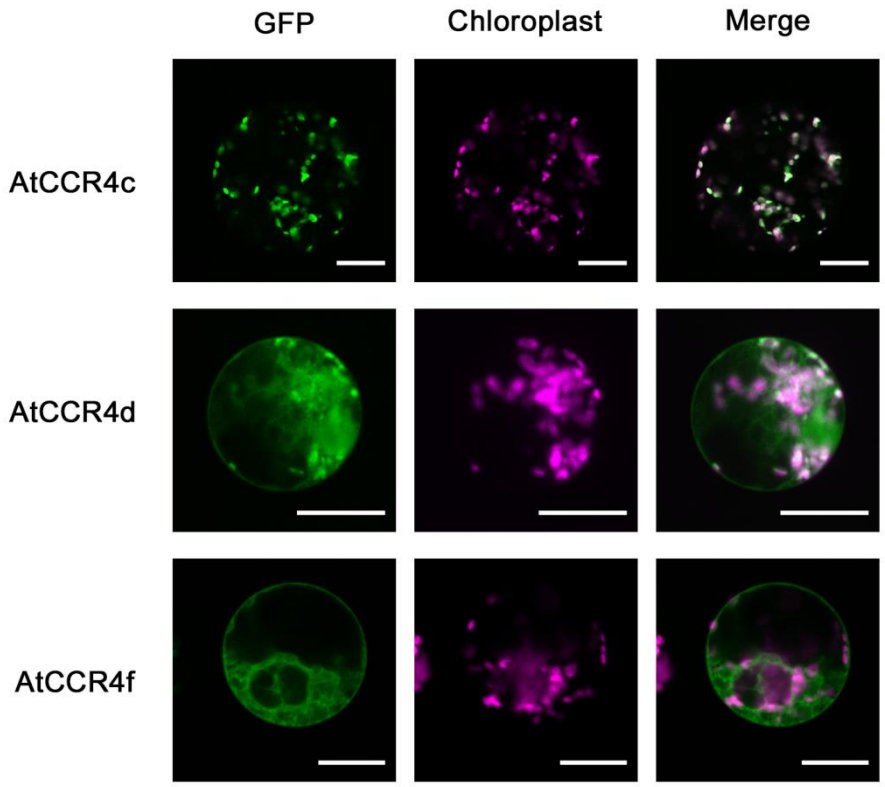

Figure 3-7. Subcellular localization of AtCCR4c/d/f

Green fluorescent protein (GFP) fusions of AtCCR4c/d/f were transiently expressed in protoplasts derived from *Arabidopsis thaliana* T87 cells. Images of GFP fluorescence are shown on the left, auto-fluorescence images of chlorophyll are presented in the middle, and merged images are on the right. Similar images were obtained in two biological replicates.

Scale bar = 20 μm

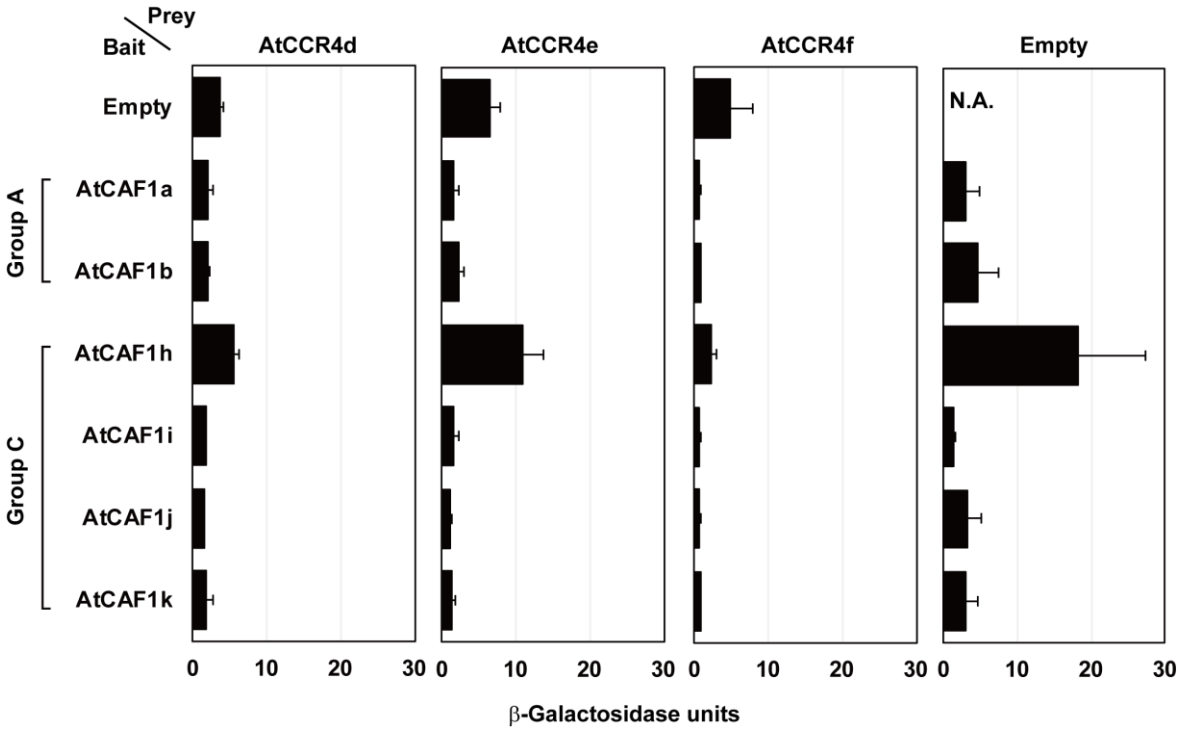

Figure 3-8. None of AtCCR4d/e/f were included in the AtCCR4-NOT complex.

Interactions between AtCCR4d/e/f and AtCAF1 isoforms were tested by yeast two-hybrid assay. β-Galactosidase units of yeast expressing AtCCR4d/e/f and AtCAF1 isoforms are shown. Means ± SD of three biological replicates are shown. N.A., not analysed.

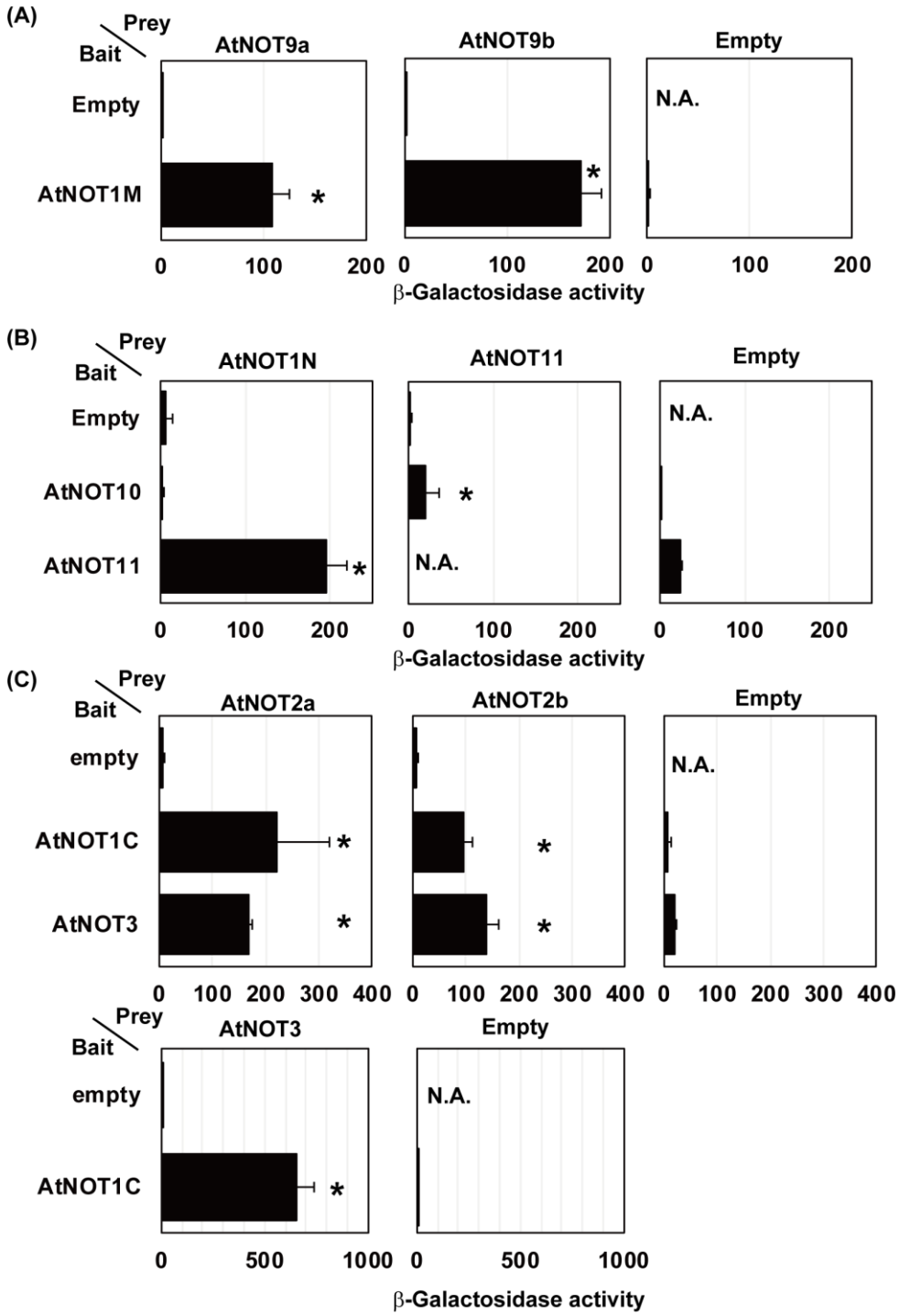

Figure 3-9. AtNOT proteins are present in the AtCCR4-NOT complex.

Interactions between AtNOT1M and AtNOT9a/b, AtNOT1N and AtNOT10/11, and among AtNOT1c, AtNOT2a/b and AtNOT3 were tested by yeast two-hybrid assay. (A) β-Galactosidase units of yeast expressing AtNOT9a/b, and AtNOT1M, (B) expressing AtNOT1N, AtNOT10, and AtNOT11, or (C) expressing AtNOT1C, AtNOT2a/b and AtNOT3. Means ± SD of three biological replicates are shown. Asterisks indicated significant differences between test sample and both of negative controls (empty vectors) according to one-sided Welch's *t*-tests. N.A., not analysed.

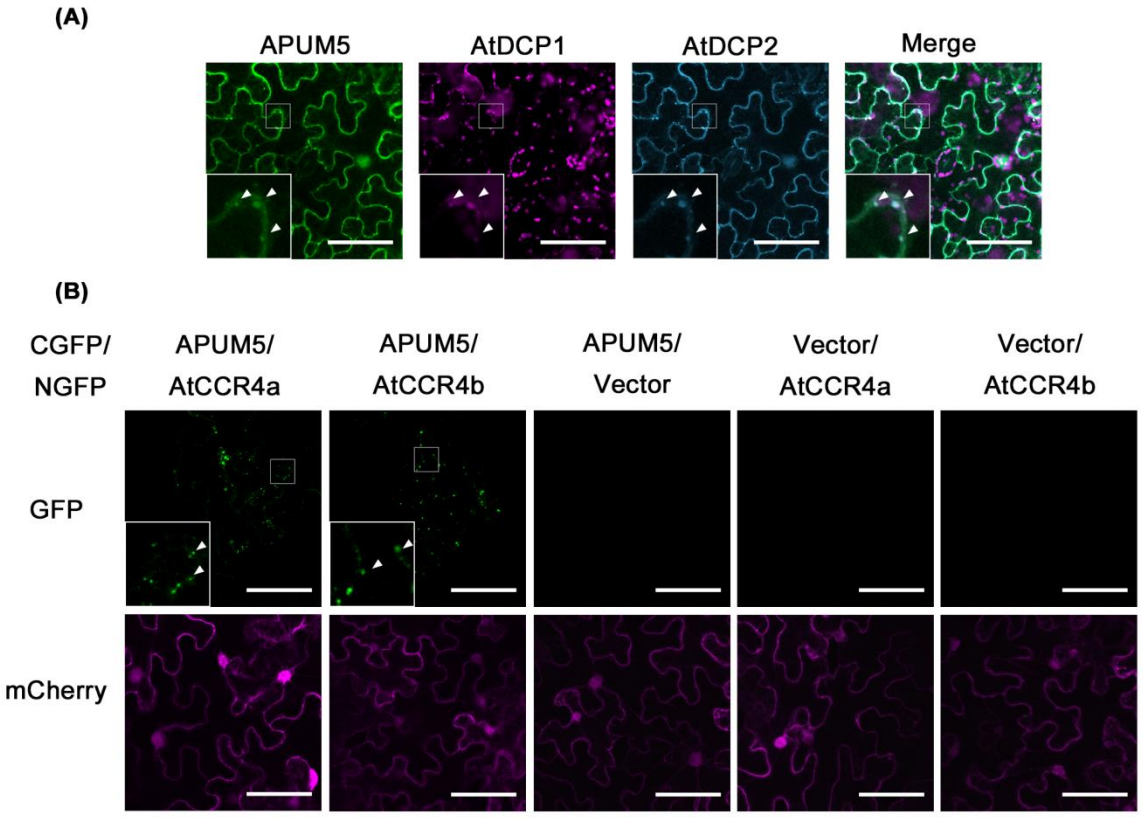

Figure 3-10. APUM5 interacts with AtCCR4 in P-bodies.

(A) The indicated fluorescent fusion proteins were transiently co-expressed in tobacco leaves by agroinfiltration. APUM5 was co-expressed with the P-body marker, AtDCP1, and AtDCP2. The areas indicated by boxes are presented in the magnified view. Arrowheads indicate the location of P-bodies. Similar images were obtained in two biological replicates. (B) Interaction analysis with biomolecular fluorescence complementation (BiFC). APUM5 tagged with the C-terminal fragment of GFP (CGFP) and AtCCR4a/b tagged with the N-terminal fragment of GFP (NGFP) were co-expressed together with mCherry in tobacco leaves by agroinfiltration. mCherry was used as a positive control for transfection. The areas indicated by boxes are presented in the magnified view as in (A). Arrowheads indicate the location of P-bodies. Similar images were obtained in three biological replicates. Scale bars = 75 μm.

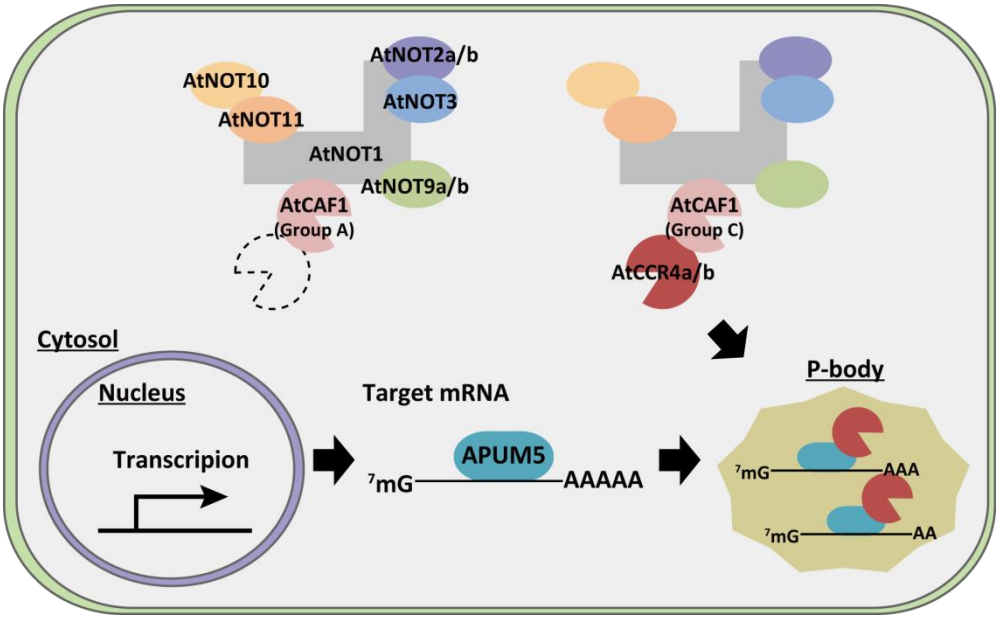

Figure 3-11. Schematic representation of two types of AtCCR4-NOT complex and APUM5.

The AtCCR4-NOT complex containing AtCCR4a/b and AtCAF1 in group C (top right) and the complex containing AtCAF1 in group A but no AtCCR4a/b (top left) are shown. APUM5 interacts with AtCCR4a/bspecifically in P-bodies.

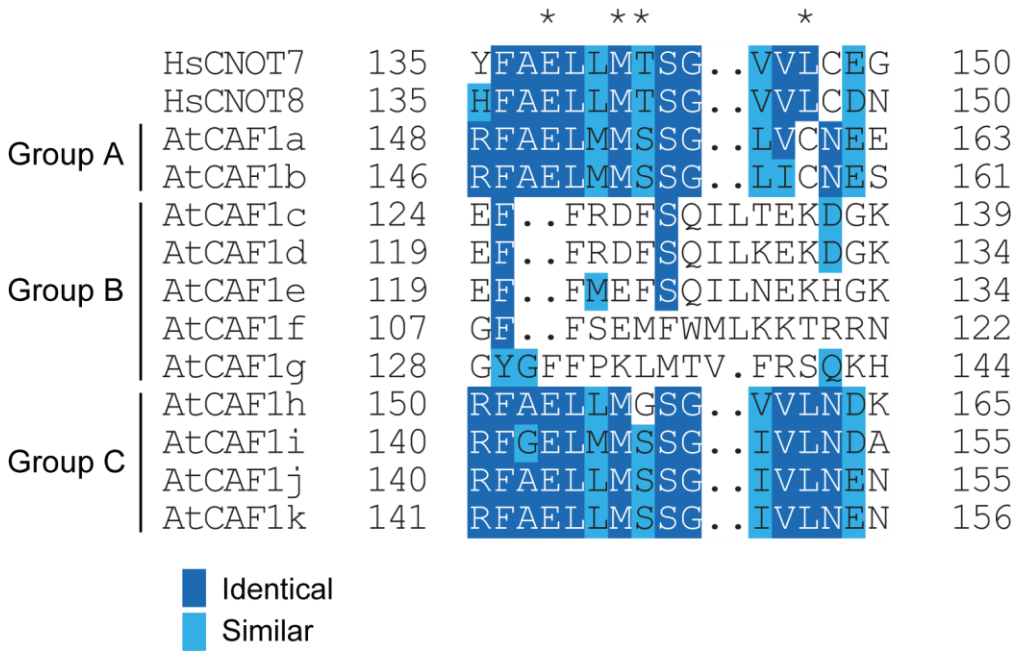

Figure 3-12. Alignment of NOT1-interacting regions of CAF1 homologs in human and Arabidopsis.

The amino acid sequences of NOT1-interacting regions of CAF1 homologs from humans and Arabidopsis were aligned using Clustal Ω with default parameters. Identical and similar residues are shaded blue and magenta, respectively. Important residues for the interactions with HsCNOT7 and HsCNOT1 are marked by asterisks.

		SEQUEST Score		Number of peptides		
AGI	**Gene name**	**FLAG-AtCCR4b**	**Mock**	**FLAG-AtCCR4b**	**Mock**	**Gene description**
AT1G15920	AtCAF1h	1.82	N.D.	1	N.D.	Polynucleotidyl transferase, ribonuclease H-like superfamily protein
AT5G10960	AtCAF1i	5.31	N.D.	4	N.D.	Polynucleotidyl transferase, ribonuclease H-like superfamily protein
AT2G32070	AtCAF1k	2.51	N.D.	1	N.D.	Polynucleotidyl transferase, ribonuclease H-like superfamily protein
AT3G58580	AtCCR4b	857.60	N.D.	39	N.D.	DNAse I-like superfamily protein
AT5G35430	AtNOT10	5.59	N.D.	12	N.D.	Tetratricopeptide repeat (TPR)-like superfamily protein
AT1G07705	AtNOT2a	2.67	N.D.	4	N.D.	NOT2 / NOT3 / NOT5 family
AT5G18230	AtNOT3	1.75	N.D.	12	N.D.	Transcription regulator NOT2/NOT3/NOT5 family protein
AT3G20800	AtNOT9a	7.43	N.D.	5	N.D.	Cell differentiation, Rcd1-like protein

Table 3-1. List of the components of the AtCCR4-NOT complex detected by IP-MS analysis. N.D., not detected.

		SEQUEST Score		Number of peptides		
AGI	**Gene name**	**FLAG-AtCCR4b**	**Mock**	**FLAG-AtCCR4b**	**Mock**	**Gene description**
AT2G34160	Alba DNA	3.18	N.D.	4	N.D.	Alba DNA/RNA-binding protein
AT2G29200	APUM1	2.44	N.D.	8	N.D.	Pumilio 1
AT3G20250	APUM5	7.17	N.D.	7	N.D.	Pumilio 5
AT4G10610	CID12	2.09	N.D.	2	N.D.	CTC-interacting domain 12
AT4G32720	La1	1.71	N.D.	11	N.D.	La protein 1
AT1G51510	Y14	1.75	N.D.	2	N.D.	RNA-binding (RRM/RBD/RNP motifs) family protein

Table 3-2. List of the RNA-binding proteins detected by IP-MS analysis. N.D., not detected.

Genes	Primer Name	Sequences
AtNOT1	AtNOT1N EnF	CACCATGTATTCAAAGACAATTGAAAATCC
	AtNOT1N EnR	GATTGTGAGGGACCAGGGTGTGA
	AtNOT1M EnF	CACCTCACACCCTGGTCCCTCACAATC
	AtNOT1M EnR	GGATCGAAAAAGGAGGATCCAGCACC
	AtNOT1C EnF	CACCTCTAATGCTGGAAACGC
	AtNOT1C EnR	CTAGTGAGAATTGTCTGAGA
AtNOT2a	AtNOT2a EnF	CACCATGTCAAGTTTACTTAATTCC
	AtNOT2a EnR	TCAATGTTGAGAATCTTGAGAA
AtNOT2b	AtNOT2b EnF	CACCATGTCAAACCTTCATTCATCTC
	AtNOT2b EnR	TCAAAGCTGCAGCAAGCTTGG
AtNOT3	AtNOT3 EnF	CACCATGGGTGCGAGCCGGAAATTAC
	AtNOT3 EnR	CTATACGACGAGTTCATCTTC
AtNOT9a	AtNOT9a EnF	CACCATGGCGAATCTACCTTCTTC
	AtNOT9a EnR	TCAAAGCATGTGCTCAAATC
AtNOT9b	AtNOT9b EnF	CACCATGGCTAATCTTCCTCCTCC
	AtNOT9b EnR	TTAATTCACAAACATATGAGCC
AtNOT10	AtNOT10 EnF	CACCATGGATTCTCGAGATTCGTTATCAT
	AtNOT10 EnR	CTATGAGGCTCTCACTTCCAATCT
AtNOT11	AtNOT11 EnF	CACCATGAATCGATCAACGATGATG
	AtNOT11 EnR	TTATTCATCCAATTGTTTCAAAAGC
AtCAF1a	AtCAF1a EnF	CACCATGGCGATCATTAAACCAAACCG
	AtCAF1a EnR	TTAAAAAACCTCAAGCCCATACA
AtCAF1b	AtCAF1b EnF	CACCATGATCAAATCAGAAGCAGATC
	AtCAF1b EnR	TCAAAAAACCTCTAAACCATAC
AtCAF1e	AtCAF1e EnF	CACCATGAGCGGTGAAGTTTG
	AtCAF1e EnR	TCACAATACGTAGTTCCTTCC
AtCAF1g	AtCAF1g EnF	CACCATGAACGAGATTCATCAA
	AtCAF1g EnR	CTACTCAACTACGTAGCAA
AtCAF1h	AtCAF1h EnF	CACCATGTCGCAGGCTCCGAAT
	AtCAF1h EnR	TTAATTTTTGGATCCAGTGAGC
AtCAF1i	AtCAF1i EnF	CACCATGGCGGAGACTTTGAAA
	AtCAF1i EnR	TACTACTACTACTGTTGCTAATTAA
AtCAF1j	AtCAF1j EnF	CACCATGTCTCTGTTTCTGAAAGACG
	AtCAF1j EnR	CTAGATAGCAACCTGACCATTT
AtCAF1k	AtCAF1k EnF	CACCATGTCACTGTTTCTAAAAGA
	AtCAF1k EnR	GGTCAGATTGTTCATTGA

AtCCR4a	AtCCR4a EnF	CACCATGCTTAGCGTTATACGAGTG
	AtCCR4a EnR	CTATAAAATATTGTTTCGTCTG
AtCCR4b	AtCCR4b EnF	CACCATGCTGAGCGTGATCCG
	AtCCR4b EnR	TTAACCGCGTCTTGTCCTAGG
AtCCR4c	AtCCR4c EnF	CACCATGCGTTGTGTGAATCGCGTTGATTG
	AtCCR4c EnR	TTAACCGTCCGGTTCAAAGACAA
	AtCCR4c EnR NS	ACCGTCCGGTTCAAAGACAAATT
AtCCR4d	AtCCR4d EnF	CACCATGTTTAGTTCTACAACTCTGCATCA
	AtCCR4d EnR	CTATTCCCGACGAATCTCAAACTC
	AtCCR4d EnR NS	TTCCCGACGAATCTCAAACTC
AtCCR4e	AtCCR4e EnF	CACCATGAGCGGATACGAGCGTAAGAACAC
	AtCCR4e EnR	TCATTGCCAGTCATTGACAAAGC
	AtCCR4e EnR NS	TTGCCAGTCATTGACAAAGCCGA
AtCCR4f	AtCCR4f EnF	CACCATGCGGCGTTCTCGTTTTGTTGC
	AtCCR4f EnR	TCAGCTTTTGGGCAGAGTTTTGC
	AtCCR4f EnR NS	GCTTTTGGGCAGAGTTTTGCTGC
APUM5	APUM5 EnF	CACCATGACGACTACGCAGAG
	APUM5 EnR	CTAACCTTCTGTTCCCTC
	APUM5 EnR NS	ACCTTCTGTTCCCTCTTC

Table 3-3. List of primers

Primer sequences used for constructions.

Chapter 4

General Discussion

Most of the researches regarding the control of gene expression have focused on the step of mRNA synthesis, transcription. Since the actual mRNA level is determined by the balance between mRNA synthesis and degradation, knowledge of mRNA degradation controls is also required. According to the simple kinetics of mRNA synthesis and degradation, control of mRNA degradation influence both on determination of mRNA level and speed of transition to a new mRNA level. To understand the importance of mRNA degradation control and its coordinated regulation with transcription, temporal changes of mRNA stability must be tested.

Dynamic changes of mRNA levels are generally observed in plant stress response. Therefore, I measured temporal changes of mRNA stability and accumulation in response to cold stress by genome-wide analysis. As shown in Chapter 2, I demonstrated that average transcripts were stabilized throughout cold treatment probably due to general decrease of enzyme activities for mRNA degradation under cold condition. Taking this general shift into account, I showed that several CBF responsive genes were relatively-destabilized, even though the mRNA accumulations were increased. Moreover, I demonstrated that this unexpected contradictory result occurred by accelerating the transcription rate to overcome the destabilization by using mathematical approach. These results suggest that mRNA destabilization is advantageous for the swift increase of stress-responsive genes.

Although a variety of relatively-stabilized or destabilized transcripts in response to cold stress were identified in this study, I could not find conserved sequence motifs in the 5' or 3'-UTR. As for mechanistic aspect of the mRNA degradation control in response to cold stress, genetic analyses using the mutants of mRNA degradation machineries are useful. For example, AtLSM1-7 complex, a cytoplasmic mRNA decay machinery, promotes decapping of several mRNAs to induce the degradation in response to the abiotic stresses, such as cold, drought and salt stress (Perea-Resa et al. 2016). AtLSM1-7 might be involved in the selective mRNA degradation observed in my study.

Dynamic changes of mRNA levels depending on time are also observed in developmental process. In other organisms, the involvement of mRNA degradation control in this process have been reported. For example, the regulation of maternal mRNA degradation at the early embryogenesis is important for the embryonic developmental process in fly (Bashirullah et al. 2001, Thomsen et al. 2010) During the early embryonic development and pollen maturation in plants, mRNA level is largely altered (Wickramasuriya and Dunwell, 2015, Honys and Twell, 2004). Accumulating studies using genome-wide analysis of mRNA stability during developmental processes and other stress responses will help us to understand the physiological importance of mRNA degradation control in plants.

To assess the importance of mRNA degradation controls in plants, I took another approach, in which I focused on the regulators of mRNA degradation, especially deadenylases. Because poly(A) shorting of mRNA, catalyzed by deadenylases, is the first and apparently the rate

limiting step of mRNA degradation. CCR4/CAF1 are widely conserved deadenylses in eukaryotes. They form large complex including NOT1 as a scaffold protein and various NOT proteins that are involved in multiple levels of gene expression control. Arabidopsis possesses the homologs of CCR4/CAF1. Deficient mutant of *AtCCR4a/b* showed pleiotropic phenotypes through plant growth and development, suggesting that AtCCR4a/b have specific target mRNAs responsible for each phenotype. In fact, *GBSS1* is identified as a target mRNA of AtCCR4a/b, which is responsible for the high sucrose tolerance phenotype (Suzuki et al. 2015). Although AtCCR4a/b have to recognize the specific target mRNA, AtCCR4a/b themselves do not have RNA-binding capability. Therefore, it is important to find interactors of AtCCR4a/b to reveal its function as a regulator of gene expression, as well as the target mRNA recognition mechanism.

As shown in Chapter 3, I first surveyed orthologs of the core components of the human CCR4-NOT complex in several plants, including Arabidopsis. Orthologs of all components exist in analyzed plant genome. Then, some of the orthologs were found as interactors of AtCCR4b by IP-MS analysis. Interaction among AtCCR4-NOT proteins were verified by yeast two-hybrid assay, resulting that two distinct AtCCR4-NOT complexes were identified. One type of AtCCR4-NOT complex includes both AtCCR4a/b and AtCAF1h/i/j/k, and the other includes only AtCAF1a/b as deadenylase components. To understand the functional differences of these two types of AtCCR4-NOT complex, target mRNA identification for each deadenylase is required. The expression of AtCAF1a/b is strongly induced by pathogen infection and abiotic stress treatments and responsible target transcripts are identified from the individual gene analysis (Walley et al. 2010, Liang et al. 2009). Next-generation sequencing technology made it possible to detect the poly(A) length globally (Subtelny et al. 2014, Chang et al. 2014, Harrison et al. 2015, Lim et al. 2016), which is useful to detect the target mRNA using the deficient mutant of each deadenylase.

The IP-MS analysis for identification of AtCCR4b interactor also detected several RNA-binding proteins. One of them, APUM5 is a member of Pumilio proteins that is widely conserved RNA-binding protein family in eukaryotes. Interestingly, I revealed that APUM5 was interacted with AtCCR4a/b mostly in P-bodies. Moreover, Huh and Paek (2014) demonstrated that the involvement of APUM5 in abiotic stress responses, such as drought, osmotic, and salt stresses. They also showed that APUM5 negatively regulates the expression of several stress inducible transcripts by binding to a specific motif in their 3'UTR. Overall findings provide the possibility that APUM5 is associated with mRNA degradation of stress responsive genes together with AtCCR4a/b. Further investigations of the mRNA stability as well as poly(A) length of target mRNAs under stress conditions in the *apum5* and the *atccr4a/b* mutants will address the possibility.

In this dissertation, I used two different approaches to address the importance of mRNA degradation controls in plants. Eventually, I found several transcripts regulated at the level of mRNA stability in response to cold and discussed the physiological meaning of the regulation. From the research of AtCCR4a/b interactors, I found the possible link between deadenylase and

control of stress responsive genes via APUM5. Further analyses would be required to reveal the mechanistic aspects of mRNA degradation control in response to abiotic stresses, however I believe that this study provide many prospects to the research field of mRNA degradation controls in plants.

References

Bashirullah, A., Cooperstock, R.L. and Lipshitz, H.D. (2001) Spatial and temporal control of RNA stability. *Proc. Natl. Acad. Sci. USA* **98**: 7025-7028.

Basquin, J., Roudko, V.V., Rode, M., Basquin, C., Seraphin, B. and Conti, E. (2012) Architecture of the nuclease module of the yeast Ccr4-Not complex: the Not1-Caf1-Ccr4 interaction. *Mol. Cell* **48**: 207-218.

Chang, H., Lim, J., Ha, M. and Kim, V.N. (2014) TAIL-seq: genome-wide determination of poly(A) tail length and 3' end modifications. *Mol. Cell*, **53**: 1044-1052.

Harrison, P.F., Powell, D.R., Clancy, J.L., Preiss, T., Boag, P.R., Traven, A., Seemann, T. and Beilharz, T.H. (2015) PAT-seq: a method to study the integration of 3'-UTR dynamics with gene expression in the eukaryotic transcriptome. *RNA*, **21**: 1502-1510.

Honys, D. and Twell, D. (2004) Transcriptome analysis of haploid male gametophyte development in Arabidopsis. *Genome Biol.*, **5**: R85.1-R.85.13

Huh, S.U. and Paek, K.H. (2014) APUM5, encoding a Pumilio RNA binding protein, negatively regulates abiotic stress responsive gene expression. *BMC Plant Biol.* **14**: 75.

Liang, W., Li, C., Liu, F., Jiang, H., Li, S., Sun, J., Wu, X. and Li, C. (2009) The Arabidopsis homologs of CCR4-associated factor 1 show mRNA deadenylation activity and play a role in plant defence responses. *Cell Res.* **19**: 307-316.

Lim, J., Lee, M., Son, A., Chang, H. and Kim, V.N. (2016) mTAIL-seq reveals dynamic poly(A) tail regulation in oocyte-to-embryo development. *Genes Dev.*, **30**: 1671-1682.

Perea-Resa, C., Carrasco-López, C., Catalá, R., Turečkova, V., Navak, O., Zhang, W., Sieburth, L. Jiménez-Gómez, J.M. and Salinas, J. (2016) The LSM1-7 complex differentially regulates Arabidopsis tolerance to abiotic stress conditions by promoting selecetive mRNA decapping. *Plant Cell*, **28**: 505-520.

Subtelny, A.O., Eichhorn, S.W., Chen, G.R., Sive, H. and Bartel, D.P. (2014) Poly(A)-tail profiling reveals an embryonic switch in translational control. *Nature*, **508**: 66-71.

Suzuki, Y., Arae, T., Green, P.J., Yamaguchi, J. and Chiba, Y. (2015) AtCCR4a and AtCCR4b are involved in determining the poly(A) length of *Granule-bound starch synthase 1* transcript and modulating sucrose and starch metabolism in *Arabidopsis thaliana*. *Plant Cell Physiol.* **56**: 863-874.

Thomsen, S., Anders, S., Janga, S.C., Huber, W. and Alonso, C.R. (2010) Genome-wide analysis of mRNA decay patterns during early Drosophila development. Genome Biol., 11: *Genome Biol.*, **11**, R93. doi: 10.1186/gb-2010-11-9-r93.

Walley, J.W., Kelley, D.R., Nestorova, G., Hirschberg, D.L. and Dehesh, K. (2010) Arabidopsis deadenylases AtCAF1a and AtCAF1b play overlapping and distinct roles in mediating environmental stress responses. *Plant Physiol.* **152**: 866-875.

Wickramasuriya, A.M. and Dunwell, J.M. (2015) Global scales transcriptome analysis of Arabidopsis embryogenesis in vitro. *BMC Genomics*, **16**: doi: 10.1186/s12864-015-1504-6

Acknowledgements

I would like to express my sincerely gratitude to Dr. Yukako Chiba, Associate Professor of the Graduate School of Life Science, Hokkaido University, for devoted guidance, pertinent advice, significant discussion, kind suggestion and critical review throughout my PhD study and the writing of this thesis.

I am very grateful to Dr. Junji Yamaguchi (Hokkaido University), Dr. Satoshi Naito (Hokkaido Universiy) for their critical reading. I thank Chieko Saito and Hitomi Sekihara (Hokkaido University) for technical assistance with the experimental procedure, Ayuko Kuwahara (RIKEN) for technical assistance with the microarray analysis, Dr. Yuichiro Watanabe (University of Tokyo) for providing us with the AtDCP1 and AtDCP2 clones, Dr. Tsuyoshi Nakagawa (Shimane University) for the pUGW and pGWB vector series, Dr. Shoji Mano (National Institute for Basic Biology) for the pB4 vector series, and Dr. Hironori Kaminaka (Tottori University) for pEG202gw and pJG4-5gw vectors.MM2d and T87 cell cultures were provided by the RIKEN BioResource Center. We used the Radioisotope Laboratory of the Faculty of Science, Hokkaido University.

List of Publications

Arae, T., Isai, S., Sakai, A., Mineta, K., Yokota-Hirai, M., Suzuki, Y., Kayana, S., Yamaguchi, J., Naito, S. and Chiba, Y. (2017) Co-ordinated regulations of mRNA synthesis and decay during cold acclimation in Arabidopsis cells. *Plant Cell Physiol.* **58**: 1090-1102.

Arae, T., Morita, K., Suzuki, Y., Yasuda, S., Sato, T., Yamaguchi, J. and Chiba, Y. (2018) Identification of Arabidopsis CCR4-NOT complexes with variable combinations of deadenylase subunits. *Plant Cell Physiol.*, **under review**

List of Publication (Appendix)

Suzuki, Y., Arae, T., Green, P.J., Yamaguchi, J. and Chiba, Y. (2015) AtCCR4a and AtCCR4b are involved in determining the poly(A) length of *Granule-bound starch synthase 1* transcript and modulating sucrose and starch metabolism in *Arabidopsis thaliana*. *Plant Cell Physiol.* **56**: 863-874.